Identification of novel genes and compounds for the development of precision therapeutics for dystrophic epidermolysis bullosa and associated squamous cell carcinoma

A DISSERTATION

SUBMITTED TO THE FACULTY OF THE

UNIVERSITY OF MINNESOTA

BY

Michael D. Pickett-Leonard

IN PARTIAL FULFILLMENT OF THE REQUIREMENTS

FOR THE DEGREE OF

DOCTOR OF PHILOSOPHY

Advisor: Jakub Tolar, MD, PhD

August 2021

ACKNOWLEDGEMENTS

First and foremost, I would like to express my gratitude to my advisor, Dr. Jakub Tolar, for his unwavering confidence in me, his many contributions to my professional development, and his limitless positivity. He has consistently pushed me to be independent, encouraged me to explore new opportunities, and trusted me to make important decisions. I would like to thank Dr. Elizabeth Thompson, who believed in me when I didn't believe in myself and has taught me so much about what it means to be a good scientist. I would like to thank the members of my committee, which includes Dr. Timothy Hallstrom, my committee chair; Dr. Rui Kuang, who was also my advisor in the Bioinformatics and Computational Biology (BICB); Dr. Ran Blekhman, who also served on my BICB committee; Dr. Daniel Voytas, and Dr. Paolo Provenzano. I would also like to thank my family and friends, who have supported me in countless different ways throughout my PhD.

ABSTRACT

Dystrophic epidermolysis bullosa (DEB) is a skin blistering disease caused by dominant (DDEB) or recessive (RDEB) mutations in the *COL7A1* gene, with the latter being more severe. *COL7A1* encodes type VII collagen (C7), which aggregates into structures called anchoring fibrils that maintain skin integrity by securing the epidermis to the dermis. DEB is characterized by shearing and blistering of the skin (and various mucosae) at the level of the superficial dermis. In severe cases of RDEB, this leads to fibrosis, scarring, and aggressive cutaneous squamous cell carcinoma (RDEBSCC). Using a combination of high-throughput sequencing and genome-wide screening tools we identified novel (1) genes and compounds that increase C7 production in wild-type and RDEB keratinocytes, (2) genes that become progressively dysregulated with RDEB disease progression, and (3) genes that drive or inhibit proliferation in wild-type, RDEB, and RDEBSCC keratinocytes.

In Chapter 2, we start by describing the creation and validation of a keratinocyte C7 reporter cell line, in which C7 production is linked to tdTomato fluorescence. We used this reporter line to perform a genome wide CRISPR activation (CRISPRa) screen to identify genes that increase C7 production in keratinocytes. There were 1544 CRISPRa single guide RNAs (sgRNAs), targeting 1464 distinct genes, whose abundance was substantially increased in the top 10% of tdTomato-expressing cells relative to the plasmid DNA library. Validation of the top two candidates identified in this screen, *DENND4B* and *TYROBP*, showed that CRISPRa-mediated upregulation of these genes significantly increased tdTomato fluorescence and C7 protein production, but not *COL7A1* mRNA. Pathway analysis of the 1464 gene targets identified significantly enriched upstream regulators, signaling pathways, and biological functions. We performed a targeted drug screen using compounds that act on some of these upstream regulators and signaling pathways and found that kaempferol, a plant flavonoid, was able to increase *COL7A1* mRNA and C7 protein in both wild-type and RDEB keratinocytes.

In Chapter 3, we investigate potential mechanisms of RDEBSCC development. We performed RNA-sequencing on nine sibling pairs of wild-type and RDEB keratinocytes (WTK, RDEBK) and six RDEBSCC cell lines and identified numerous genes whose expression progressively increased or decreased from WTKs to RDEBKs to RDEBSCCs, suggesting that these genes could be involved in disease progression. To identify inhibitors of proliferation in keratinocytes and RDEBSCCs, we performed CRISPRi proliferation screens in one WTK (NTERT) and three RDEBSCC (RDEBSCC2, 53, and 70) cell lines. There were 53 sgRNAs that were enriched in all four CRISPRi screens, including all three sgRNAs targeting the *TAFA3* gene. To identify drivers of proliferation in keratinocytes, we performed CRISPRa proliferation screens in one RDEBK (RDEBK8) and two WTK (NTERT and WTK1) cell lines. No sgRNAs were enriched in all three screens, but there was some overlap across each of the three possible pairs. We performed competition assays to validate some of the top hits from the CRISPRa and CRISPRi screens and found that inhibition of *PTK2B, QPRT, STAT2,* or *TAFA3* expression and upregulation of *ADAM2, CDYL2, CSF3R, DENND4B, FSTL1, GCSAM, ITGB1, ITGB3, KLHDC8A, KRT33B, SEMA5A*, or *TYROBP* expression significantly increased proliferation in NTERT keratinocytes.

Using a combination of RNA-sequencing and genome wide CRISPRai screens, we identified (1) genes that promote C7 production, (2) a novel strategy for increasing C7 production in RDEB skin, (3) genes that were progressively dysregulated from WTK to RDEBK to RDEBSCC, (4) genes that drive proliferation in wild-type and/or RDEB keratinocytes, and (5) genes that inhibit proliferation in keratinocytes and RDEBSCC cells. We also created and validated a keratinocyte C7 reporter cell line that could be used in future DEB research. Overall, this research has led to the discovery of numerous previously unexplored avenues of investigation in dystrophic epidermolysis bullosa research and a multitude of new gene targets for the development of novel targeted therapeutics.

TABLE OF CONTENTS

LIST OF FIGURES

Chapter 2: Genes and compounds that increase type VII collagen as potential treatments for dystrophic epidermolysis bullosa

Chapter 3: Identification of novel drivers and inhibitors of proliferation in keratinocytes and progressively dysregulated genes in RDEB disease progression

LIST OF TABLES

CHAPTER 1

INTRODUCTION

Epidermolysis bullosa

Epidermolysis bullosa (EB) is a heterogeneous group of rare genetic disorders that are characterized by varying degrees of skin blistering (Has 2020a). According to epidemiological studies done using EB registry data from various countries, the incidence and point-prevalence of EB as a whole range from 1.4-41.3 per million live births and 2.82-54.0 per million population, respectively (Kero 1984, Inaba 1989, Pavicic 1990, McKenna 1992, Abahussein 1993, Horn 1997, Fine 2000, Tadini 2005, Abu Sa'd 2006, Kho 2010, Hernandez-Martin 2013, Danescu 2015, Fine 2016, Baardman 2020). EB is divided into four main subtypes based on the level at which skin cleavage and blistering occur and the gene in which the disease-causing mutation is located. EB simplex (EBS) is characterized by intraepidermal skin cleavage and can be caused by mutations in *KRT5*, *KRT14*, *KLHL24*, *DST*, *EXPH5*/*SLAC2B*, *PLEC*, or *CD151/TSPAN24* genes. Junctional EB (JEB) is characterized by skin cleavage at the dermal-epidermal junction and can be caused by mutations in the *LAMA3, LAMB3, LAMC2*, *COL17A1*, *ITGA6*, *ITGB4*, or *ITGA3* genes. Kindler EB (KEB) is an extremely rare form of EB in which cleavage and blistering can occur at multiple levels (intraepidermal, junctional, and/or dermal) and is exclusively caused by mutations in the *FERMT1/KIND1* gene. Dystrophic EB (DEB) is characterized by skin cleavage and blistering that occurs beneath the lamina densa in the superficial dermis and is exclusively caused by mutations in the *COL7A1* gene. The breakdown of EB types by percentage is approximately 70% EBS, 5% JEB, 25% DEB, and less than 0.1% KEB, which is so rare that fewer than 300 individuals with KEB have been documented since its initial description in the 1950s (Has 2020a). The four types of EB are further divided into subtypes based on the severity of the blistering and/or the nature of the disease-causing mutation, leading to over 30 clinical subtypes of EB (Fine 2014, Has 2020a, Has 2020b). As of 2020, the most recent reclassification of inherited EB, thousands of pathogenic variants across the 16 EB-related genes have been documented (Has 2020a).

The COL7A1 gene and type VII collagen

Dystrophic epidermolysis bullosa (DEB) is caused by mutations in the *COL7A1* gene, which encodes type VII collagen (C7). C7 is a member of the collagen superfamily, which includes 28 collagens (C1-C28) and 20 other proteins with collagen-like characteristics (Theocharidis & Connelly 2019). Collagens are made up of three polypeptide α chains that twist around each other to form a right-handed triple helix, and these chains can be identical or different (Theocharidis & Connelly 2019).

The human *COL7A1* gene is located on the short arm of chromosome 3 (3p21.31) and contains 118 exons spanning over 31 kilobases (Parente 1991, Greenspan 1993, Christiano 1994a, 1994b). Translation of the ~8.9kb *COL7A1* mRNA produces the polypeptide α1 chain of type VII collagen (C7α1), which contains 2944 amino acids (aa) (Christiano 1994b). The precursor form of C7, procollagen VII (pro-C7), is made up of three identical α chains, which self-assemble into a homotrimer in the endoplasmic reticulum before being secreted into the extracellular space (Morris 1986, Burgeson 1993, Christiano 1994a, 1994b; Bruckner-Tuderman 1995). Secreted pro-C7 homes to the dermal-epidermal junction (DEJ), dimerizes, and undergoes further processing to yield mature C7 (Morris 1986, Sakai 1986, Bruckner-Tuderman 1995, 1999). Mature C7 molecules aggregate laterally into structures called anchoring fibrils, which interact with ECM proteins in the basement membrane and superficial dermis.

Anchoring fibrils (AFs), along with anchoring filaments and hemidesmosomes, form supramolecular structures called anchoring complexes that are dispersed throughout the dermal-epidermal junction (DEJ) and serve to anchor the epidermal basement membrane (and therefore the epidermis itself) to the underlying dermis. AFs originate in the lamina densa (bottom of basement membrane), extend into the papillary dermis, and then either loop back into the lamina densa or bind to anchoring plaques in the dermis (Burgeson 1993). Since each C7α1 chain can interact with ECM proteins independent of the other chains, each molecule of C7 can interact with numerous ECM proteins. Interstitial collagen fibers in the dermis also get “caught” by passing through the looping structure of AFs, which provides additional structural integrity (Chung & Uitto 2010). C7α1 polypeptides are organized into three major domains, and each of these domains plays important roles in the structure, maturation, processing, and/or protein-protein interactions of C7.

The first non-collagenous (NC1) domain of C7 mediates interactions between C7 and other extracellular matrix (ECM) proteins of the basement membrane and dermis. The first exon of *COL7A1* is not part of NC1, as it contains the 5'-untranslated region (UTR) and the 16aa signal peptide, which is eventually cleaved (Christiano 1994b). NC1 spans exons 2-28 (aa 17-1253) and has a mass of ~145 kilodaltons (kDa) (Burgeson 1985, 1990, 1993; Christiano 1992, 1994a, 1994b). The NC1 domain contains two von Willebrand factor type A-like motifs, vWFA1 (exons 2-5, aa 38-211) and vWFA2 (exons 24-26, aa 1054-1229), nine consecutive fibronectin type III motifs (FNIII1-9, exons 6-23, aa 234-1051), and a proline- and cysteine-rich domain (exons 27-28) (Burgeson 1985, 1990, 1993; Christiano 1992, 1994a, 1994b). The NC1 domain also contains three conserved asparagine residues that undergo N-linked glycosylation (Asn337, Asn786, Asn1109), which may influence C7 secretion (Chen 1997). The FNIII7-9 motifs mediate binding of C7 to type IV collagen (C4) and the β3/γ2 chains of laminin-332 (Lam332), the two main binding partners of C7 in the basement membrane (Chen 1997a, 1999a; Brittingham 2006). The vWFA2 motif mediates binding of C7 to type I collagen (C1), integrin α2β1, and to a lesser extent, Lam332 (Villone 2008, Wegener 2013, Gebauer 2020). The NC1 domain also binds fibronectin (FN) and thrombospondin-1 (TSP1), two glycoproteins that play important roles in signal transduction and ECM structure and function (Chen 1997a, Aho & Uitto 1998, Atanasova 2019a). It has also been shown that each NC1 domain in a molecule of C7 can interact with a protein, enabling up to six Lam332/C4 interactions per dimer.

The triple helix domain (THD), a hallmark of the collagens and collagen-like proteins that make up the collagen superfamily, is crucial for proper assembly and structural integrity of the collagen triple helix. The THD makes up the majority of C7α1, spanning from exon 29 to the first half of exon 112 (aa 1254-2784) (Bentz 1983, Burgeson 1985, Christiano 1994a, Christiano 1994b). The triple helical structure is achieved by hundreds of sequential glycine (Gly)-X-Y repeats, where X is usually proline and Y is usually hydroxyproline (Bentz 1983, Burgeson 1985, 1990, 1993; Christiano 1994a, 1994b). There are 64 exons in the THD that are in-frame multiples of nine base pairs (bp), which is thought to preserve the overall structural integrity of the THD and enable mutation-containing exons in this region to be easily removed or skipped (Bentz 1983, Burgeson 1985, 1990, 1993; Christiano 1994a, 1994b). There are also 18 small (1-10aa) interruptions and one large interruption (39aa) to the Gly-X-Y repeats that occur throughout the THD, which are highly conserved and increase the flexibility of the polypeptide (Bentz 1983, Burgeson 1985, 1990, 1993; Christiano 1994a, 1994b). The large interruption, which is referred to as the hinge region, occurs near the middle of the THD and is encoded by the last three bases of exon 70, all of exon 71, and the first 36 bases of exon 72 (Bentz 1983, Burgeson 1985, 1990, 1993; Christiano 1994a, 1994b).

The second non-collagenous (NC2) domain of C7 is much smaller than NC1 or THD but plays a crucial role in pro-C7 dimerization. NC2 spans from the second half of exon 112 through the first part of exon 118 and has a mass of ~30kDa (Burgeson 1993, Christiano 1994a, 1994b). Pro-C7 dimerization begins with the antiparallel alignment of the C-termini, which requires an intact NC2 domain (Bachinger 1990, Colombo 2003). Dimerization is stabilized by the formation of disulfide bonds between conserved cysteine residues in the NC2 domain (Cys2802 or Cys2804) and the C-terminal end of the THD (Cys2634) (Morris 1986, Bachinger 1990, Burgeson 1990, Christiano 1994a, 1994b; Colombo 2003). Dimerization is further stabilized/promoted by partial cleavage of the NC2 domains by bone morphogenetic protein 1 (BMP1) (Bachinger 1990, Burgeson 1990, Rattenholl 2002, Colombo 2003).

Dystrophic epidermolysis bullosa: Clinical subtypes

COL7A1 mutations can be inherited in autosomal dominant (DDEB) and autosomal recessive (RDEB) fashions, with the latter generally being more severe (Has 2020a). There have also been cases of compound heterozygosity in which there is a dominant mutation on one allele and a recessive mutation on the other allele (Has 2020a). DDEB and RDEB are classified into various clinical subtypes according to the extent of C7 production and AF formation, the severity and distribution of blistering, and the presence or absence of various cutaneous and extracutaneous manifestations (Mariath 2020). DDEB is classified as intermediate, localized, pruriginosa, or self-improving, and RDEB is classified as severe, intermediate, inversa, localized, pruriginosa, or self-improving (Has 2020a, Has 2020b, Mariath 2020).

Intermediate and localized DDEB

Clinically, intermediate DDEB is characterized by generalized blistering, milia (small white bumps), nail dystrophy (misshapen, damaged, or discolored finger/toenails), atrophic scarring (indented scars), and albopapuloid lesions (small, white/pale, raised bumps) (Mariath 2020). Localized DDEB is characterized by blistering that is largely restricted to the hands and feet, milia, nail dystrophy, and occasionally some atrophic scarring (Fine 2014, Mariath 2020).

DDEB is most frequently caused by mutations that affect the structure of the collagenous triple helix domain of C7, which impacts the assembly and stability of procollagen α1(VII) chains into the C7 trimer (Varki 2006, Dang & Murrell 2008, Chung & Uitto 2010, Mariath 2020). The triple helix domain of C7 is composed of Gly-X-Y repeats with 19 small interrupting sequences and spans from exons 29-112 (Christiano 1994a, Christiano 1994b). Glycine substitutions that disrupt the Gly-X-Y repeats in the triple helix domain are the most common mutation type in DDEB, but other mutation types (indels, other missense mutations, splice site variants, large in-frame deletions) have also been documented (Hammami-Hauasli 1998, Sakuntabhai 1998, Varki 2006, Dang & Murrell 2008, Chung & Uitto 2010, Has 2020a, Mariath 2020). Most DDEB-associated glycine substitutions occur near the small amino acid sequences that interrupt the Gly-X-Y repeats, which enhance the flexibility of the C7 peptide and contribute to its overall structure (Mellerio 1998, Mecklenbeck 1999, Has 2020a). Exon 73, for example, is a well-established hotspot for glycine substitutions, and in addition to being the largest exon in *COL7A1*, is directly downstream of the largest interruption (39 amino acids vs 1-10 amino acids for the other 18 interruptions) of the Gly-X-Y repeats (Christiano 1994a, Christiano 1994b, Mecklenbeck 1999, Has 2020a).

Specific glycine substitutions can also exhibit substantial heterogeneity between and within families, highlighting the complex nature of some *COL7A1* mutations. The most common DDEB-causing mutation, p.G2043R in exon 73, has been documented in families from a variety of countries, including (but not necessarily limited to) the United States, Mexico, Scotland, Italy, Hungary, Norway, and Finland (Christiano 1995, Christiano 1996, Cserhalmi-Friedman 1997, Winberg 1997, Mellerio 1998). Only one member of the Mexican family had any symptoms, despite having thirteen siblings, and this individual presented with a traditional intermediate DDEB-phenotype: blistering, scarring, nail dystrophy, loss of nails, and albopapuloid lesions (Mellerio 1998). The Scottish family, however, had three affected individuals from three separate generations, and while the generation II individual presented with blistering, scarring, and nail dystrophy and loss, the generation III individual (offspring of generation II) had more severe, recurrent blistering and milia, but barely any nail dystrophy (Mellerio 1998).

While largely associated with localized and intermediate DDEB, some glycine substitutions are only associated with RDEB, and others can be recessive or dominant depending on the context (Mecklenbeck 1999, Almaani 2011, Turczynski 2016, Has 2020a). For example, p.Gly1770Ser resulted in severe DEB in two brothers and a cousin that were homozygous for the mutation (suggesting RDEB), localized blistering, inflammation, and nail abnormalities in the mother and nail abnormalities in the father of the two brothers, who were both heterozygous (suggesting DDEB), and no abnormalities whatsoever for the parents of the cousin, who were both heterozygous (suggesting RDEB) (Almaani 2011).

<u>Severe, intermediate, and localized RDEB</u>

Severe RDEB is usually caused by mutations that create premature termination codons (PTCs) in both *COL7A1* alleles, resulting in little to no C7 protein production or AF formation

(Christiano 1994, Dang & Murrell 2008, Mariath 2020). Cutaneous manifestations of severe RDEB include generalized blistering leading first to mutilating scars and eventually to pseudosyndactyly (fusion of the fingers and toes) and joint contractures; milia, nail dystrophy, and aggressive cutaneous squamous cell carcinoma (cSCC) (Fine 2014, Has 2020a, Has 2020b, Mariath 2020). Extracutaneous manifestations of severe RDEB include blistering in oral and gastrointestinal epithelia and the corneas, esophageal stenosis (narrowing or tightening), chronic ulcers, anemia, and developmental delay (Mariath 2020).

Intermediate RDEB is often the result of a PTC-causing mutation on one allele and a missense mutation (or other type of less severe mutation) on the other such that some mutant C7 protein is produced, and some AF formation occurs (Gardella 1996, 2002; Jarvikallio 1997, Kern 2006, Dang & Murrell 2008, van den Akker 2009, Danescu 2015, Mariath 2019, Mariath 2020). Clinically, intermediate RDEB is characterized by generalized (but less severe) blistering and scarring that can sometimes (but less frequently) lead to pseudosyndactyly, joint contractures, esophageal stenosis, and corneal blistering, as well as milia and nail dystrophy (Mariath 2020).

Localized RDEB is most frequently caused by splice site mutations that result in exon skipping, where one or more exons are removed during the splicing process (Gardella 1996, Hovnanian 1997, Terracina 1998, Dang & Murrell 2008, Toyonaga 2015, Mariath 2019, Mariath 2020). Splice site mutations that cause localized RDEB affect largely non-essential exons that can be removed without having a significant impact on the stability of C7 or its ability to form AFs. Clinical manifestations of localized RDEB are essentially identical to those of localized DDEB (mild blistering restricted to hands/feet, milia, nail dystrophy, atrophic scarring), so a genetic test is usually required to determine the mode of inheritance in these cases (Mariath 2020).

<u>Rare DEB subtypes: pruriginosa, self-improving, and inversa</u>

The pruriginosa, self-improving, and inversa subtypes of DEB are associated with very specific mutations and clinical criteria. The pruriginosa subtype is characterized by pruritus (itch), especially on lower limbs, some blistering and scarring, lichenified (thick/leathery) papules (small, raised bumps up to 1cm) with milia, nodules (small, raised, solid lesions up to 2cm), and/or plaques (elevated region of skin larger than 1cm in diameter), nail dystrophy, and occasionally albopapuloid lesions (McGrath 1994, Fine 2010, Mariath 2020). Pruriginosa DEB can be caused by both dominant and recessive mutations, including specific types of glycine substitutions (McGrath 1994, Varki 2006, Fine 2010, Has 2020a, Mariath 2020).

Self-improving DEB, also referred to as transient bullous dermolysis of the newborn, is characterized by generalized blistering at birth (or shortly after birth) that rapidly improves during the first few months of life, often without significant scarring (Christiano 1997, Has 2020a, Mariath 2020). Specific splice site mutations and glycine substitutions have been shown to cause self-improving DEB, but the rarity of this subtype makes it difficult to gauge the true mutation spectrum (Christiano 1997, Fassihi 2005, Shi 2015, Has 2020a, Mariath 2020).

Inversa RDEB (RDEB-I) is extremely rare and is caused by specific missense mutations in arginine and glycine residues that are postulated to affect the thermostability and folding of C7 (Chiaverini 2010, Fine 2010, van den Akker 2011, Has 2020a, Mariath 2020). Individuals with RDEB-I are usually homozygous for one of these missense mutations or are compound heterozygotes with a missense mutation on one allele and a PTC-causing mutation on the other (Chiaverini 2010, van den Akker 2011). RDEB-I initially presents with generalized blistering (and scarring) that decreases with age, while severe blistering of oral, esophageal, anal, and genital mucosae increases with age (Chiaverini 2010, Fine 2010, van den Akker 2011, Has 2020a, Mariath 2020).

Epidemiology

The incidence and prevalence of DEB have been estimated to be between 0.2-14.1 per million live births and 2.82-20.4 per million population, respectively, based on data from EB registries in various countries (Kero 1984, Inaba 1989, Pavicic 1990, McKenna 1992, Abahussein 1993, Horn 1997, Fine 2000, Tadini 2005, Abu Sa’d 2006, Kho 2010, Hernandez-Martin 2013, Danescu 2015, Fine 2016, Baardman 2020). Using data from the National Epidermolysis Bullosa

Registry from 1986-2002, the incidence of DDEB and RDEB in the United States were estimated to be 2.12 and 3.05 per million live births, respectively and the prevalence of DDEB and RDEB were estimated to be 1.49 and 1.35 per million population, respectively (Fine 2016). A more recent epidemiological study using data from the Dutch EB Registry from 1988-2018 estimated the incidence of DDEB and RDEB to be 8.6 and 5.5 per million live births and the point-prevalence of DDEB and RDEB to be 6.1 and 2.1 per million (Baardman 2020). Over 90% of EB cases in this dataset were backed up by genetic confirmation, suggesting that (1) DEB (and EB overall) may be more common than previously thought and (2) DDEB may be more common than RDEB (Baardman 2020).

Management of DEB

There is currently no cure for DEB or other forms of EB, so general patient care is focused on prevention and management of wounds and blisters to minimize pain, scarring, and the risk of infections, but other considerations are also important (Has 2020a, 2020b, Mariath 2020). Wound and blister care involves (1) puncturing and draining the blister (when applicable), (2) applying cleansers and washing the wound regularly to reduce the risk of infection, (3) applying moisturizer to keep the wound bed from drying out, (4) applying antibacterial and/or antimicrobial ointments, (5) applying the primary (contact) layer of dressings, which are non-adherent so as not to disturb healing skin, and (6) applying secondary/tertiary dressings such as gauzes, foams, and other specialty dressings to support and protect the contact layer (DEBRA). Other aspects of DEB management include chronic and acute pain management, reducing itch, regular dental/oral exams, maintaining proper nutrition to minimize the risk of anemia and/or malnutrition, physical and/or occupational therapy, regular monitoring for squamous cell carcinoma (cSCC) development (DEBRA, El Hachem 2014, Rashidghamat & McGrath 2017, Bruckner-Tuderman 2020). Wound dressings with type I collagen, such as Integra (Integra LifeSciences, Plainsboro, NJ) and Helicoll (Encoll, Fremont, CA) significantly improved wound closure in RDEB patients (relative to regular wound dressings) but the observed benefits dissipated as soon as the treatment stopped (Wiegand 2010, Gorell 2015, Rashidghamat & McGrath 2017).

A recent survey of EB patients (n=63) and caregivers (n=93), including 31 DDEB and 53 RDEB respondents, highlighted the challenges of effectively managing EB and the far-reaching impacts it can have on life decisions (Bruckner 2020). 10 DDEB (~32%) and 32 RDEB respondents (~60%) reported that over 30% of the patient's body was covered by wounds, and another 9 DDEB and 15 RDEB reported 10-30% wound burden (Bruckner 2020). Furthermore, 6 DDEB (~19%) and 34 RDEB (~64%) respondents reported that their regular wound care took at least two hours, and 13 RDEB respondents needed over four hours for wound care (Bruckner 2020). All surveyed patients and nearly 70% (65/93) of caregivers reported working fewer hours due to EB, with over 70% (46/63) of patients and over 50% (53/93) of caregivers reporting that they decided not to work at all (Bruckner 2020). Financial burden due to EB was reported by over 50% of patients and caregivers, including 31.7% and 20.4% reporting "a lot" and 22.2% and 37.6% reporting "a moderate amount", respectively (Bruckner 2020). Patients and caregivers also reported making other life decisions due to EB, such as switching to homeschooling (36.5% and 40.9%), moving to a more affordable home (42.9% and 35.5%), deciding not to have children (patients only) or more children (58.7% and 60.2%), deciding not to date (55.6% and 30.1%), and divorce or separation (42.9% and 46.2%) (Bruckner 2020). Responses from patients and caregivers also highlighted the desire for new treatment options that reduced wound burden, including accelerating wound closure, reducing pain, itch, and risk of infection, and making wound dressing easier (Bruckner 2020). Reducing the risk of skin cancer (cutaneous squamous cell carcinoma, cSCC) was also a top concern (Bruckner 2020).

Allogeneic cell transplantation and injection for treating DEB

Blistering and wounding are the source of many challenges associated with DEB, both in terms of everyday life and long-term complications. In addition to generalized skin fragility, individuals with more severe DEB often have chronic wounds that will not heal, increasing the risk of severe infections, fibrosis, scarring, and cutaneous squamous cell carcinoma. To address these needs, many different therapeutic approaches that aim to improve skin integrity and reduce blistering and wounding have been explored. Numerous studies have evaluated the potential of healthy allogeneic cell types to treat DEB.

Keratinocytes and fibroblasts

Many early strategies for treating DEB involved transplantation or injection of C7-producing cells from healthy donors, such as keratinocytes (KERs) and/or dermal fibroblasts (FBs). Allogeneic approaches using KERs and/or FBs have repeatedly been found to be safe, but their ability to improve wound healing and/or provide functional C7 are mixed. KERs are the primary producers of C7 in the skin, with multiple studies finding substantially higher *COL7A1* expression and C7 production in KERs than in FBs (Stanley 1985, Bruckner-Tuderman 1987, Konig & Bruckner-Tuderman 1992, Ryynanen 1992, Goto 2006a). One study found that when KERs and FBs from a DEB patient were transduced with a retroviral vector containing *COL7A1* cDNA, KERs had 3.2-fold higher *COL7A1* expression even though the total RNA content of FBs was 3.4-fold higher (Goto 2006). The same study also found that grafts composed of untransduced KERs and transduced FBs produced significantly more C7 than grafts composed of transduced KERs and non-transduced FBs, suggesting that FBs might be more effective than KERs at producing C7 when transferred onto a wound (Goto 2006). Indeed, preclinical studies in mice and skin equivalents have shown that intradermally-injected allogeneic FBs can produce C7 at the DEJ and that C7 has a relatively long half-life, suggesting that this approach could provide therapeutic benefit to DEB patients (Woodley 2003, Fritsch 2008, Kern 2009).

The preference for FBs over KERs is reflected in the published literature, as most approaches using allogeneic skin cells to treat DEB use FBs or a combination of KERs and FBs, with very few using only KERs. One study reported that application of allogeneic KERs to the chronic wounds of a DEB patient resulted in successful wound healing without rejection or inflammation for at least four months and production of AFs that were visible for at least six weeks (McGuire 1987). Another study that used allogeneic KERs to treat RDEB wounds, however, found no significant improvement in wound healing in grafted vs ungrafted sites (McGrath 1993). Regardless of whether FBs produce more C7 than KERs *in vivo*, FBs are easier and less expensive to culture and less prone to senescence than KERs, which has contributed to the increased use of allogeneic FBs to treat DEB. Various studies have reported that allogeneic FBs can improve wound healing, increase C7 production, and increase C7 deposition at the DEJ in DEB patients (Wong 2008, Natsuga 2010, Nagy 2011, Petrof 2013, Venugopal 2013, Moravvej 2018). One of the main concerns of using allogeneic cells for any therapeutic approach is the risk of rejection, but there were no instances of immune rejection across any of these studies (Wong 2008, Natsuga 2010, Nagy 2011, Petrof 2013, Venugopal 2013, Moravvej 2018).

While allogeneic fibroblasts have been shown to possess some therapeutic benefit for people with DEB, there are several important caveats that limit their potential usefulness, including their ability to increase C7 in the skin and the duration of the therapeutic benefits. In Wong *et al.* (2008), all five patients showed increased C7 production relative to pre-injection levels at two weeks post-injection, but only three of the five still showed increased C7 production at three months post-injection. Furthermore, the increase in C7 production was due to higher production of mutant C7 by patient cells rather than the allogeneic FBs providing full-length C7, suggesting that the therapeutic benefit of allogeneic FBs is more indirect (Wong 2008). In a follow-up experiment, one of the five patients from Wong *et al.* (2008) received a second injection of allogeneic FBs, and biopsies were taken at various time points (day 7, 15, 30, 90, 180, 270, and 360) after the injection (Nagy 2011). *COL7A1* expression and C7 production were increased relative to baseline levels by day 15 but returned to baseline by day 180 and day 360, respectively (Nagy 2011). Natsuga *et al.* (2010) used cultured dermal substitutes (CDS) containing allogeneic FBs to treat DEB wounds and found no increase in C7 production even though wound re-epithelialization was observed. One of the two phase II clinical trials did not measure C7 production (Petrof 2013). The other phase II clinical trial found increased C7 production in three of the five patients relative to their respective baselines, but similar increases were observed for FB-treated and vehicle-treated wounds, suggesting that the new C7 was being produced by the patients' cells and not the FBs (Venugopal 2013). A more recent study found increased C7 production in DEB wounds for at least 12 weeks after being treated with allogeneic FBs via intradermal injection and amniotic membrane scaffold, with the former showing more robust increases in C7 than the latter (Moravvej 2018). Interestingly, this study (Moravvej 2018) and Petrof *et al.* (2013) used fibroblasts from neonatal foreskin, whereas Wong *et al.* (2008) used fibroblasts from a parent and a separate healthy donor, Natsuga *et al.* (2010) used fibroblasts from a "young donor", and Venugopal *et al.* (2013), used fibroblasts from a 23-year-old male donor, so it is possible that neonatal fibroblasts naturally produce more full-length C7 or are more robust than fibroblasts from older donors in some way.

Another limitation of allogeneic FBs is their lack of long-term efficacy, with most studies showing loss of most or all therapeutic benefit within a year. Petrof *et al.* (2013) found that FB-treated wounds showed a higher degree of wound closure (measured by erosion surface area) and a more rapid rate of closure than vehicle-treated wounds, but the largest differences between the groups was the first post-injection measurement (50% reduction vs 32% reduction at day 7 post-injection) and these differences were gone after day 28. Venugopal *et al.* (2013) found that wounds healed by up to 50% in both FB-treated and vehicle-treated sites by six months post-injection, and there no statistically significant differences in average wound size between FB-treated, vehicle-treated, and untreated wounds across any of the measured time points. Three of the five patients in Wong *et al.* (2008) showed increased skin integrity for at least three months post-injection (last time point for follow-up), but two patients did not show any sign of therapeutic benefit. Natsuga *et al.* (2010) reported that chronic ulcers became re-epithelialized within a month of treatment, but no additional follow-ups were reported. Moravvej *et al.* (2018) found that both FB delivery methods (intradermal injection and amniotic membrane scaffold) resulted in significantly decreased wound size relative to untreated wounds, with the intradermal injection showing higher rates of closure than the amniotic membrane scaffold.

KERs and FBs communicate and influence the behavior of one another through the secretion of cytokines, growth factors, and other proteins. A recent review of the interactions between KERs and FBs highlights the variety of effects that these cell types can have on one another (Russo 2020). There is substantial evidence that KER viability is increased in the presence of FBs, with numerous studies reporting that KERs showed increased proliferation and production of basement membrane proteins, decreased apoptosis, and consistent/regular differentiation (Russo 2020). The effects of KERs on FBs are less consistent, which is likely due to differences in culture conditions, experimental systems, and KER differentiation status (Russo 2020). Previous work has shown that C7 was higher (measured via immunofluorescence) in co-cultures of KERs and FBs than in monocultures of either cell type, suggesting that allogeneic approaches that use both KERs and FBs may be more effective for treating DEB wounds (Stanley 1985, Bruckner-Tuderman 1987, Konig & Bruckner-Tuderman 1991, Ryynanen 1992).

Apligraf (Graftskin, Organogenesis Inc, Canton, MA), a tissue-engineered skin equivalent containing bovine type I collagen and human KERs and FBs derived from neonatal foreskin, has shown therapeutic benefit in EB patients (including DEB) in multiple studies (Falabella 2000, Fivenson 2003a, 2003b; Phillips 2003). One study that used Apligraf to treat wounds in 15 EB patients (7 RDEB, 2 DDEB, 5 EBS, 1 JEB) found that 82% of acute wounds were healed after six weeks and 79% were still healed after 18 weeks, with patients reporting favorable healing outcomes (Falabella 2000). In a separate study, 58 wounds across five RDEB patients treated with Apligraf showed rapid healing, decreased itch and pain, and significant increases in hand range of motion (<25% to >90% in some cases), with recurrent blistering only occurring in areas of chronic trauma (Fivenson 2003a). Apligraf has also shown promise in improving wound healing and skin integrity in the hands of DEB patients after surgery to alleviate pseudosyndactyly (Fivenson 2003b, Phillips 2003).

Other allogeneic approaches that have been used to treat DEB include amniotic membrane, bone marrow/hematopoietic stem cells, mesenchymal stromal cells (MSCs), and human cord blood-derived unrestricted somatic stem cells (USSCs). Grafting of amniotic membrane or cryopreserved placental membrane onto chronic wounds decreased pain and stiffness but showed mixed results in their ability to induce re-epithelialization (Martinez Pardo 1999, Niknejad 2008, Lo 2010, Gibbons 2015, Nevala-Plagemann 2015, Rashidghamat & McGrath 2017, Marinkovich 2019).

Bone marrow transplantation

Several important discoveries about the characteristics of stem cell populations in bone marrow led to the investigation of bone marrow transplant (BMT) as a potential treatment for RDEB, including (1) the ability to give rise to cell types from all three germ layers (including epithelial cells), (2) the ability to home to injured tissue and promote wound healing, and (3) the ability to engraft and promote wound healing in the skin (Jiang 2002, Peister 2004, Kunter 2006, Ortiz 2007, Phinney 2007; Togel 2007, Tolar 2007, 2009). The initial trial of BMT in children with RDEB showed increased expression and deposition of C7 at the DEJ in five of six individuals, with the sixth showing some improvement without an increase in C7 (Wagner 2010). At eight years post-BMT, patients showed increased C7, reduced blistering and the presence of donor cells in the skin, but no mature AFs were detected (Tolar 2013). Although BMT has the potential to considerably improve disease symptoms in individuals with RDEB, it is an extremely invasive and arduous process. Continued refinement of the pre-BMT conditioning process and the cell types used for transplantation have made this process safer, but there are still considerable risks associated with BMT, including death. These considerations have driven investigation and development of less invasive alternatives.

Mesenchymal stromal cells

Mesenchymal stem/stromal cells (MSCs) have emerged as a potential middle ground option between skin cell grafts and BMT. MSCs are a multipotent, self-renewing population of adult stem cells that have been the focus of substantial research effort over the past decade (Conget 1999, 2010; LeBlanc 2005, Caplan 2006, Rashidghamat & McGrath 2017). MSCs were initially identified in bone marrow but can be isolated from a wide variety of other tissues, including adipose, umbilical cord (and umbilical cord blood), placenta, skin, skeletal muscle, and more (Li 2021). Subsequent research has shown that MSCs home to wounds and contribute to wound healing, possess both immunomodulatory and anti-inflammatory characteristics, and are immune-privileged, suggesting that they could be used to improve wound healing in DEB (Li 2021). The first trial in RDEB-severe patients, in which two patients received intradermal injection of bone marrow-derived MSCs (BM-MSCs), showed improved wound healing and deposition of C7 at the dermal-epidermal junction for approximately four months (Conget 2010). Subsequent studies have shown mixed results, with one trial showing similar results to the first (El-Darouti 2016), while another found no consistent clinical benefit (Petrof 2015). Overall, MSCs have shown some promising results in improving wound healing in DEB, but the observed inconsistencies indicate that further investigation and optimization are needed.

Molecular therapeutics for increasing C7 production in DEB

Allogeneic approaches have been shown to provide some therapeutic benefit in DEB skin, but the potential of these therapies is limited by spatial restrictions (specific wounds), lack of long-term benefit (therapeutic benefit was often lost within a year), safety risks (for BMT), or feasibility (time and cost to prepare treatments). Another major limitation for allogeneic approaches was that most of the therapeutic benefits could be attributed to general support of wound healing rather than deposition of full-length C7, even when C7-producing cells (KERs and FBs) were used. These shortcomings highlight the need for treatments that provide systemic, long-term improvements in wound healing. Molecular therapeutics that aim to induce production of fully (or mostly) functional C7 in the skin include gene therapy, gene editing, protein therapy and compounds that mediate exon skipping or readthrough of premature termination codons (PTCs) in the context of specific DEB-causing mutations. Although some of these therapies have shown promising results in preclinical and early clinical trials, there are often risks associated and none have yet moved beyond clinical trials to full regulatory approval.

Gene therapy

Gene therapy approaches seek to restore C7 production through the addition of a fully functional copy of *COL7A1*, usually in the form of complementary DNA (cDNA), into the patient's skin cells. These modified skin cells are then returned to the patient via graft or injection. While this type of approach is not suitable for most cases of DDEB due to the dominant-negative effect of these mutations, it could theoretically be used for all cases of RDEB. Introduction of *COL7A1* cDNA into patient cells is usually mediated by retroviral or lentiviral vectors, but non-viral vectors such as transposon-based systems and specialized polymers have also been tested (Has 2020c). Insertional mutagenesis has always been a potential risk of approaches that use integrating vectors, so stringent quality control is needed to confirm the location of the insertion site. Three early phase clinical trials for gene therapy in RDEB have been completed, and several more are planned, recruiting patients, or already ongoing.

In two of the completed clinical trials, RDEB patient keratinocytes were transduced with a retroviral vector containing a full-length *COL7A1* expression cassette, assembled into epidermal grafts, and transplanted onto chronic wounds. The use of these grafts was evaluated in a phase I trial (Siprashvili 2016) in four patients and a phase I/IIa trial (Eichstadt 2019) in seven patients (NCT01263379). In both trials, grafts were applied to six distinct wounds on each patient, resulting in 24 and 42 (only 38 were eligible for evaluation) total treated wounds, respectively (Siprashvili 2016, Eichstadt 2019). At three months post-treatment, C7 expression was detected in 90% (9/10) and 73% (11/15) of graft site biopsies and wound healing of at least 50% was observed for 100% and 95% (36/38) of treated wounds, respectively (Siprashvili 2016, Eichstadt 2019). At twelve months post-treatment, C7 expression was detected in 42% (5/12) and 43% (3/7) of graft site biopsies and 83% (20/24) and 68% (26/38) of wounds still showed at least 50% healing with marked differences observed between treated and untreated sites (Siprashvili 2016 and Eichstadt 2019). At two years post-treatment (phase I/IIa trial only), C7 expression was detected in biopsies from two of the three patients that had them and 71% (27/38) of wounds still showed at least 50% healing (Eichstadt 2019).

The results of these studies have led to the authorization of another phase I/IIa trial (same clinical trial identifier) in ten patients, which is already underway, and a phase III trial (NCT04227106) in the recruitment phase that aims to include 10-15 patients. The C7 expression results are particularly encouraging because (1) the investigators used an antibody against the NC2 domain of C7 (near the C-terminus) for immunofluorescence and (2) morphologically normal AFs were observed in multiple patients, both of which suggest that the modified KERs were producing fully (or mostly) functional C7. Although these grafts likely do not increase skin integrity or prevent blistering in RDEB skin long-term, they were able to reliably induce healing of chronic wounds for up to a year (at least two years in some patients) without any adverse events, suggesting that they could be a useful tool for treating particularly problematic wounds.

In the other completed trial, RDEB patient fibroblasts were transduced with a lentiviral vector containing a full-length copy of *COL7A1* and the modified cells were injected intradermally into unwounded patient skin. This approach was evaluated in a single-center, open-label phase I trial in four patients and found no adverse safety outcomes (Lwin 2019, NCT02493816). The FB trial found significant increases in C7 (relative to respective baselines) in three out of four patients at three months post-treatment and two out of four patients at twelve months post-treatment, but these increases were highly variable (<1.50-fold to >26-fold) and no mature AFs were detected (Lwin 2019). Furthermore, C7 immunofluorescence was performed with an antibody against the NC1 domain of C7, so the observed increases in C7 may not be due to production of full-length C7 (Lwin 2019). There is a separate phase I/II trial evaluating the use of intradermally-injected patient fibroblasts in six adult and six pediatric patients that is currently underway and a phase III trial that is in the recruiting phase and aims to recruit up to 24 patients (both trials under NCT04213261). Unlike the completed FB trial, these new trials plan to inject FBs into wounds, which may or may not result in more pronounced therapeutic effects.

There are currently four other clinical trials for gene therapy approaches in RDEB, and the results of these trials could provide significant insight into which cell type(s) and delivery method(s) provide the most therapeutic benefit for DEB patients. NCT04186650 is a phase I/II trial in which patient KERs and FBs are transduced with a self-inactivating retroviral vector containing full-length *COL7A1* cDNA, assembled into skin equivalent grafts, and transplanted onto wounds. The results of this trial will be interesting because it is entirely possible that grafts containing both modified KERs and FBs have more therapeutic potential than grafts that only contain KERs, which would suggest that more effort should be directed toward skin equivalent grafts.

NCT02984085 is a phase I/II trial in which patient KERs are transduced with a γ-retroviral vector containing full-length *COL7A1* cDNA, assembled into epidermal grafts, and transplanted onto wounds. The investigators in this trial explicitly state that biopsies will include KER stem cells (holoclones) and the resulting grafts will be transplanted back onto the site from which the cells were taken after preparation of the wound bed. Siprashvili *et al.* (2016) remarked that while the grafts used in that trial likely contained modified KER stem cells, the decline in therapeutic benefit after a year could be attributed to lower numbers of KER stem cells in the biopsies and/or competition of uncorrected cells in the wound bed. Eichstadt *et al.* (2019) also suggested that the decrease in therapeutic benefit over time could be due to fewer KER stem cells in the initial biopsies. In an earlier study, a JEB patient that was treated with modified epidermal grafts experienced therapeutic benefit after 3.5 years (Mavilio 2006). The biopsies used to create the epidermal grafts were taken from the patient's palms, which are known to contain a higher percentage of KER stem cells (Mavilio 2006). While biopsies cannot be easily obtained (if at all) from the palms of RDEB patients, these results suggest that increasing the percentage of KER stem cells in epidermal grafts could increase their durability.

NCT03536143 and NCT04491604 are phase II and phase III trials, respectively, in which a topical gel containing a non-integrating, replication-deficient Herpes simplex virus 1 (HSV-1) vector with two copies of the *COL7A1* gene is applied to RDEB patient skin. Since the vector does not integrate into the genome and cannot be passed on through cell division, there is essentially no risk of insertional mutagenesis, but the therapeutic benefits of this approach are inherently more transient than the other types of approaches discussed in this section. Although a single treatment may not provide long-term benefit, this therapy can be easily re-applied by the patient or their caregiver(s). Overall, the usefulness of this type of approach will depend on a variety of factors, which include but are not limited to (1) the extent and (2) the duration of the therapeutic benefits, (3) the number of cells that take up the construct relative to the amount used, (4) whether the vector can reach KER stem cells, and (5) the prevalence of autoimmune activity against the C7 produced by the vector.

<u>Gene editing</u>

Gene editing seeks to provide C7 function through the endogenous *COL7A1* locus by correcting specific disease-causing mutations rather than providing new copies of the gene. Most gene editing tools rely on the creation of a DNA double-strand break (DSB) in the gene of interest near the disease-causing mutation. This DSB activates the homologous recombination (HR) machinery, which uses a template to repair the DNA. Under natural conditions, the other allele is usually used as the repair template, but by providing an exogenous donor template with the wild-type sequence, gene editing can be achieved. There are several types of gene editing tools, including zinc finger nucleases (ZFNs), meganucleases, transcription activator-like effector nucleases (TALENs), and clustered regularly interspaced short palindromic repeats (CRISPR). ZFNs and meganucleases have not been used to correct *COL7A1* mutations, so they will not be discussed further.

The creation of TALENs was a significant leap for the field of gene editing. TALENs have higher specificity and activity, lower toxicity and off-target effects, and significantly more binding sites than ZFNs or meganucleases. TALEN design and assembly are also just as straightforward, if not more so, than ZFNs, but without the same concerns of losing activity due to context-dependence of some ZFN subunits (Sun & Zhao 2013). TALENs are composed of transcription activator-like effectors (TALEs), which recognize and bind specific sequences of DNA, and a nuclease domain (usually FokI) to mediate the DSB (Sun & Zhao 2013). TALEs are modular DNA-binding proteins that were originally isolated from the *Xanthomonas* genus of plant pathogens and subsequently optimized for use as a gene editing tool (Bogdanove & Voytas 2011). TALEs contain a targeting domain composed of repeats of 33-35 amino acids where each repeat binds preferentially to a specific nucleotide due to the variable residues at positions 12 and 13 (Bogdanove & Voytas 2011). Since each repeat recognizes a specific nucleotide, TALEs can be readily assembled to target a specific DNA sequence.

Our group was the first to use TALENs to correct COL7A1 mutations (Osborn 2013). Primary RDEB fibroblasts were transfected with TALENs (as plasmid DNA or mRNA) and the donor molecule (as plasmid DNA) using the Neon Transfection System (Invitrogen, Carlsbad, CA) to correct a PTC mutation in exon 14 of *COL7A1* with minimal off-target effects (Osborn 2013). A separate group has used TALENs to correct the c.6527insC *COL7A1* mutation, a highly recurrent mutation in Spanish RDEB patients (Chamorro 2016). This group also used TALENs to delete the c.6527insC mutation via non-homologous end joining (NHEJ) (Mencia 2018). TALENs have also been used in the context of DDEB to knock out the allele bearing the dominant-negative mutation (c.8068_8084delinsGA) without affecting the wild-type allele (Shinkuma 2016).

Over the past decade, the CRISPR-Cas9 system has become the gold standard of gene editing. CRISPR-Cas functions as an adaptive immune system in prokaryotes by storing small sequences of viral DNA in host chromosomes that allow the prokaryote to recognize subsequent infection attempts and degrade the viral DNA. The viral DNA sequences are stored in a CRISPR array separated by direct repeat sequences (Nidhi 2021). The CRISPR array gets transcribed into a precursor CRISPR RNA (pre-crRNA) and processed to create mature CRISPR RNAs (crRNAs) which have homology to specific viruses. When a virus infects a prokaryote that has a crRNA that corresponds to that virus, the crRNA directs a complex of Cas (CRISPR-associated) proteins to the viral DNA, the crRNA binds the viral DNA, and the Cas protein complex cleaves the viral DNA, causing it to be degraded (Nidhi 2021). Many different types of CRISPR-Cas systems exist, but CRISPR-Cas9 is the most widely used by far. As a gene editing system, CRISPR-Cas9 is made up of the Cas9 protein and a single guide RNA (sgRNA), which contains a 20-nucleotide sequence that corresponds to the locus of interest and the Cas9-binding sequence.

CRISPR-Cas9 has been used by numerous groups to correct *COL7A1* mutations. Our group used CRISPR-Cas9 to correct the 4317delC *COL7A1* mutation in primary RDEB fibroblasts, which were then reprogrammed into iPSCs and successfully differentiated into keratinocytes, MSCs, and hematopoietic progenitor cells (Webber 2016). CRISPR-Cas9 has also been used to correct or mitigate other RDEB-causing mutations, such as c.6527insC (Hainzl 2017, Bonafont 2019), c.189delG (Izmiryan 2018), c.5819delC (Takashima 2019), c.2470insG and c.3948insT (Jackow 2019), and c.425A>G (Kocher 2019), c.6081delC (Kocher 2020), and the DDEB-causing mutation, c.8068_8084delinsGA (Shinkuma 2016). CRISPR-Cas9 nickases, in which one of the Cas9 nuclease domains is inactivated, have also been used to mediate gene editing of *COL7A1* mutations. One study showed that both single and double-nicking (two single-strand breaks on the same strand) strategies could efficiently correct the c.425A>G mutation with fewer potential off-target effects than traditional CRISPR-Cas9 (Kocher 2019).

Gene editing approaches, especially those using CRISPR-Cas9, have shown great promise in treating genetic disorders such as DEB. Gene editing has numerous advantages over gene therapy, including no risk of insertional mutagenesis, restoring C7 function through the endogenous *COL7A1* locus rather than providing a new copy that could potentially be silenced, and lower cytotoxicity due to decreased cargo size. There are still some risks associated with gene editing, such as off-target effects, but many studies have shown that off-target effects are extremely uncommon. There are several clinical trials for CRISPR/Cas9-based gene editing currently recruiting/underway, including knockout of CCR5 in CD34+ cells for individuals infected with HIV (NCT03164135), generation of chimeric antigen receptor (CAR)-T cells targeting CD19 and either CD20 or CD22 for individuals with relapsed or refractory leukemia and lymphoma (NCT03398967), and knockout of cytokine-induced SH2 protein (CISH) in tumor infiltrating lymphocytes for individuals with metastatic gastrointestinal epithelial cancers (NCT04426669), among others. Although gene editing approaches for DEB are still in the preclinical stage, this could soon change as more clinical trials evaluate the safety and efficacy of gene editing approaches in other contexts.

Protein therapy

Like gene therapy, protein therapy seeks to restore C7 function by direct addition of functional C7 through local or intravenous injection. Preclinical work in mouse skin and human skin equivalents (transplanted onto the backs of mice) has shown that recombinant C7 protein homes to skin wounds, but not unwounded skin, when injected intradermally or intravenously (Woodley 2004, Woodley 2013). It is possible that recombinant C7 could home to other areas of the body that are affected in individuals with DEB, such as oral mucosa, esophagus, and the gastrointestinal tract, but further research is needed to determine whether this is the case (Woodley 2013, Has 2020c). While this type of approach has the benefits of being straightforward and applicable to all RDEB cases, it does not have the same potential for providing long-term benefit and would almost certainly require regular injections.

Exon skipping and read-through of premature termination codons

Exon skipping refers to altered splicing of the pre-mRNA molecule such that a specific exon is not included in the final mRNA, resulting in a slightly truncated protein. Natural exon skipping has been observed in multiple individuals with DEB and JEB and can significantly ameliorate disease symptoms in some cases (McGrath 1999, Schwieger-Briel 2015, Kowalewski 2016, Bremer 2019). Antisense oligonucleotides (ASOs) are small, synthetic nucleic acid molecules that can induce exon skipping by binding to pre-mRNA. Preclinical work has shown that ASO-mediated exon skipping of some *COL7A1* exons produces a partially functional protein that can be successfully deposited at the DEJ (Goto 2006, Bornert 2016, Bremer 2016, Turczynski 2016). This work paved the way for an ongoing phase I/II clinical trial of an ASO targeting exon 73 of *COL7A1*, a well-known mutation hotspot (NCT03605069). This approach cannot be applied to all *COL7A1* mutations because some exons are essential, but when applicable, ASOs have the potential to provide significant benefit to individuals with DEB.

PTC read-through refers to the suppression of nonsense mutations by enabling the incorporation of a different amino acid during translation, thus enabling translation of the entire protein. Ataluren/PTC124, one of the first read-through compounds identified, has shown efficacy in promoting read-through of PTCs that cause Duchenne muscular dystrophy, cystic fibrosis, and others, but several studies have shown that it does not consistently induce read-through of PTCs in *COL7A1* (McElroy 2013, Cogan 2014, Atanasova 2017). Gentamicin, an aminoglycoside antibiotic, has been shown to promote read-through of PTCs in *COL7A1* in both preclinical work (Cogan 2014) and a clinical trial (NCT02698735, Woodley 2017). There is also an ongoing phase I/II clinical trial for intravenous gentamicin to promote PTC read-through in RDEB (NCT03392909), but topical application may be more desirable due to the potential liver toxicity associated with long-term systemic use of gentamicin (Walker 1988). Amlexanox, which has traditionally been used to treat canker sores, has also been shown to induce PTC read-through in *COL7A1* (Atanasova 2017).

Cutaneous squamous cell carcinoma

Cutaneous squamous cell carcinoma (cSCC), which originates in epidermal keratinocytes, is one of the most common types of non-melanoma skin cancer in the general population (Que 2018, Fania 2021). cSCC is not part of the U.S. National Tumor Registry, which makes accurate estimates of incidence and prevalence difficult for the U.S. population. In other countries, there is substantial variation among estimates of cSCC incidence, including between countries with similar demographics in the same geographic region (Fania 2021). For example, studies from Sweden, Scotland, and Germany reported incidences of 9-96 per 100,000 males and 5-68 per 100,000 females (Katalinic 2003, Brewster 2007, Andersson 2011, Fania 2021). Even countries that actively track cSCC may be significantly underestimating its frequency since it is not uncommon for these figures to be based on pathology reports, which do not account for cSCCs that are not surgically excised (Fania 2021). Regardless of the true incidence of cSCC in any given year, the incidence of cSCC has been rapidly increasing over the past few decades. A Mayo Clinic study found a 263% increase in the incidence of cSCC among residents of Olmsted County, MN between the periods of 1976-1984 and 2000-2010 (Muzic 2017). A separate study using data on the Medicare fee-for-service population from 2006-2012 found a 14% increase in the number of NMSC-associated procedures with a BCC to cSCC ratio of 1:1 (Rogers 2015).

The average age of onset for cSCC is in the mid-60s, which is due in part to the gradual progression of cSCC, with cells going through multiple intermediate stages before reaching the invasive cSCC stage (Xiang 2014, Martincorena 2015, Que 2018). Aside from age, the major risk factors for cSCC are chronic UV exposure, fair skin, smoking, and immunosuppression (Xiang 2014, Martincorena 2015, Que 2018, Fania 2021). cSCC has an extremely high mutation rate (5-fold higher than lung SCC, 4-fold higher than melanoma), and many of these mutations (as high as 80%) are UV-induced (Wikonkal 1999, TCGA Research Network 2012, Pickering 2014, Cho 2018). Despite having a low rate of metastasis (2-4%), a high five-year survival rate (>90%), and a high cure rate for surgical excision (>90%), cSCC accounts for up to 75% of all NMSC deaths (Brougham 2012, Skulsky 2017, Kim 2018, Fania 2021). This is largely because BCC, the other major type of NMSC, is more common and has even more favorable outcomes than cSCC.

Cutaneous squamous cell carcinoma in individuals with EB

The first major report on cSCC in EB used data from the National EB Registry (NEBR) from 1986-2002 and a second round of data collection in 2006 (n = 2745 patients) to estimate the risks of developing and dying from cSCC for each subtype of EB (Fine 2009). cSCC was most common in people with RDEB-severe (formerly Hallopeau-Siemens RDEB), followed by RDEB-inversa (authors note that frequency may be inflated due to small sample size), RDEB-intermediate (formerly non-Hallopeau-Siemens RDEB), and JEB-severe (formerly Herlitz JEB), with all other subtypes at or below 1% (Fine 2009). For individuals with RDEB-severe, the risk of developing a first cSCC and the risk of death due to cSCC were estimated to be 7.5% and 12.7%, respectively, at age 20, but skyrocket soon after, with estimated cumulative risks of 67.8% and 57.2% by age 35, 80.2% and 87.3% by age 45, and 90.1% and 87.3% by age 55 (Fine 2009). The most common age range for developing a first cSCC was 25-35 in people with RDEB-severe, and these patients frequently develop multiple primary cSCCs, with a median of 3-3.5 per patient (Fine 2009). cSCC in RDEB (henceforth referred to as RDEBSCC) tends to develop in areas of chronic wounding and scarring, such as the hands and feet, which are especially prone to fibrosis, scarring, joint contractures, and pseudosyndactyly (Fine 2009).

The findings of a more recent study that reviewed published literature on cSCC in EB largely supported those of Fine et al. (Montaudie 2016). Of the 117 EB patients with cSCC (across 69 publications) discussed in this paper, 88 had DEB (81 recessive, 7 dominant), 19 had JEB, 3 had EBS, and 7 had KEB which supports the assertion that people with RDEB are at the highest risk of developing cSCC (Montaudie 2016). Many of the RDEBSCC cases did not specify subtype (53/81), preventing further insight into the risks of cSCC development for people with RDEB-intermediate and RDEB-inversa (Montaudie 2016). This study found that 45 out of 117 patients (36 RDEB, 7 JEB, and 2 KEB) had at least two primary cSCCs, which is in line with the finding that EB patients (especially RDEB) at a high risk of developing cSCC often develop multiple primary tumors (Fine 2009, Montaudie 2016). Over 85% of cSCCs occurred on the upper (30.8%) or lower (54.7%) extremities, which is also consistent with previous findings (Fine 2009, Montaudie 2016).

The therapeutic outlook for RDEBSCC, both short-term and long-term, is much less favorable than that of DEB. Several compounds have shown limited success in slowing or stopping RDEBSCC progression, such as the EGFR antagonist cetuximab and a variety of immune checkpoint inhibitors (cemiplimab, nivolumab, pembrolizumab), but these successes are generally restricted to isolated case reports (Arnold 2009, Kim 2013, Diociaiuti 2019, Khaddour 2020, Piccerillo 2020, Reimer 2020). A recent study showed that rigosertib, a multikinase inhibitor, induced apoptosis in ten distinct RDEBSCC cell cultures without significantly impacting the growth of non-cancerous keratinocytes, leading to the authorization of two early-stage clinical trials (NCT03786237 and NCT04177498) to evaluate its use in patients (Atanasova 2019b). Rigosertib was initially identified as a potential treatment for RDEBSCC based on its ability to inhibit polo-like kinase 1 (PLK1), which had been identified as a potential therapeutic target for RDEBSCC (Gumireddy 2005, van de Weerdt and Medema 2006, Watt 2011, Liu 2017, Atanasova 2019b). When RDEBSCCs were treated with rigosertib or a specific inhibitor of one of its major target pathways, PLK1 inhibition (using siRNA) showed the most similarity to rigosertib treatment, but differences in PLK1 expression across RDEBSCC cell lines did not correlate with differences in sensitivity to rigosertib (Atanasova 2019b). These results suggest that further investigation is needed to elucidate the mechanism(s) of action of rigosertib in RDEBSCCs, but the ability of rigosertib to induce apoptosis in RDEBSCCs with minimal toxicity is encouraging, nonetheless.

CHAPTER 2

GENES AND COMPOUNDS THAT INCREASE TYPE VII COLLAGEN PRODUCTION AS POTENTIAL TREATMENTS FOR DYSTROPHIC EPIDERMOLYSIS BULLOSA

SUMMARY

Dystrophic epidermolysis bullosa (DEB) is a skin-blistering disease caused by mutations in *COL7A1*, which encodes type VII collagen (C7). There is no cure for DEB, but previous work has shown potential therapeutic benefit of increased production of even partially functional C7. Genome-wide screens using CRISPR-Cas9 have enabled the identification of genes involved in cancer development, drug resistance, and other genetic diseases, suggesting that they could be used to identify drivers of C7 production. A keratinocyte C7 reporter cell line was created and used in a genome wide CRISPR activation (CRISPRa) screen to identify genes and pathways that increase C7 expression. The CRISPRa screen results were used to develop a targeted drug screen to identify compounds that upregulate C7 expression. The C7-tdTomato cell line was validated as an effective reporter for detection of C7 upregulation. The CRISPRa screen identified *DENND4B* and *TYROBP* as top gene hits plus pathways related to calcium uptake and immune signaling in C7 regulation. The targeted drug screen identified several compounds that increase C7 expression in keratinocytes, of which kaempferol, a plant flavonoid, also significantly increased C7 mRNA and protein in DEB patient cells.

INTRODUCTION

Epidermolysis bullosa (EB) is a heterogeneous group of genetic skin-blistering disorders characterized by increased fragility and impaired structural integrity of the skin (Fine 2014). Dystrophic EB (DEB) is a subtype of EB that is exclusively caused by mutations in the COL7A1 gene, which encodes collagen type VII α1 chain. Type VII collagen protein (C7) is formed by the assembly of three proα1(VII) polypeptide chains into a homotrimer. C7 is the main component of anchoring fibrils, which provide mechanical strength and stability to the skin by anchoring the epidermis to the dermis (Colombo 2003, Has 2020a). DEB has a wide spectrum of disease severity and can be caused by either dominant (DDEB) or recessive (RDEB) mutations. DEB subtypes are based on clinical criteria, but disease severity often correlates with COL7A1 mutation type (Christiano 1996, Ishiko 2004, Varki 2006, van den Akker 2011, Eichstadt 2019, Has 2020a).

RDEB generalized severe (RDEB-GS) makes up about 10% of DEB cases and is frequently caused by two COL7A1 null mutations that result in little to no functional expression of C7. RDEB other (RDEB-O) and RDEB inversa (RDEB-I) typically result from missense mutations or both null and missense mutations and have intermediate phenotypes. DDEB has the mildest phenotype and often results from a single glycine substitution in the triple helical domain (Eichstadt 2019). Patients with missense mutations in one or both alleles can often form AFs in reduced numbers and/or with morphological alterations, which can lessen disease severity (Varki 2006). While DEB disease severity often correlates with COL7A1 mutation type, a variety of other genetic, epigenetic, and non-genetic disease-modifying factors can obscure this correlation (Fine 2014, Has 2020a, 2020b).

Despite significant advances in developing molecular therapeutics for DEB, there is currently no cure (Fine 2014, Has 2020a, 2020b, 2020c). The strategies of supplying functional C7 to the skin include direct application of a gene therapy vector containing full-length COL7A1 cDNA, C7 protein therapy, and allogeneic transplant of bone marrow-derived cells or skin cells (Badiavas 2003, Kataoka 2003, Brittan 2005, Woodley 2007, Wong 2008, Kern 2009, Tolar 2009, Fujita 2010, Wagner 2010, Petrof 2013, 2015; Venugopal 2013, Iinuma 2015, Nevala-Plagemann 2015, El-Darouti 2016, South 2016, Webber 2017, Has 2020c). These experimental therapies are generally only accessible to individuals with the most severe DEB phenotypes, in which the disease-causing mutations in COL7A1 result in complete loss of C7 (Has 2020c) with no therapy other than wound treatment for most DEB patients. While complete restoration of fully functional C7 in the skin would be ideal, previous work has shown that even partial C7 function (~10%) can be sufficient to improve disease symptoms (Has 2020c). Identifying genes and/or compounds that can increase production, secretion, and/or deposition of C7 protein into the skin could significantly improve the quality of life for many DEB patients, especially those who are not eligible for other types of experimental treatments.

Genome-wide screening methods have identified targetable genes and pathways for precision medicine development and helped elucidate mechanisms of drug action and resistance (Kampmann 2018, Lin 2019). One such screening approach, called CRISPR activation (CRISPRa), utilizes the clustered regularly interspaced short palindromic repeats (CRISPR)-associated protein 9 (Cas9) system to activate gene expression in a targeted manner. The CRISPRa system employs a catalytically dead Cas9 (dCas9) fused to a transcriptional activation domain such as VP64 (Sanson 2018). Localization of the dCas9-VP64 fusion to the promoter region of a gene with a single guide RNA (sgRNA) will increase expression of the target gene without making genetic alterations. A genome-wide CRISPRa screen utilizes dCas9-VP64 in conjunction with a library of sgRNAs that are designed to target the promoter regions of thousands of different genes (Sanson 2018). CRISPRa screens have been used successfully in the cancer field, and we reasoned that these powerful screening techniques could be adapted for a rare genetic disease like DEB.

Increasing C7 expression in the skin holds the promise of preventing blistering and could form the basis of precision medicine for DEB. Toward this goal, we engineered a keratinocyte C7 reporter cell line by tagging the endogenous C-terminus of COL7A1 with a red fluorescent marker (tdTomato), called C7-tdTomato. In this reporter, tdTomato is produced in equal molarity with one proα1(VII) polypeptide chain and serves as a readout of C7 expression. We next performed a genome-wide CRISPRa screen with the C7-tdTomato cells and a library of sgRNAs targeting over 18,000 genes (Sanson 2018) to identify genes that can increase tdTomato/C7 expression. Several promising gene candidates, including DENND4B (DENN domain containing 4B) and TYROBP (transmembrane immune signaling adapter protein), and pathways, including toll-like receptor and interferon signaling and calcium uptake, were identified, leading us to test 25 potential targeted therapies for increasing C7 expression in keratinocytes. Kaempferol, a plant flavonoid, significantly increased *COL7A1* gene expression and C7 protein levels in multiple wild-type and RDEB keratinocyte cell lines, demonstrating its potential therapeutic benefit for DEB patients. In summary, creation of a C7 reporter cell line and adaptation of CRISPRa screening to a rare disease gene resulted in a promising precision medicine candidate for DEB.

RESULTS

Engineering and validation of a C7-tdTomato reporter cell line

To develop a targeted therapy for DEB patients and screen potential therapeutics, we created a C7 reporter line by modifying the immortalized N/TERT keratinocyte cell line. The fluorescent protein tdTomato was inserted into the endogenous *COL7A1* locus using a genome engineering technique called homology-independent knock-in (Lackner 2015) **(Figure 2A)**. Fluorescence-activated cell sorting (FACS) was used to collect the edited cells, resulting in a stable, tdTomato-positive population, which we call C7-tdTomato in the remainder of this paper (**Figure 2B**). A combination of PCR and sequencing was used to confirm correct integration in the C7-tdTomato clones, and two isolated clones were heterozygous for the tdTomato knock-in

(**Figure 2C, S1-S2)**. To validate the C7-tdTomato reporter cell line, we stimulated C7 expression with TGF-β which resulted in a significant 2.1-fold increase in tdTomato mean fluorescence intensity **(Figure 2D)**. Increased C7 expression was further confirmed by qRT-PCR and Western blot **(Figure 2E-F, S3A)**. Proportional expression of COL7A1 and tdTomato was demonstrated through high correlation of qRT-PCR data (**Figure S4)**. Taken together, these results demonstrate that measurable increases in tdTomato fluorescence directly correlate with increases in collagen VII mRNA and protein, validating the functionality of the C7-tdTomato reporter line.

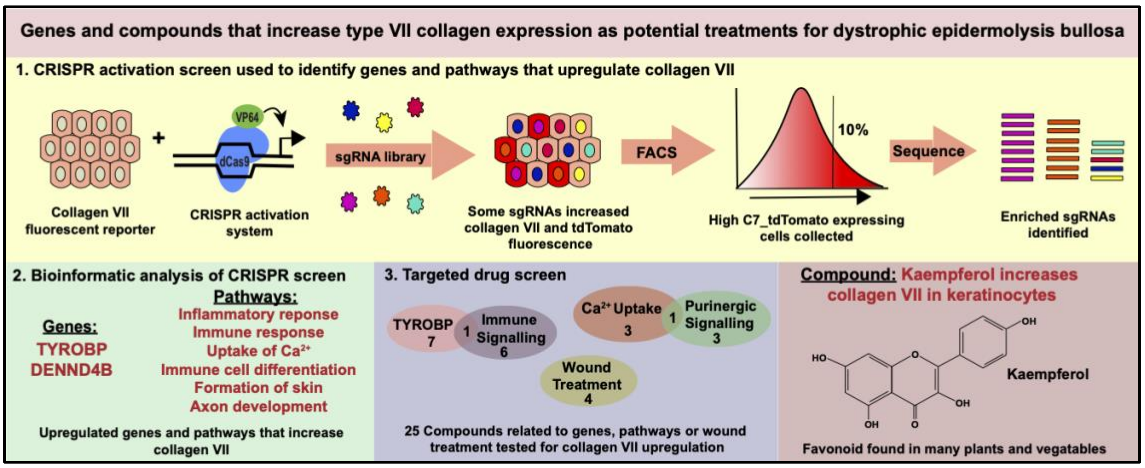

Figure 1: Graphical abstract outlining the methodology used to screen for positive regulators of C7 production. C7-tdTomato keratinocytes were transduced with dCas9-VP64 and an sgRNA library targeting ~18,000 genes. Cells were sorted into low, mid, and high populations based on tdTomato fluorescence using FACS. sgRNAs that were enriched in the high population were identified by PCR-amplifying the sgRNA region of the library construct from gDNA and using high-throughput sequencing. Bioinformatic analysis of enriched sgRNAs guided selection of compounds for a targeted drug screen. Kaempferol was the only compound that increased C7 at the mRNA and protein level in both WTKs and RDEBKs.

CRISPRa screen with C7-tdTomato reveals positive regulators of C7

After confirming the CRISPRa system was functional in our C7-tdTomato cells transduced with dCas9-VP64 (**Figure S5A)**, we performed the CRISPRa screen. The C7-tdTomato+dCas9-VP64 cells were transduced with the lentiviral sgRNA library at 50%

transduction efficiency with the intention of integrating one sgRNA per cell and a minimum of 500 cells per guide (McDade 2016). To identify genes that increase C7 production, the top 10% of tdTomato-expressing cells (tdTomato-high) were collected using FACS **(Figure S6)**. The bottom 10% and middle 80% of tdTomato-expressing cells (tdTomato-low & tdTomato-mid, respectively) were also collected for comparison. Genomic DNA was isolated from the tdTomato-high cells, and the sgRNA region of the guide construct was PCR-amplified and sequenced to a depth of ~20 million reads. Fold changes were calculated between the relative abundance of each sgRNA in the tdTomato-high population and in the plasmid DNA library and converted into Z-scores. At a cutoff of Z > 1.75 (FC ~ 2.5), 1544 enriched sgRNAs were identified.

To identify the most promising gene candidates, we sorted the enriched sgRNAs based on Z-score and looked for genes that had more than one sgRNA enriched. Only two genes, *COL7A1* and *DENND4B*, had sgRNAs with a Z-score greater than 5. There were 78 genes (including *DENND4B*) that had more than one enriched sgRNA, but only one, *TYROBP*, showed enrichment of all three sgRNAs. One of two *DENND4B* sgRNAs and two of three *TYROBP* sgRNAs were increased at least 1.5-fold relative to tdTomato-low. *DENND4B* and *TYROBP* were also the only two genes with all three sgRNAs represented among the cells with high C7 expression in the secondary CRISPRa screen **(Figure 3A)**. Based on these results, we selected sgRNAs targeting *DENND4B* and *TYROBP* to validate our screen. C7-tdTomato+dCas9-VP64 cells transduced with sgRNAs targeting *DENND4B*, *TYROBP*, or *COL7A1* all showed significantly increased tdTomato fluorescence relative to NT sgRNA **(Figure 3B-C)**. While *COL7A1* mRNA was not significantly increased in cells with sgRNAs targeting *DENND4B* or *TYROBP* **(Figure 3D)**, C7 protein levels were significantly increased relative to NT sgRNA **(Figure 3E, S3B)**. These results suggest that (1) increasing expression of *DENND4B* and *TYROBP* results in increased C7 production, and (2) these effects occur at the translational or post-translational level rather than the level of transcription.

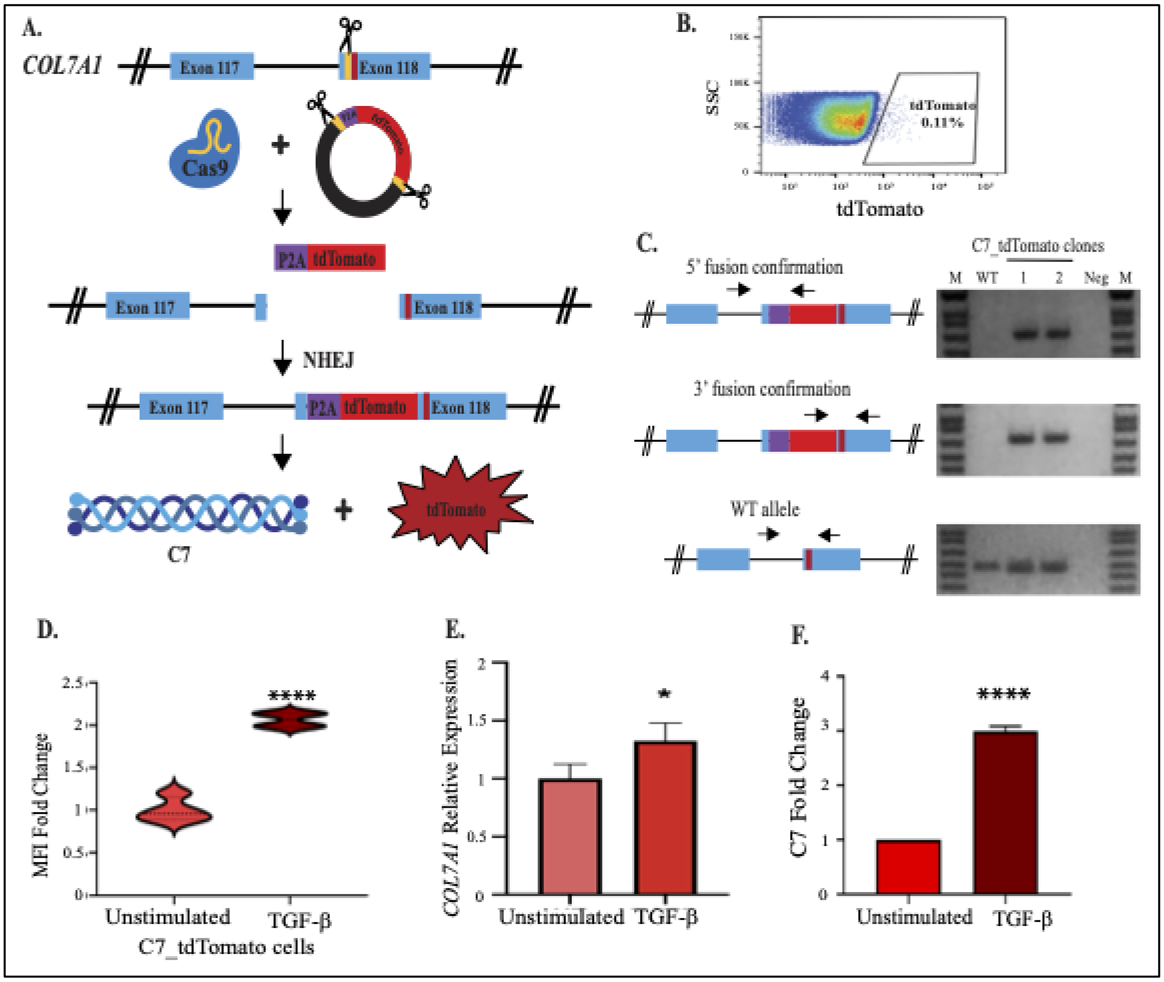

Figure 2: Creation of C7 reporter cell line, C7-tdTomato. A. Targeting scheme for creating the C7-tdTomato reporter with P2A self-cleaving peptide (purple), tdTomato gene (red), and *COL7A1* gRNA sequence (yellow). Cas9 and gRNA (yellow) **B.** FACS used to isolate edited cells. **C.** PCR was used to confirm correct 5' and 3' integration of the P2A-tdTomato into the *COL7A1* gene C-terminus and heterozygous knock-in. **D.** Mean fluorescence intensity (MFI) for replicate samples of C7-tdTomato cells unstimulated and with TGF-β **E.** qRT-PCR analysis of C7-tdTomato cells unstimulated and with TGF-β. **F.** Quantification of Western blot analysis of C7-tdTomato cells unstimulated and with TGF-β for C7 expression (see **Figure S3A** for blots).

We also probed our list for genes with products that interact with DENND4B and TYROBP to identify potential signaling pathways/mechanisms. *DENND4B* encodes a RAB guanine nucleotide exchange factor that may be involved in membrane trafficking and/or vesicle-mediated transport. The only gene product in our list that has been shown to interact with

DENND4B is CTU2 (cytosolic thiouridylase subunit 2), but the only evidence for this interaction is from a single co-immunoprecipitation experiment (Huttlin 2017). *TYROBP* encodes a protein that interacts with a variety of immune cell surface receptors to mediate their activation, including natural killer cells, neutrophils, macrophages, and dendritic cells (Tomasello 2005). In contrast to DENND4B, there were several gene products identified in the screen that are known to interact with TYROBP, including CD69, LAT2, MMP9, SIGLEC1/CD169, SIGLEC14, and SIRPB1 (**Figure S9**).

To identify mechanisms of increasing C7 production, we used Ingenuity Pathway Analysis (IPA, QIAGEN) to identify upstream regulators, signaling pathways, and biological functions that were significantly enriched and predicted to be activated ($Z > 2.0$) based on the list of genes. The upstream regulators were dominated by components of interferon signaling, including type I, II, and III interferons, interferon-induced genes, interferon regulatory factors, and components of pathways directly upstream (toll-like receptors) and downstream (JAK/STAT, MAPK) of interferon signaling **(Table S1)**. There were also other immune regulators, such as cytokines/chemokines (and receptors), growth factors, and transcription factors that mediate expression of immune signaling genes **(Table S1)**. The thirteen diseases/functions and ten canonical pathways also contained terms related to immune cell functions, including cytokine production, cell-cell communication, and differentiation **(Tables S2-S3)**. There were also terms relevant to keratinocytes, such as “inflammatory response,” “Ca2+ uptake,” “formation of skin”, “IL-15 production,” “retinoic acid-mediated apoptosis signaling,” and “retinol biosynthesis” **(Table S2-S3)**. Taken together, these results identified numerous signaling pathways and processes that could potentially be targeted to increase C7 production.

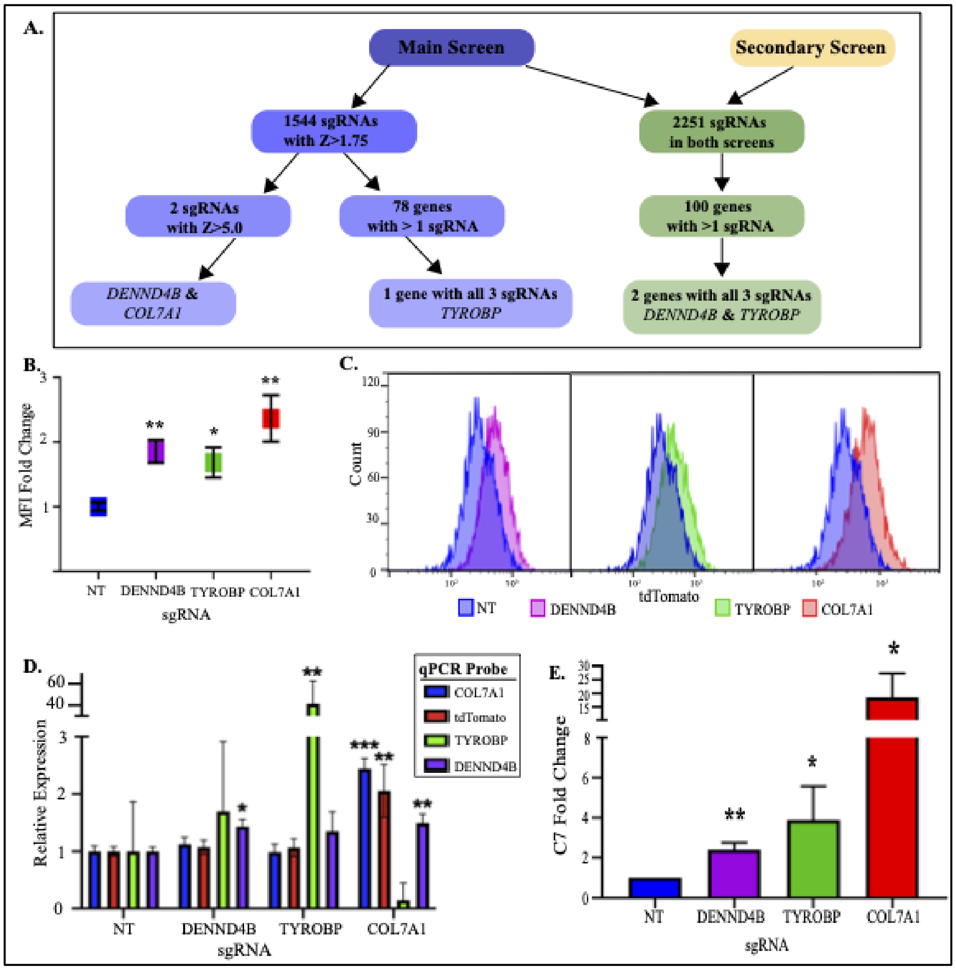

Figure 3: Results and validation of CRISPRa screen. A. Flow diagram of CRISPRa screen sequencing results analysis. **B.** C7-tdTomato + dCas9-VP64 cells were transduced with sgRNA lentivirus for NT, *DENND4B*, *TYROBP*, or *COL7A1*. Analyzed by FACS for tdTomato MFI and normalized to NT. **C.** Representative histograms for each sgRNA transduction compared to NT. **D**. qRT-PCR of each sgRNA transduction with corresponding probes. Ct values were normalized to NT control. **E.** Quantification of Western blot analysis of C7 expression after sgRNA transduction (see **Figure S3B** for blots).

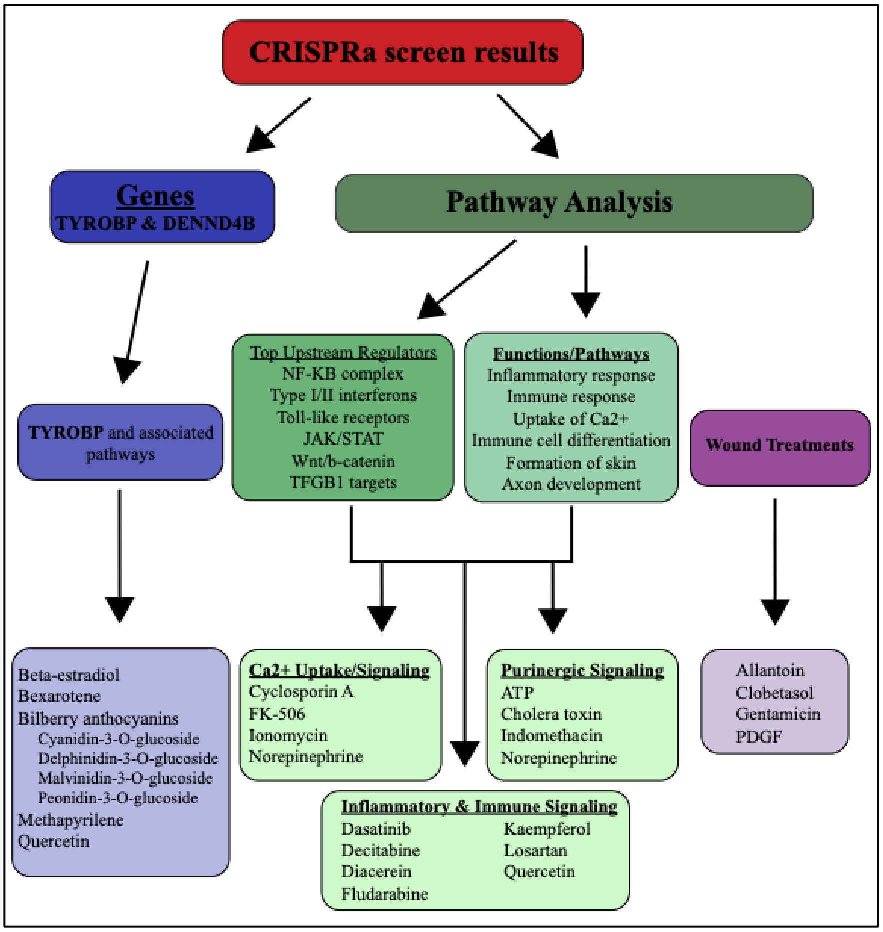

Figure 4: Flow diagram for development of the targeted drug screen based on CRISPRa screen results. We chose compounds that had been previously shown to increase TYROBP, compounds that either promote or inhibit signaling through Ca2+, purinergic receptors, inflammatory mediators, and/or immune signaling pathways, and compounds that have been previously used to increase wound healing.

Targeted Drug Screen

To determine whether any of the genes/pathways identified in our screen could be effectively targeted to increase C7 production in keratinocytes, we performed a targeted drug screen **(Figure 4)**. Using literature searches, we selected compounds shown to (1) increase TYROBP expression, (2) activate/inhibit immune signaling pathways (especially chronic inflammation), (3) activate/inhibit calcium uptake/signaling, and/or (4) activate/inhibit purinergic signaling **(Figure 4, Table S3)**. We also chose some compounds that had previously been shown to improve wound healing.

Drugs were initially tested at three concentrations to evaluate toxicity and identify the best concentration for induction of tdTomato/C7 expression, and drugs that induced the largest increase in fluorescence were screened again **(Figure 5A, Table S5)**. Adenosine triphosphate (ATP), dasatinib, diacerein, indomethacin, kaempferol, and the four bilberry anthocyanins (BA; cyanidin, delphinidin, malvidin, and peonidin) reproducibly and significantly increased tdTomato fluorescence and C7 protein levels **(Figure 5B)**. Besides TGF-β, dasatinib, kaempferol, and two BAs (cyanidin and peonidin) also significantly increased *COL7A1* mRNA expression **(Figure 5C)**. Drugs that increased C7 were tested in two additional keratinocyte cell lines that were developed by immortalizing primary wild-type (WT1) and RDEB (RDEB8) keratinocytes.

Indomethacin, kaempferol, and peonidin significantly increased *COL7A1* mRNA in WT1, but only kaempferol increased *COL7A1* mRNA in RDEB8 **(Figure 6A)**. RDEB8 keratinocytes showed a significant decrease in *COL7A1* mRNA when treated with dasatinib **(Figure 6A)**. Most importantly, kaempferol (and to a lesser extent indomethacin) significantly increased C7 protein expression in RDEB8 keratinocytes **(Figure 6B, S3C)**.

Kaempferol was further evaluated with several additional keratinocyte cell lines. Three wild-type (WT4, WT9, and WT10) and three RDEB (RDEB4, RDEB8 and RDEB9) keratinocyte cell lines were tested with and without kaempferol treatment. Again, kaempferol significantly increased *COL7A1* expression in all keratinocyte cell lines tested (**Figure 6C**). Additional testing was focused on the RDEB8 cells since it was our only RDEB patient cell line with a *COL7A1* missense mutation. Kaempferol increased C7 protein expression in both RDEB8 and WT9 keratinocytes (**Figure 6D**). Finally, immunofluorescence without cell permeabilization was used to detect extracellular deposition of C7. There was a visible increase in extracellular C7 staining with kaempferol treatment compared to untreated RDEB8 keratinocytes (**Figure 6E**). Overall, these results suggest that kaempferol may provide therapeutic benefit to DEB patients by increasing C7 production and extracellular deposition in patients with a missense mutation.

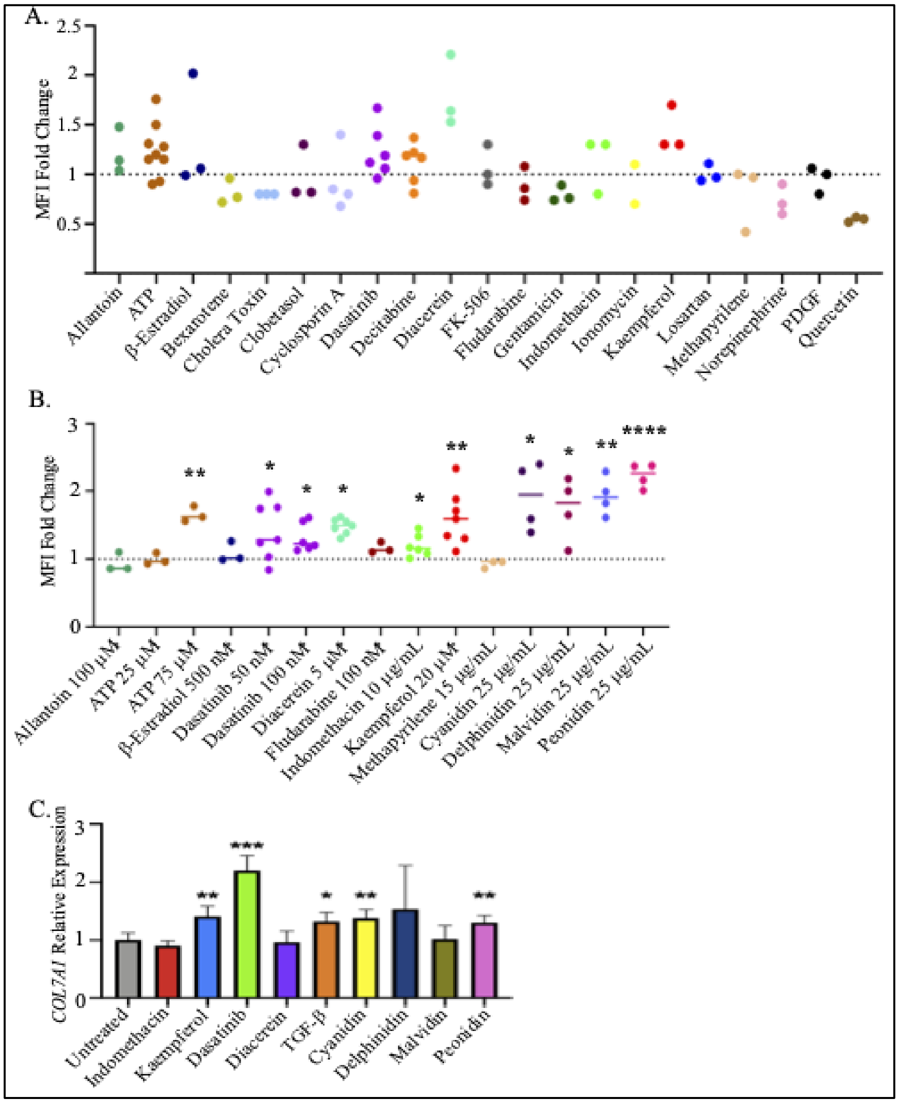

Figure 5: Drug screen with C7-tdTomato cells. C7-tdTomato cells were incubated with the indicated compound for 3 days and collected for analysis. **A.** FACS analysis, each point represents a different concentration of the corresponding drug. For specific drug concentrations and associated MFI see **Table S6**. MFI normalized to average MFI of untreated C7-tdTomato cells. **B.** FACS analysis, each point represents a replicate sample with indicated drug concentration. Bar represents mean. **C.** qRT-PCR of samples treated with the indicated drug concentration in B. Ct values were normalized to untreated controls.

DISCUSSION

Wound management is currently the only treatment available for most DEB patients, highlighting the need for effective precision medicines. Therapeutics that enable sustained production of full-length C7 in the skin, such as gene editing and gene therapy, have shown promise in preclinical and clinical studies, but since they are still experimental, they are inaccessible to most DEB patients. Previous work has shown that increasing production of partially functional, mutant C7 protein in patients with missense mutations could potentially improve skin integrity and reduce blistering. In this study, we successfully identified new genetic mechanisms and compounds for increasing C7 production in DEB keratinocytes by merging the power of CRISPRa screens with a C7 reporter cell line. The CRISPRa screen identified two genes, *DENND4B* and *TYROBP*, that reproducibly increased production of C7 protein, but not mRNA. This suggests that their ability to increase C7 is related to translation, stability, modification, secretion, and/or deposition of C7 protein.

DENND4B encodes a RAB guanine nucleotide exchange factor involved in vesicle-mediated transport, suggesting that it could facilitate C7 processing and/or cellular export, but additional testing and confirmation are necessary. DENND4B is expressed in keratinocytes and seems to have feedback regulation with C7, since DENND4B expression significantly increased with both *DENND4B* and *COL7A1* sgRNAs **(Figure 3D)**. *TYROBP* encodes a protein that mediates the activation of immune signaling pathways by interacting with a variety of immune receptors through its immunoreceptor tyrosine-based activation motif (Tomasello 2005). TYROBP is normally expressed in lymphoid and myeloid cell types, as well as osteoclasts in bones and microglia in the brain, but not keratinocytes (Tomasello 2005). Multiple genes encoding proteins known to interact with TYROBP were enriched, including signal regulatory protein β (SIRPB1). SIRPB1 activation in macrophages has been shown to suppress the release of TNFα, a proinflammatory cytokine known to inhibit C7 expression in keratinocytes (Dietrich

2000, Hayashi 2004, Gaikwad 2009). This suggests that TYROBP/SIRPB1-expressing macrophages could potentially increase C7 production through inhibition of TNFα in the skin, but additional experiments are needed to test this hypothesis.

Without functional C7, RDEB skin blisters with minor trauma and wounds do not heal properly, resulting in chronic inflammation, fibrosis, and susceptibility to infection. RDEB skin and serum show increased levels of pro-inflammatory cytokines and other mediators of immune signaling relative to healthy controls (Breitenbach 2015, Esposito 2016, Cianfarani 2017). Using IPA, we identified numerous immune-related upstream regulators, canonical pathways, and diseases/functions that were predicted to be activated based on our gene list. Many of the top upstream regulators were involved in interferon and toll-like receptor signaling, which are important initiators of immune responses **(Table S1)**. These results led us to test compounds that modulate these signaling pathways and/or increase production of TYROBP, including bexarotene, BAs, decitabine, diacerein, kaempferol, methapyrilene, and norepinephrine. Six of these compounds including all 4 BAs, diacerein and kaempferol significantly increased fluorescence in the C7-tdTomato cells (**Figure 5B**), reconfirming the important influence of TYROBP and immune signaling in C7 expression.

Genes encoding components of purinergic signaling and calcium signaling—important regulators of keratinocyte proliferation, differentiation, adhesion, and cell signaling—were also enriched in our pathway analysis. The enrichment of genes with products involved in these processes led us to test compounds that affect calcium uptake and purinergic signaling, including ATP itself, cholera toxin (increases cAMP), cyclosporin A and FK-506 (inhibit calcineurin signaling), indomethacin (decreases cAMP), and norepinephrine (increases purinergic signaling). While none of these compounds significantly increased C7 production in the RDEB keratinocyte line we tested, the complex interplay of these pathways and their potential impact on C7 function warrants further investigation, particularly indomethacin.

The CRISPRa screen directed the selection of drugs for our targeted screen and over a third of the compounds tested significantly and consistently increased tdTomato fluorescence/C7 expression **(Figure 5B)**. This screen also led to the potentially therapeutic discovery that kaempferol can increase both *COL7A1* mRNA expression and C7 protein expression in RDEB patient keratinocytes **(Figure 6A-C)**. Kaempferol, a plant flavonoid, could increase C7 production through multiple mechanisms due to its wide-ranging effects on cells. Kaempferol has been shown to reduce inflammation, oxidative stress, DNA damage, fibrosis, and cancer development in a variety of different cell types (Chen 2013, Wang 2018, Liu 2019, Sekiguchi 2019). Kaempferol was found to help heal wounds in both normal and diabetic rats (Ambiga 2007, Ozay 2019), and suppress fibrosis and oxidative stress in a mouse model of systemic sclerosis (Sekiguchi 2019), but has not been tested in human wound healing or in conjunction with DEB. Our findings, taken together with previous research, suggest that kaempferol could provide substantial therapeutic benefits to individuals with DEB. Further development and testing of kaempferol as a therapeutic for wound healing and for DEB is necessary.

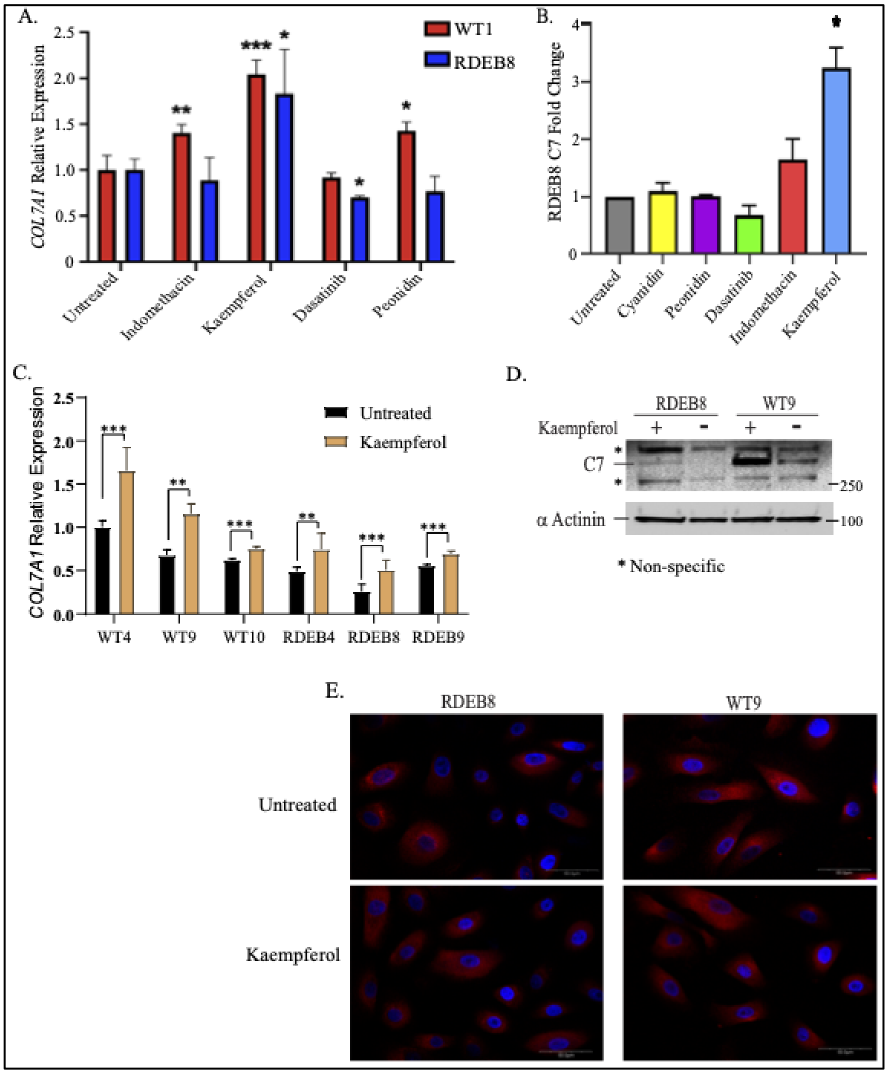

Figure 6: Drug screen and kaempferol testing with WT and RDEB keratinocytes. A. qRT-PCR of WT and RDEB8 cells treated with the indicated drug. (See **Figure 5B, Table S6** for drug concentrations) **B.** Quantification of Western blot analysis of C7 expression in RDEB8 cells treated with indicated drug **C.** *COL7A1* qRT-PCR for keratinocytes +/- 20µM kaempferol. Ct values were normalized to WT4. **D**. C7 Western blot for RDEB8 and WT9 keratinocytes +/- 20µM kaempferol (15µg protein per well). **E.** C7 (red, Cy3) and DAPI (blue) immunofluorescence for RDEB8 and WT9 keratinocytes +/- 20µM kaempferol (See **Figure S3C, S8C-D** for blots).

MATERIALS AND METHODS

Cell culture: Keratinocytes were maintained in keratinocyte complete media (KCM): EpiLife medium +60 μM calcium/EpiLife Defined Growth Supplement (EDGS, ThermoFisher). Cells were cultured with 50 U/mL penicillin-streptomycin, unless otherwise indicated. Patient keratinocytes were obtained and subsequently immortalized following informed consent, IRB approval, and in accordance with the Declaration of Helsinki Principles. The RDEB cell lines used in this study had the following *COL7A1* mutations: RDEB4: c.4078G>T (p.Gly1360*) / c.8075delG (p.Gly2692Alafs*94); RDEB8: c.4738_4740delinsA (p.Val1580Thrfs*28)/c.425A>G (p.Lys142Arg); and RDEB9: c.5888G>A (p.Trp1963*)/c.5888G>A (p.Trp1963*).

qRT-PCR: Total RNA was isolated using the RNeasy Mini Kit (QIAGEN) and reverse transcribed using SuperScript II Reverse Transcriptase (ThermoFisher) according to manufacturer's instructions. *GAPDH* was used as the reference gene. The comparative Ct method was used to calculate gene expression differences. Samples were run in duplicate in each plate, and each sample was run on a minimum of 3 separate plates.

Western blot: Cell lysates were collected from the cell culture plate with lysis buffer using a cell scraper. Primary antibodies: rabbit anti-C7 (ab93350, Abcam, 1:500) and mouse anti-α-actinin (sc-17829, Santa Cruz, 1:1000). Secondary antibodies: goat anti-mouse IgG HRP and goat anti-rabbit IgG HRP (BioRad, 1:5000). Quantification was performed using ImageJ.

FACS analysis: Cells were fixed in 4% paraformaldehyde and FACS was performed at the University of Minnesota (UMN) Flow Cytometry Resource facility. Analyses were performed with FlowJo software (v10).

Immunofluorescence: WT9 and RDEB8 cells were plated in chamber slides coated with collagen IV and grown in KCM media with or without 20μM kaempferol for 3 days. Cells were fixed in 4% paraformaldehyde and stained with polyclonal rabbit anti-human collagen VII antibody (LSBio) without permeabilization to detect extracellular C7 deposition. Secondary antibody used was donkey anti-rabbit IgG Cy3 (Jackson Immunoresearch) along with DAPI nuclear stain.

Statistical Analysis: Statistical analysis was performed with GraphPad Prism 9.1.0. Multiple unpaired t-test comparisons with a minimum of 3 technical replicates for all analyses. Significance was determined by *p*-values: $*p < 0.05$; $**p < 0.01$; $***p < 0.001$; $****p < 0.0001$.

Drug Screens: Cells were plated in 6-well plates, and when the cells reached 25% confluency, the specified drug was added at the specified concentration in 2 mL KCM. After 3 days, cells were harvested for analysis.

<u>Creating the C7-tdTomato cell line</u>

CRISPR/Cas9 homology-independent knock-in was used to insert P2A-tdTomato into the *COL7A1* gene via NHEJ, as previously described (Lackner 2015). Briefly, the tdTomato gene was amplified from pCDH-EF1-Luc2-P2A-tdTomato plasmid (Addgene; 72486) with primers containing *COL7A1* guide, P2A, and BspQI restriction site sequences and cloned into the donor plasmid with BspQI digestion. N/TERTs were edited with Cas9, *COL7A1* guide, and donor plasmid, and edited cells were isolated using FACS (**Figure 2B**). Primer sequences can be found in **Table S5**.

Guide selection: Three guide sequences preceding the stop codon in *COL7A1* were identified using CRISPOR (Concordet 2018) and evaluated for cutting efficiency. The guides were cloned into the px458 plasmid as previously described, and 0.5mg of each guide plasmid was transfected in triplicate into HEK293T cells (1×10^6 cells; Neon transfection system: 1100V, 20ms, 2 pulses). Cells recovered for 2 days, then DNA was isolated and the Cas9 cut site was PCR-amplified and sequenced. Based on TIDE analysis, guide 1 had the highest indel formation and was selected for targeting in the N/TERT cells (**Figure S1**).

Plasmid donor DNA: A plasmid containing P2A-tdTomato flanked with the *COL7A1* guide 1 sequence was engineered as the donor DNA for knock-in gene tagging. CRISPR/Cas9 targeting of guide 1 sequence can linearize the P2A-tdTomato donor DNA and create a double-strand DNA break in *COL7A1* for NHEJ incorporation of the tag (**Figure 2A**). The donor plasmid was created by PCR amplification of the P2A and tdTomato gene from the pCDH-EF1-Luc2-P2A-tdTomato plasmid (Addgene; 72486) with primers containing guide 1 target sequence and BspQI restriction enzyme sites (BSPQ1-guide1-P2A-F and BSPQ1-guide1-tdT-R). The amplified product was incorporated into the pGG-MCS-ROCK plasmid with BspQI digestion and T4 ligation. The plasmid was sequence-confirmed and referred to as pGuide1-P2A-tdTomato-Guide1.

Transfection and FACS sorting: N/TERTs were transfected with 1.5μg donor pGuide1-P2A-tdTomato-Guide1 and 2μg px458-Guide1 in triplicate (1×10^6 cells; Neon transfection system: 1500V, 20ms, 2 pulses). Transfected cells were expanded for 4 weeks and then FACS was used to identify tdTomato positive cells (at UMN Flow Cytometry Resource facility). Approximately 0.1% of the cells were positive for tdTomato (**Figure 2B**). A second round of FACS was used to further purify the targeted population and the tdTomato positive cells were sorted into a 96 well plate at 5, 10, and 20-cell densities. Colonies grew in all three cell dilutions and were visually screened by fluorescent microscopy for tdTomato expression.

Confirmation of C7-tdTomato cell line: PCR and Sanger sequencing were used to confirm the correct integration **(Figure 2C**, **S2)**. Primer sequences are provided in **Table S5**. Cells were stimulated with TGF-β (5ng/μL) and collected for analysis after 3 days **(Figure 2D-F)**.

Performing CRISPRa Screens

Vectors and plasmid library for CRISPRa screen: Cells were transduced with a lentiviral vector containing dCas9-VP64-Blast (Addgene, 61425) as previously described (Piccioni 2018). Cells were expanded and maintained in blasticidin selection. The CRISPRa screen was performed using the human CRISPRa single guide RNA (sgRNA) library Calabrese (Set A) in the pXPR-502 backbone (Addgene, 1000000111). The library contained 56,762 sgRNAs targeting 18,885 genes with three sgRNAs per gene. Individual sgRNAs were engineered with customizable plasmid, pXPR-050 (Addgene, 96925) as previously described (Sanson 2018).

Individual sgRNA lentiviral plasmid cloning: Individual sgRNA sequences from the CRISPRa library were cloned into pXPR_050. The forward and reverse oligos for each sgRNA were annealed by incubation in 1X T4 ligase buffer at 95˚C for 5 minutes and cooled to room temperature for 20 minutes. The annealed oligos were Golden Gate cloned into pXPR_050 with Esp31 digestion and T4 ligase. Ligated plasmids were transformed and plated on LB agar plates with 100µg/mL carbenicillin. Colony screening was performed using PCR with the U6 promoter forward primer and sgRNA reverse primer. Correctly cloned colonies were grown overnight in LB +100µg/mL carbenicillin, pDNA was isolated, and the sgRNA sequence was confirmed using Sanger sequencing. Primer sequences can be found in **Table S5**.

CRISPRa sgRNA Library Amplification: 400ng of the sgRNA library was electroporated into 100µL STBL4 electrocompetent *E. coli* cells (Invitrogen). To maintain library diversity, transformed bacteria were plated on twenty 150cm^2 agar plates containing 100µg/mL carbenicillin and grown for 18 hours at 30˚C. Bacterial colonies were scraped from the plates and library plasmid DNA (pDNA) was isolated using the ZymoPURE II Plasmid Midiprep Kit (Genesee Scientific). Library pDNA was sequenced to confirm sgRNA representation and distribution (**Figure S7A**).

Lentivirus production: ~8×10^6 HEK293T cells were seeded in 0.1% gelatin coated T-150 flasks with 293T complete media (DMEM + 10% FBS, 1× GlutaMAX, 50 U/mL penicillin-streptomycin). The next day, 293T cells were transfected using Lipofectamine 2000 with cargo plasmid (15µg), and 3rd generation lentivirus packaging plasmids: pMDGLg/pRRE (10µg), pRSV-rev (1µg) and pMD2.G (2µg) and incubated overnight. The next day, media was removed and replaced with 293T complete media without GlutaMAX. After 36 hours, virus production was confirmed with Lenti-X GoStix (Takara), media was collected, and virus was concentrated with Lenti-X concentrator (Takara) according to manufacturer’s instructions. Pelleted virus was reconstituted in EpiLife media. Virus was stored at -80˚C in single use aliquots. sgRNA library virus production for screens was performed in 10-20 × T-150 flasks.

Virus transduction efficiency testing: 6×10^6 N/TERTs were resuspended in 6ml transduction solution containing KCM, 10µM ROCK inhibitor (BD BioSciences), 30µL LentiBlast A, and 6µL LentiBlast B (Oz Biosciences). Cells were equally distributed to each well of a 6-well plate that had been pre-coated with type IV collagen. Different amounts of CRISPRa library lentivirus were added to each well (0, 25, 50, 75, 100, and 125 µL). The next day, cells were harvested from each well, washed with KCM, and divided 50% to selection media (KCM +2 µg/mL puromycin), and 50% to regular KCM. Cells were grown for 4 days with media changes on day 1 and 3 before being harvested and counted. Transduction efficiency was determined for each well (virus concentration) by calculating the percentage of cells that survived in puromycin selection and compared to the well that did not receive any lentivirus (**Figure S7B**).

CRISPRa Main screen: The CRISPRa screen was performed as previously described (Piccioni 2018). Briefly, ~90 million C7-tdTomato+dCas9-VP64 cells were transduced with the sgRNA library at ~30-50% transduction efficiency to achieve 500× coverage for each sgRNA (McDade 2016, Piccioni 2018, Sanson 2018). After 24 hours, cells were pooled and plated with KCM + 2µg/mL puromycin. After 3 days in selection media, cells were switched to regular KCM for 24 hours before FACS. Cells were sorted into low (bottom 10%), mid (~75%), and high (top 10%) populations based on tdTomato mean fluorescence intensity (MFI). The tdTomato-high population contained 650,782 cells **(Figure S4)**.

Secondary Screen: This screen was conducted as described, with the following differences: approximately 35 million C7-tdTomato + dCas9-VP64 cells were transduced. Cells were in puromycin selection for 5 days, and the tdTomato-high population contained 439,602 cells.

Sequencing: Genomic DNA (gDNA) was isolated from each population and the sgRNA region was PCR-amplified using primers containing Illumina P5 and P7 adapter sequences. Successful amplification was confirmed via gel electrophoresis. Agencourt AMPure XP beads (Beckman Coulter) were used to clean up PCR products/sequencing libraries. Library concentrations were determined using a NanoDrop (Thermo Fisher). Libraries were diluted, denatured, and sequenced on an Illumina MiniSeq using 75-cycle kits according to the manufacturer's instructions (Illumina). Primer sequences can be found in **Table S5**.

<u>Analyzing Screen Data</u>

Read Processing and Alignment: Reads were first filtered using Cutadapt (Martin 2011) based on the presence of the CACCG sequence that appears immediately 5' to the sgRNA sequence in the construct. After trimming the CACCG sequence and any bases preceding it, the first 20 bases in each read represented the sgRNA sequence. Reads were then trimmed from the 3' end to leave only the 20-base sgRNA sequence. After filtering and trimming, the reads were analyzed to determine every unique 20-base sequence and the number of reads that corresponded to each unique sequence. The list of unique sequences was cross-referenced with the list of sgRNA library sequences to identify which sgRNAs were present. No mismatches were tolerated. Raw read counts for each sgRNA were converted into counts-per-million (CPM) sgRNA reads to normalize for differences in read totals across populations and the starting material (library pDNA).

Calculating sgRNA Enrichment: For each sgRNA, the fold change (FC) was calculated by dividing the screen CPM by the pDNA CPM. Log2-transformed FC values (logFC) were used to calculate a Z-score for each sgRNA via the following formula: (sgRNA logFC - mean logFC) / (standard deviation of logFC). sgRNAs with a Z-score greater than 1.75 were used for pathway and gene set enrichment analyses.

Pathway and Gene Set Enrichment Analysis: Ingenuity Pathway Analysis (IPA, QIAGEN) was used to identify upstream regulators, diseases, functions, and canonical pathways that significantly overlapped and/or were predicted to be activated/inhibited based on the list of candidate genes and the fold change values. Results for enriched upstream regulators and diseases/functions were filtered based on activation Z-score and overlap p-value.

SUPPLEMENTARY FIGURES

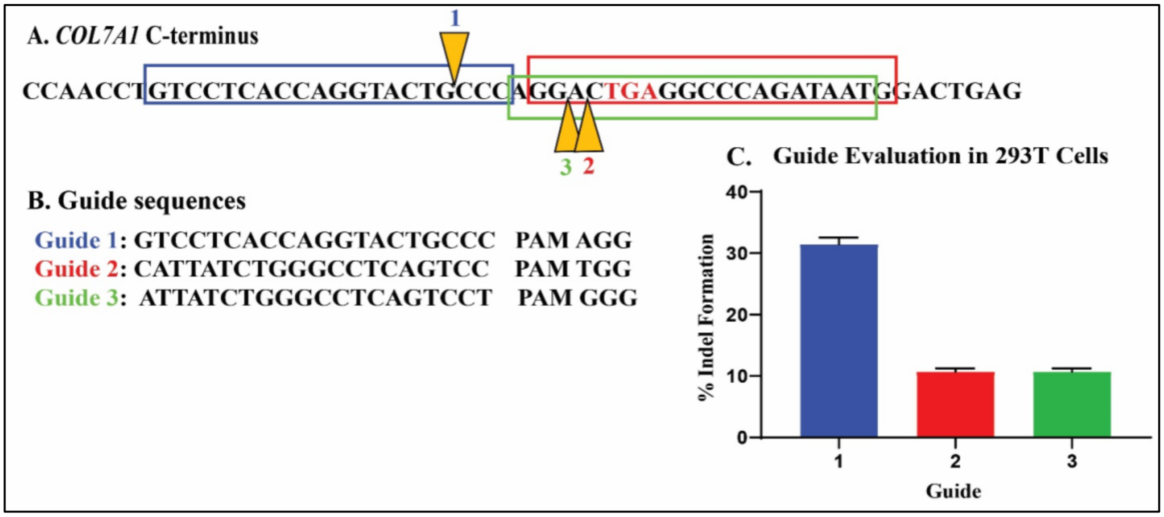

Figure S1: Gene targeting design for creation of C7-tdTomato keratinocyte reporter cell line. A. N-terminal sequence of *COL7A1* with stop codon indicated in red letters. Three different guide sequences highlighted by blue (guide 1), red (guide 2) and green (guide 3) colored rectangles. Location of Cas9 cut site indicated with yellow triangles and numbered for each guide. **B.** Sequences and PAM for each guide. **C.** Guides were evaluated by transfection into 293T cells along with Cas9 and cutting efficiency of each guide was determined by % indel formation from TIDE analysis.

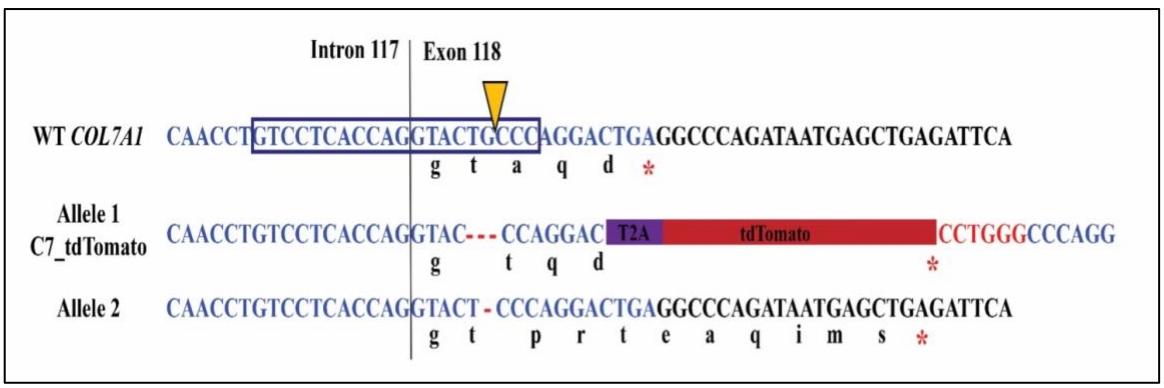

Figure S2: Sequence analysis of C7-tdTomato cells. Sequence analysis of the C7-tdTomato cell line indicated a heterozygous knock-in of tdTomato into the C-terminus of *COL7A1*. Allele 1 contains a 3bp deletion at the Cas9 cut site and in-frame integration of P2A-tdTomato insert into the *COL7A1* C-terminus. Allele 2 contains a single nucleotide deletion at the Cas9 cut site and frameshift resulting in a slightly longer peptide sequence.

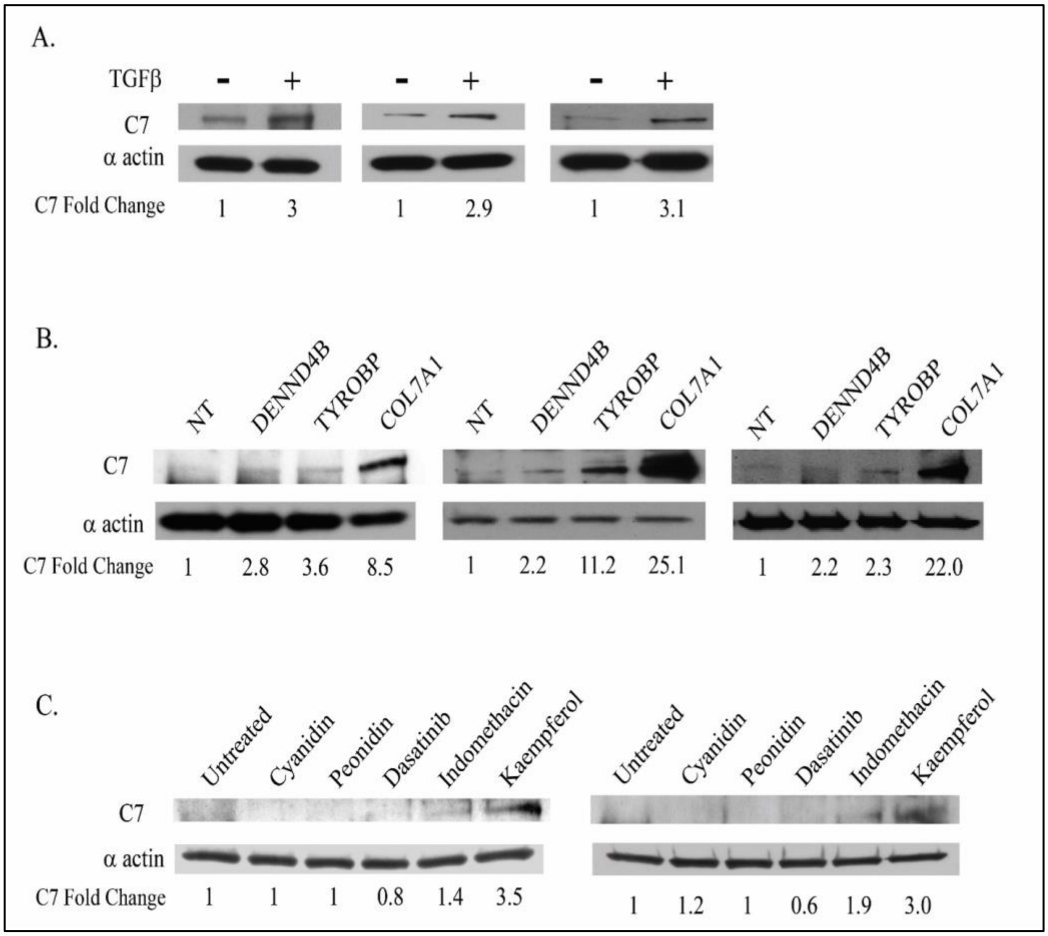

Figure S3: Western blot analysis. Western blot (WB) analysis for C7 protein (size 295 kDa) performed on whole cell lysates including extracellular matrix collected from culture plates with α-actinin (size 100 kDa) as loading control. **A.** WB images of three replicates of TGF-β (5 ng/mL) stimulation (+) for 3 days compared to unstimulated (-) cells with 10.0 µg protein loaded per well. C7 protein levels were normalized to the unstimulated well. **B.** WB images of three replicate transductions of C7-tdTomato +dCas9-VP64 cells with sgRNAs for NT (control), *DENND4B*, *TYROBP*, and *COL7A1* (9.6µg protein was loaded per well). Cells were in puromycin selection for 5 days to ensure sgRNA integration. C7 protein levels were normalized to the NT sgRNA well. **C.** Western blots for two replicates of RDEB keratinocytes incubated with the respective compound for 3 days (12.5µg protein loaded per well). Drug concentrations were as follows: cyanidin 25µg/mL, peonidin 25µg/mL, dasatinib 50nM, indomethacin 10µg/mL, and kaempferol 20µM. C7 protein levels were normalized to the untreated well.

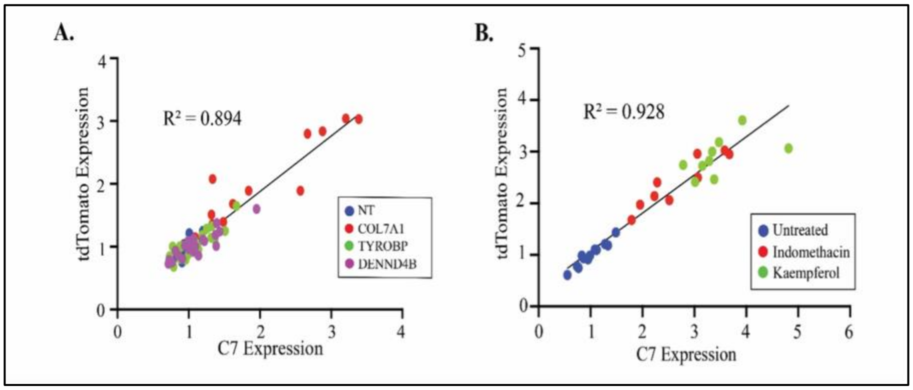

Figure S4: Correlation of C7 and tdTomato Expression in C7-tdTomato cells. Correlation curves of qRT-PCR data for tdTomato (y-axis) and C7 (x-axis) for **A.** C7-tdTomato + dCas9-VP64 cells transduced with specified sgRNAs and **B.** drug-treated C7-tdTomato cells. Ct values for each gene were normalized to the mean Ct value of cells transduced with non-targeting sgRNAs (A) or untreated cells (B).

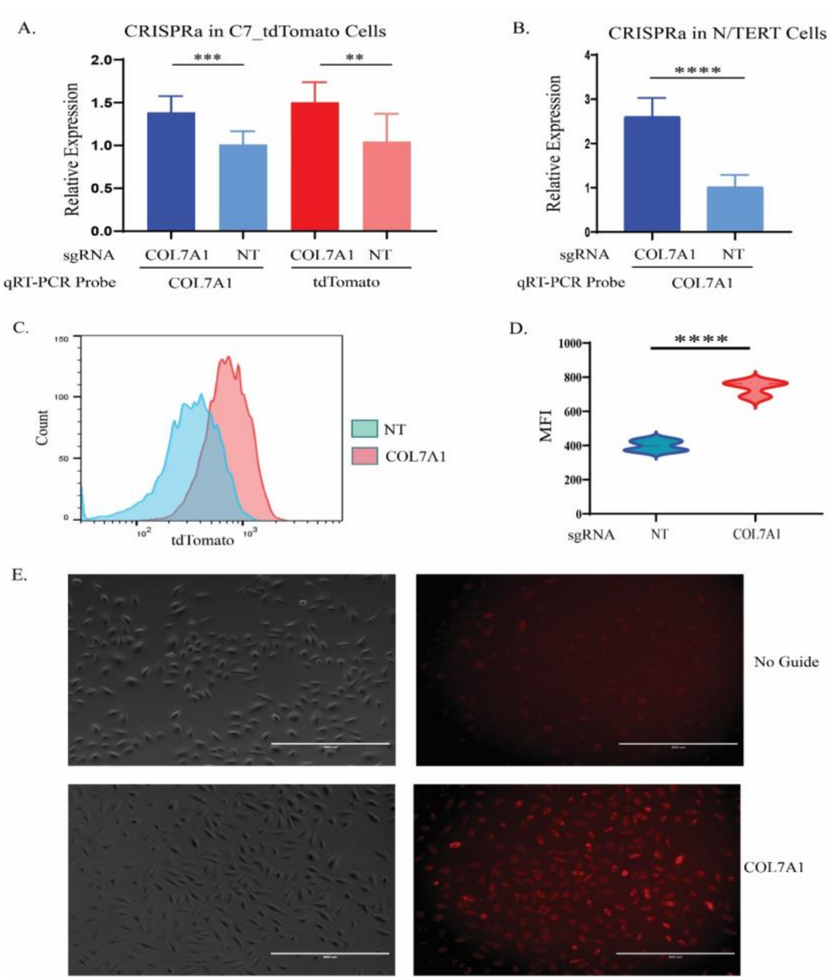

Figure S5: Validation of the CRISPRa System in C7-tdTomato cells. A. qRT-PCR demonstrates induced transcription by the CRISPRa system. C7-tdTomato +dCas9_VP64 cells transduced with a pool of *COL7A1* sgRNA exhibited proportional upregulation of *COL7A1* and tdTomato mRNA compared to NT sgRNA. **B.** N/TERTs + dCas9_VP64 also demonstrated upregulation of *COL7A1* mRNA with *COL7A1* sgRNAs compared to NT sgRNA. FACS analysis shows induced tdTomato/C7 protein expression by the CRISPRa system, as measured by mean fluorescence intensity (MFI). **C.** Histogram comparing C7-tdTomato + dCas9_VP64 cells transduced with either *COL7A1* sgRNAs or NT sgRNA. **D.** The tdTomato MFI plotted for replicate samples transduced with each guide. **E.** Fluorescent microscopy images represent tdTomato fluorescence upregulation in C7-tdTomato + dCas9_VP64 cells transduced with *COL7A1* sgRNAs. Bright field images shown for comparison.

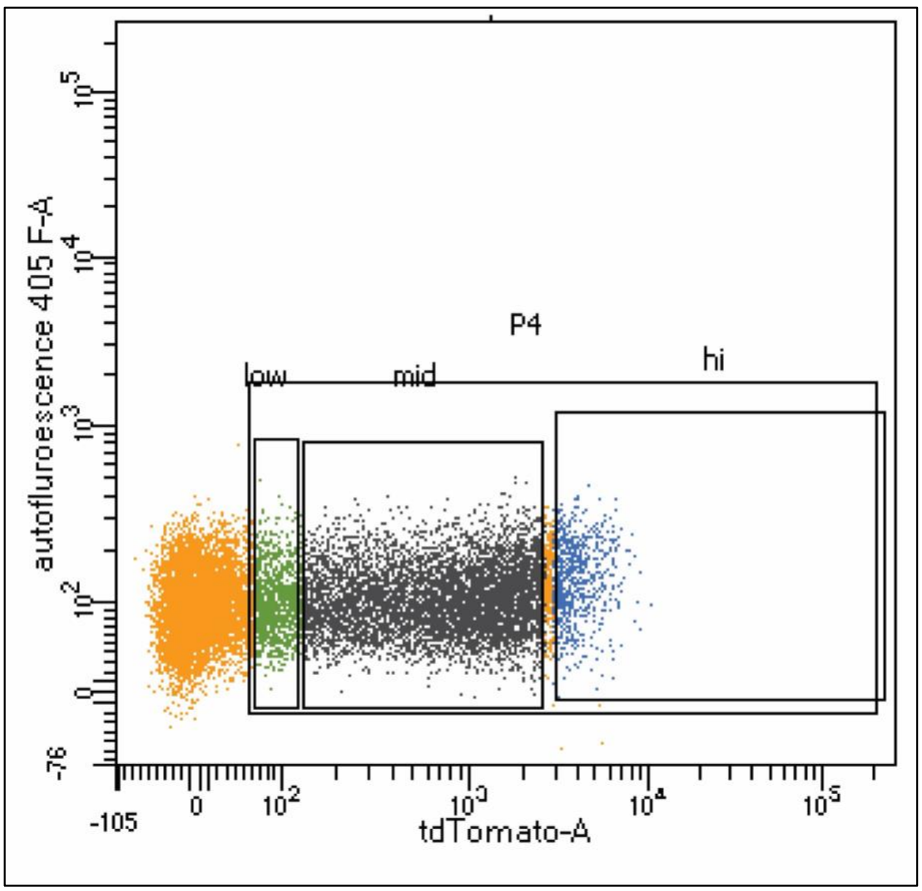

Figure S6: CRISPRa Main Screen FACS Sort. The lentiviral sgRNA library was transduced into the C7-tdTomato +dCas9_VP64 cells and selected for integration. FACS was used to collect the highest tdTomato/C7 expressing cells for PCR and sequence analysis. The box labeled "hi" corresponds to the tdTomato-high population (650,782 cells).

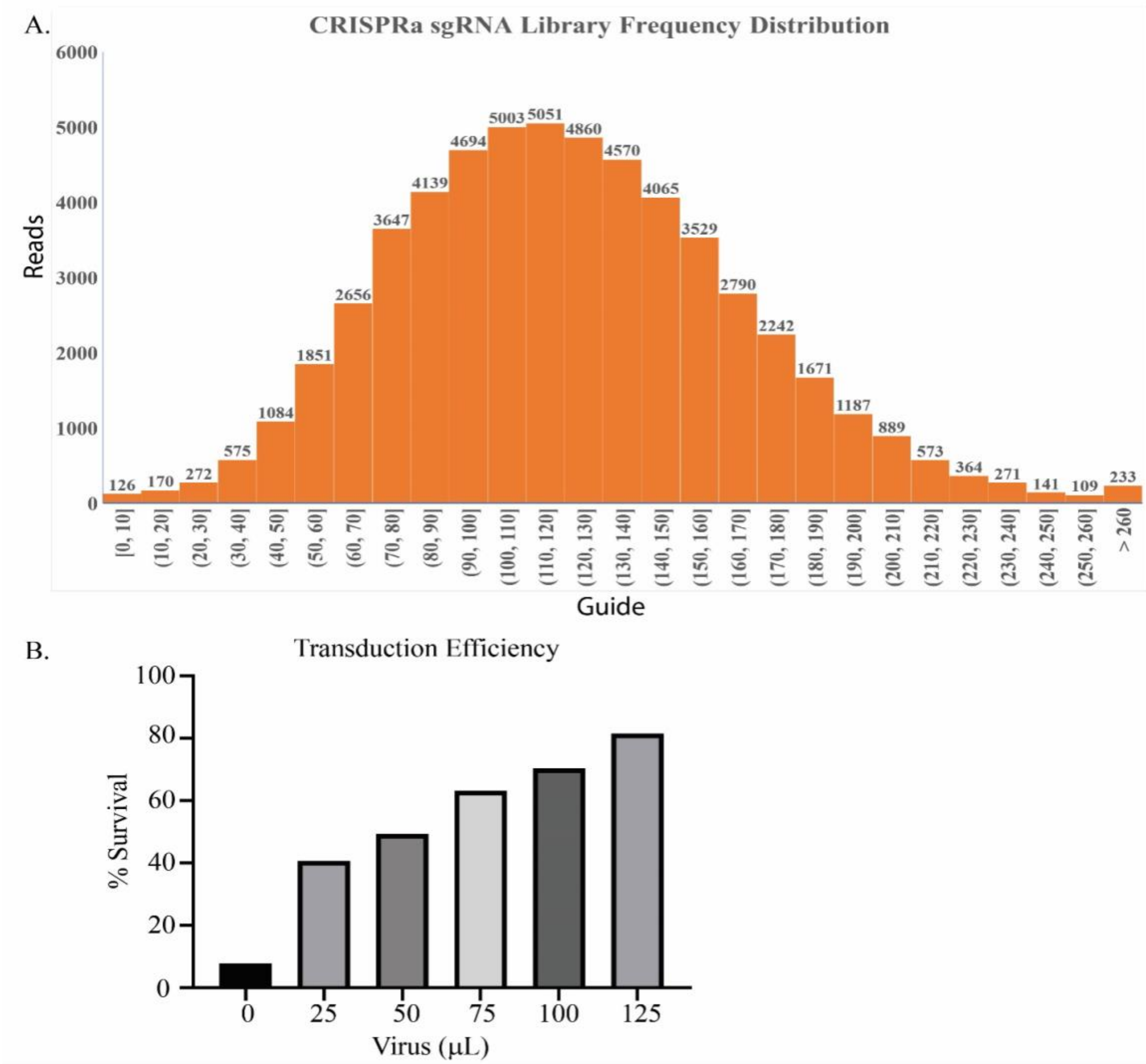

Figure S7: sgRNA Library Validation. A. sgRNA distribution was assessed by plotting the number of unique 20-base sequences in the sgRNA library by the number of reads corresponding to each unique sequence, resulting in a normal distribution of the unique sgRNA representation in the library. **B.** The transduction efficiency assay was performed with the N/TERTs using one aliquot of a large production batch of sgRNA library lentivirus to determine the volume of sgRNA library lentivirus to use for CRISPRa screen. Optimal transduction efficiency for the CRISPRa screen is 30-50% to maximize the number of transduced cells with only one sgRNA/cell (Piccioni 2018, Sanson 2018).

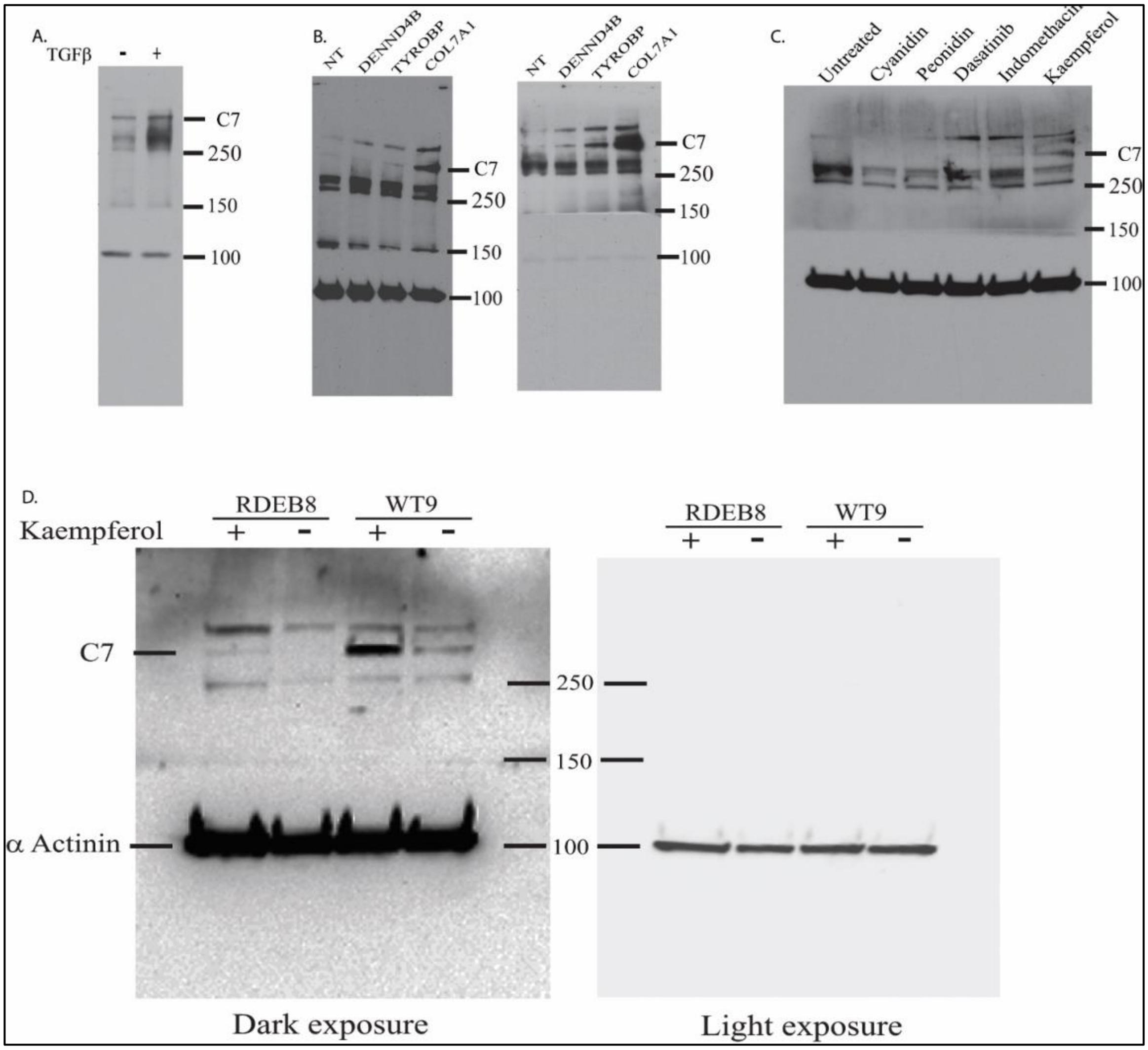

Figure S8: Western blot analysis. Representative Western blots (WB) for C7 protein (size 295 kDa) performed on whole cell lysates, including extracellular matrix, collected from culture plates with α-actinin (size 100 kDa) as loading control. **A.** TGF-β (5ng/mL) stimulation (+) and unstimulated (-) cells (10.0µg protein loaded per well). **B.** Replicate transductions of C7-tdTomato +dCas9-VP64 with sgRNAs for NT (control), *DENND4B*, *TYROBP*, and *COL7A1* (9.6µg protein loaded per well). **C.** RDEB8 cells treated with respective compound (12.5µg protein loaded per well). Drug concentrations were the same as **Figure 4B**. C7 protein levels were normalized to the untreated well. **D.** RDEB8 and WT9 cells incubated with 20mM kaempferol (+) and untreated (-) cells (15µg protein loaded per well).

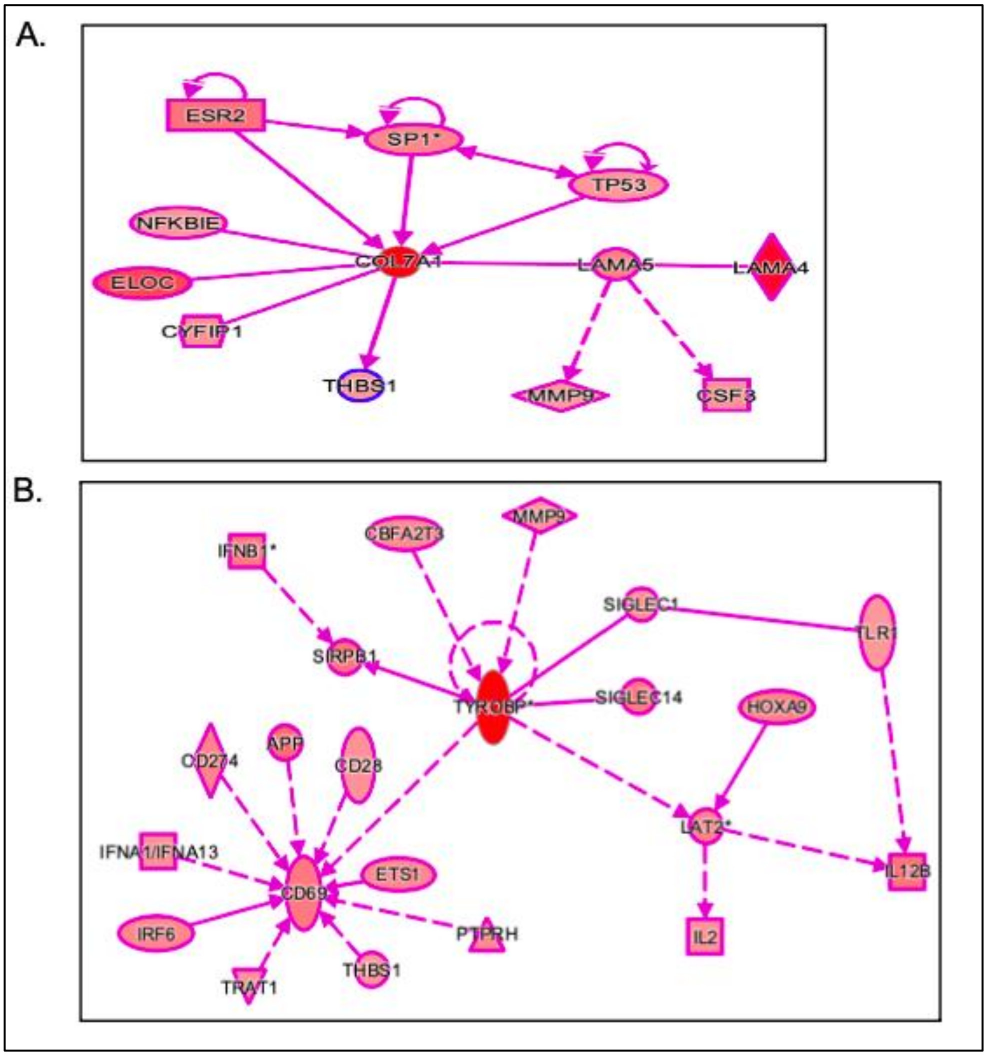

Figure S9: Pathway analysis of CRISPRa screen. A. Map of interactions between C7 and genes enriched in the screen whose products have been previously shown to interact with C7. **B.** Map of interactions between TYROBP and genes enriched in the screen whose products have been previously shown to interact with TYROBP.

SUPPLEMENTARY TABLES

Table S1: Upstream regulators that had significant overlap p-values ($p < 0.05$) and were predicted to be activated ($Z > 2.0$) or inhibited ($Z < -2.0$) in the tdTom-high population by Ingenuity Pathway Analysis (IPA). Overlap p-value is calculated based on the number of genes in the gene list that are known to be regulated by a given regulator. Activation Z-score is based on the changes in gene expression (or in this case, sgRNA abundance) relative to the known regulatory effect of a given regulator on that gene.

Upstream Regulator	Activation Z-Score	p-value of overlap	Downstream Genes	Consistent with Activation
NFkB complex	5.809	3.08E-02	52	38
IFN-γ	5.716	4.03E-02	106	76
TLR9	4.681	1.63E-02	24	23
SMARCA4	4.585	3.58E-02	51	33
IRF7	4.434	2.16E-03	21	21
TLR4	4.100	1.01E-02	36	22
PRL	3.912	1.64E-02	27	24
RAF1	3.904	8.03E-03	23	18
IFNA2	3.818	4.71E-03	26	22
STAT1	3.630	3.09E-02	32	23
IRF3	3.603	2.62E-02	20	17
CEBPB	3.360	3.10E-02	37	26
IFN-β	3.273	1.64E-03	19	14
SREBF1	3.243	2.62E-02	24	17
KLF4	3.223	3.93E-02	27	21
IFNL1	3.097	3.87E-02	10	10
IFI16	3.080	2.13E-02	10	10
SRC	3.059	8.77E-03	15	12
CTNNB1	3.023	2.27E-02	74	25
SASH1	3.000	3.00E-02	9	9
DOCK8	3.000	2.54E-02	9	9
JUNB	2.903	2.70E-02	16	9
CREBBP	2.856	3.05E-02	34	11
EP300	2.841	2.23E-02	38	12
ERK1/2	2.816	2.52E-02	28	21
TRAF6	2.749	2.76E-02	9	8
TLR8	2.635	2.42E-02	7	7
EP400	2.630	1.35E-02	7	7
SMPD1	2.611	3.95E-02	7	7
E2F2	2.611	3.51E-02	9	7

CHUK	2.595	4.05E-02	20	14
PTGS2	2.539	2.13E-02	19	12
IFNB1	2.534	1.57E-02	28	16
FLT1	2.530	1.18E-02	11	9
ARHGAP21	2.449	4.71E-02	6	6
USF2	2.390	3.91E-02	8	6
CTCF	2.357	3.71E-02	14	8
OSM	2.322	3.26E-02	46	31
RNY3	2.236	2.30E-02	5	5
Hmgn3	2.219	1.06E-02	6	5
IL17C	2.213	2.30E-02	5	5
MAPK3	2.204	4.14E-02	10	7
CXCL12	2.191	6.51E-03	22	16
JUN	2.172	1.41E-02	43	20
PGR	2.167	1.28E-02	29	19
FGF2	2.165	4.89E-02	35	20
TGFA	2.164	4.34E-03	12	10
CCR2	2.111	4.86E-02	12	9
TNFRSF1B	2.075	2.65E-02	12	8
ESRRA	2.032	4.55E-04	24	6
GRB2	-2.121	1.70E-02	8	7
RICTOR	-2.216	1.39E-02	27	20
miR-30a-3p	-2.224	1.17E-02	5	5
LINC00941	-2.433	2.76E-02	6	6
SIRT1	-2.589	2.65E-02	36	22
PAX1	-2.646	2.17E-02	7	7
miR-21-5p	-2.947	3.00E-02	9	9
miR-146a-5p	-3.317	3.89E-02	11	11
IL1RN	-3.845	1.42E-02	15	15
GRIN3A	-4.123	6.15E-04	17	17

Table S2: Diseases and functions that had significant overlap ($p < 0.05$) and were predicted to be activated ($Z > 2.0$) in the tdTom-high population according to IPA.

Diseases or Functions Annotation	Activation Z-score	p-value of overlap	# Genes
Inflammatory response	4.321	3.16E-04	107
Immune response of leukocytes	4.173	8.34E-03	41
Differentiation of PBMCs	2.828	1.45E-03	8
Uptake of Ca2+	2.816	9.72E-03	12
Transport of carboxylic acid	2.522	7.94E-03	16
Reactivation of virus	2.433	7.08E-03	6
Axonogenesis	2.392	9.25E-03	31
Differentiation of TREG cells	2.368	2.05E-03	6
Response of peritoneal macrophages	2.252	5.25E-03	8
Differentiation of peripheral blood monocytes	2.236	7.39E-03	5
Internalization of virus	2.200	4.01E-03	6
Formation of skin	2.132	4.03E-04	60
Shape change of axons	2.084	3.80E-03	15

Table S3: Canonical pathways that had significant overlap ($p < 0.05$) and were predicted to be activated ($Z > 2.0$) in the tdTom-high population according to IPA.

Ingenuity Canonical Pathways	Activation Z-score	p-value	# Genes
IL-15 Production	3.606	3.24E-02	13
Triacylglycerol Degradation	3.000	1.82E-03	9
Retinoic acid Mediated Apoptosis Signaling	3.000	1.00E-02	9
Retinol Biosynthesis	2.646	3.39E-03	8
Crosstalk between Dendritic and Natural Killer Cells	2.646	4.37E-02	10
Thyroid Hormone Metabolism II	2.449	2.57E-02	6
Role of PI3K/AKT Signaling in Influenza Pathogenesis	2.333	1.48E-02	9
Apelin Liver Signaling Pathway	2.236	1.86E-02	5
IRF Activation by Cytosolic Pattern Recognition Receptors	2.121	3.63E-02	8

Table S4: Compounds used in targeted drug screen, rationale, and associated publications.

Drug	Function/Rationale	Reference
Allantoin	Wound healing	Murrell 2020
ATP	Increases purinergic signaling	Borges de Silva 2020
β-estradiol	Increases C7 & TYROBP	Haure-Mirande 2017; Reese 2018
Bexarotene	Increases TYROBP; decreases inflammation	Lefterov 2015; Zuo 2019
Cyanidin-3-O-glucoside	Increases TYROBP; decreases inflammation	Li 2020
Cholera Toxin	Increases cAMP & purinergic signaling	Simard 2020
Clobetasol	Skin treatment	Warner 2008
Cyclosporin A	Skin treatment; decreases Ca2+ signaling	Santini 2001
Dasatinib	Tyrosine kinase inhibitor; inhibits ephrin B	Zhu 2015; Mavrogonatou 2020
Decitabine	Affects TGFB Signaling	Sufaru 2017
Delphinidin-3-O-glucoside	Increases TYROBP; decreases inflammation	Li 2020
Diacerein	Wound healing in EBS; IL1B inhibitor	Prodinger 2019
FK-506	Skin treatment; decreases Ca2+ signaling	Santini 2001
Fludarabine	Nucleoside analog; inhibits HIF1a & VEGF	Fang 2004; Xue 2007
Gentamicin	Antibiotic; increases C7	Woodley 2017
Indomethacin	Decreases purinergic signaling	Ehrlich 1986
Ionomycin	Increases Ca2+ signaling	Malsy 2019
Kaempferol	May increase TYROBP through p53; decreases inflammation and fibrosis	Chen & Chen 2013; Liu 2019; Zajkowicz 2018
Losartan	Decreases inflammation & fibrosis	Nystrom 2015
Malvidin-3-O-glucoside	Increases TYROBP; decreases inflammation	Li 2020
Methapyrilene	Increases TYROBP	Haure-Mirande 2017
Norepinephrine	Increases purinergic & TGF-β signaling	Luckett-Chastain 2009
PDGF	Wound healing treatment	Beer 1997; Gope 2002
Peonidin-3-O-glucoside	Increases TYROBP; decreases inflammation	Li 2020
Quercetin	Inhibits PI3K/Akt/mTOR signaling	Zhu 2015, Mavrogonatou 2020

Table S5: Primer and sgRNA sequences.

Purpose	Name	Sequence
Create DSBs in COL7A1 C-terminus	COL7A1 G1	GTCCTCACCAGGTACTGCCC PAM AGG
	COL7A1 G2	CATTATCTGGGCCTCAGTCC PAM TGG
	COL7A1 G3	ATTATCTGGGCCTCAGTCCT PAM GGG
Create P2A-tdTomato insert	BSPQ1_G1_P2A_F	GACGCTCTTCACCGGTCCTCACCAGGTACTGCCCA GGACGCTACTAACTTCAGCCTGCT
	BSPQ1_G1_tdT_R	GACGCTCTTCCATGGTCCTCACCAGGTACTGCCCA GGTTACTTGTACAGCTCGTCCA
PCR confirmation of C7-tdTomato fusion	5': COL7A1_CC_F2	CTTCCATGTTCCCTCCTTTA
	5': tdTomato-R2	GGTCTTCTTCTGCATTACG
	3': tdTomato-F1	CGCTGATCTACAAGGTGAA
	3': COL7A1_CC_R1	AATCAGCACCATGTCATCA
	WT: COL7A1_F2	CTTCCATGTTCCCTCCTTTA
	WT: COL7A1_R2	ATGTCATCACAGGCTTGG
PCR confirmation of dCas9-VP64 integration	dCas9_4121_F1	AGAACCGCCAGAAGAAGA
	dCas9_4846_R1	TCTCAGGATGTCGCTCAG
Oligo sequences for cloning individual CRISPRa (Ca) and CRISPRi (Ci) sgRNAs into sgRNA expression plasmid	COL7A1_Ca_G1_F	CACCGTCCTCACCAGGTACTGCCC
	COL7A1_Ca_G1_R	AAACGGGCAGTACCTGGTGAGGAC
	COL7A1_Ca_G2_F	CACCGCATTATCTGGGCCTCAGTCC
	COL7A1_Ca_G2_R	AAACGGACTGAGGCCCAGATAATGC
	COL7A1_Ca_G3_F	CACCGATTATCTGGGCCTCAGTCCT
	COL7A1_Ca_G3_R	AAACAGGACTGAGGCCCAGATAATC
	TYROBP_Ca_G1_F	CACCGAATCAGGCCCAGACACCCAG
	TYROBP_Ca_G1_R	AAACCTGGGTGTCTGGGCCTGATTC
	TYROBP_Ca_G2_F	CACCGCCCCAGCAACTAGACGTGAA
	TYROBP_Ca_G2_R	AAACTTCACGTCTAGTTGCTGGGGC
	TYROBP_Ca_G3_F	CACCGCCTTCACGTCTAGTTGCTGG
	TYROBP_Ca_G3_R	AAACCCAGCAACTAGACGTGAAGGC
	DENND4B_Ca_G1_F	CACCGAGTCAGCCTATGGGTGTGTG
	DENND4B_Ca_G1_R	AAACCACACACCCATAGGCTGACTC
	DENND4B_Ca_G2_F	CACCGCAGCCTATGGGTGTGTGTGG
	DENND4B_Ca_G2_R	AAACCCACACACACCCATAGGCTGC
	DENND4B_Ca_G3_F	CACCGTATAGTCTGAGATTCCAACT

	DENND4B_Ca_G3_R	AAACAGTTGGAATCTCAGACTATAC
	COL7A1_Ci_G1_F	CACCGAGACCAGGACTCGGGCTGGA
	COL7A1_Ci_G1_R	AAACTCCAGCCCGAGTCCTGGTCTC
	COL7A1_Ci_G2_F	CACCGCGCAGGCAAGACCAGGACT
	COL7A1_Ci_G2_R	AAACAGTCCTGGTCTTGCCTGCGC
	COL7A1_Ci_G3_F	CACCGCGGACGCGCAGGCAAGACC
	COL7A1_Ci_G3_R	AAACGGTCTTGCCTGCGCGTCCGC
	NT_G1_F	CACCGACAAAGATCGCATGGCATAC
	NT_G1_R	AAACGTATGCCATGCGATCTTTGTC
TaqMan qRT-PCR Probes	COL7A1 Probe	Hs00164310_m1
	TYROBP Probe	Hs00924511_g1
	DENND4B Probe1	Hs00208230_m1
	DENND4B Probe2	Hs00972874_m1
	GAPDH Probe	Hs02786624_g1
	tdTomato Probe	Mr07319439_mr
PCR primers for amplifying sgRNA sequence from sgRNA expression construct	P5 Primer	5’AATGATACGGCGACCACCGAGATCTACACTCTTTCCCTACACGACGCTCTTCCGATCT[s]TTGTGGAAAGGACGAAACACCG
	P7 Primer	5’CAAGCAGAAGACGGCATACGAGATNNNNNNNNGTGACTGGAGTTCAGACGTGTGCTCTTCCGATCTTCTACTATTCTTTCCCCTGCACTGT
PCR F Primers containing variable Illumina P5 adapter sequences - denoted as [s] in P5 PCR primer	CRISPRa_P5_0	AATGATACGGCGACCACCGAGATCTACACTCTTTCCCTACACGACGCTCTTCCGATCTTTGTGGAAAGGACGAAACACCG
	CRISPRa_P5_1	AATGATACGGCGACCACCGAGATCTACACTCTTTCCCTACACGACGCTCTTCCGATCTCTTGTGGAAAGGACGAAACACCG
	CRISPRa_P5_2	AATGATACGGCGACCACCGAGATCTACACTCTTTCCCTACACGACGCTCTTCCGATCTGCTTGTGGAAAGGACGAAACACCG
	CRISPRa_P5_3	AATGATACGGCGACCACCGAGATCTACACTCTTTCCCTACACGACGCTCTTCCGATCTAGCTTGTGGAAAGGACGAAACACCG
	CRISPRa_P5_4	AATGATACGGCGACCACCGAGATCTACACTCTTTCCCTACACGACGCTCTTCCGATCTCAACTTGTGGAAAGGACGAAACACCG

	CRISPRa_P5_6	AATGATACGGCGACCACCGAGATCTACACTCTTTCCCTACACGACGCTCTTCCGATCTTGCACCTTGTGGAAAGGACGAAACACCG
	CRISPRa_P5_7	AATGATACGGCGACCACCGAGATCTACACTCTTTCCCTACACGACGCTCTTCCGATCTACGCAACTTGTGGAAAGGACGAAACACCG
	CRISPRa_P5_8	AATGATACGGCGACCACCGAGATCTACACTCTTTCCCTACACGACGCTCTTCCGATCTGAAGACCCTTGTGGAAAGGACGAAACACCG
PCR R Primers containing Illumina P7 adapter sequences and barcodes for multiplexing	CRISPRa_P7_BC1	CAAGCAGAAGACGGCATACGAGATCGGTTCAAGTGACTGGAGTTCAGACGTGTGCTCTTCCGATCTTCTACTATTCTTTCCCCTGCACTGT
	CRISPRa_P7_BC2	CAAGCAGAAGACGGCATACGAGATGCTGGATTGTGACTGGAGTTCAGACGTGTGCTCTTCCGATCTTCTACTATTCTTTCCCCTGCACTGT
	CRISPRa_P7_BC3	CAAGCAGAAGACGGCATACGAGATTAACTCGGGTGACTGGAGTTCAGACGTGTGCTCTTCCGATCTTCTACTATTCTTTCCCCTGCACTGT
	CRISPRa_P7_BC4	CAAGCAGAAGACGGCATACGAGATTAACAGTTGTGACTGGAGTTCAGACGTGTGCTCTTCCGATCTTCTACTATTCTTTCCCCTGCACTGT
	CRISPRa_P7_BC5	CAAGCAGAAGACGGCATACGAGATATACTCAAGTGACTGGAGTTCAGACGTGTGCTCTTCCGATCTTCTACTATTCTTTCCCCTGCACTGT

Table S6: Mean fluorescence intensity fold change data for initial testing of compounds used in targeted drug screen.

Drug	Concentration	MFI FC	Drug	Concentration	MFI FC
Allantoin	25uM	1.14	Decitabine	10uM	1.22
	50uM	1.04		20uM	0.94
	100uM	1.48	Diacerein	12.5uM	1.53
ATP	6.25uM	0.95		25uM	1.64
	12.5uM	1.31		50uM	2.21
	12.5uM	1.22	FK-506	2.5ug/mL	1.32
	25uM	1.15		5ug/mL	0.88
	25uM	1.45		10ug/mL	0.96
	50uM	1.76	Fludarabine	10nM	0.74
	100uM	0.93		100nM	1.08
	200uM	1.28		1uM	0.86

	400uM	1.15	PDGF	2.5ug/mL	0.76
β-estradiol	100nM	0.99		5ug/mL	0.74
	1uM	1.06		10ug/mL	0.89
	10uM	2.02	Indomethacin	2.5ug/mL	0.78
Bexarotene	250nM	0.72		5ug/mL	1.28
	500nM	0.77		10ug/mL	1.34
	1uM	0.96	Ionomycin	250nM	1.13
Cholera toxin	2.5ug/mL	0.78		500nM	0.74
	5ug/mL	0.77	Kaempferol	5uM	1.27
	10ug/mL	0.80		10uM	1.33
Clobetasol	250nM	0.82		20uM	1.66
	500nM	1.30	Losartan	100nM	0.97
	1uM	0.82		1uM	0.94
Cyclosporin A	500nM	0.80		10uM	1.11
	1uM	0.68	Methapyrilene	5ug/mL	0.97
	2uM	0.85		10ug/mL	0.42
	5uM	1.39		20ug/mL	1.00
Dasatinib	6.25nM	1.06	Norepinephrine	2.5uM	0.87
	12.5nM	1.19		5uM	0.69
	25nM	0.96		10uM	0.64
	50nM	1.39	PDGF	2.5ng/mL	0.80
	100nM	1.67		5ng/mL	1.00
	200nM	1.12		10ng/mL	1.06
Decitabine	0.875uM	1.37	Quercetin	25nM	0.57
	1.75uM	1.17		50nM	0.52
	2.5uM	1.19		100nM	0.55
	5uM	0.81			

CHAPTER 3

IDENTIFICATION OF NOVEL DRIVERS AND INHIBITORS OF PROLIFERATION IN KERATINOCYTES AND PROGRESSIVELY DYSREGULATED GENES IN RDEB DISEASE PROGRESSION

SUMMARY

Recessive dystrophic epidermolysis bullosa (RDEB) is a severe genetic skin blistering disease caused by loss or reduced function of type VII collagen, which is encoded by *COL7A1*. RDEB is characterized by extreme skin fragility resulting in repeated wounding and blistering, progressively worsening fibrosis and scarring, and eventually aggressive cutaneous squamous cell carcinoma (cSCC). People with RDEB start to develop cSCC much earlier than the general population and often develop multiple primary tumors, which rapidly progress and metastasize. RDEBSCC can be difficult to diagnose and is essentially untreatable even when caught early, highlighting the need for more effective diagnostic tools and biomarkers. RNA-sequencing and genome-wide CRISPR activation/inhibition (CRISPRai) screens of wild-type, RDEB, and RDEBSCC keratinocytes were used to identify novel candidate genes that could be useful in studying the development and progression of RDEB and RDEBSCC. There were 90 genes whose expression progressively increased or decreased from wild-type to RDEB to RDEBSCC, including *SEMA5A*, which was also identified in two CRISPRa screens as a potential driver of proliferation in keratinocytes. Another gene, *QPRT*, was massively downregulated in RDEBSCC cells relative to both wild-type and RDEB keratinocytes and was one of only 52 genes that were enriched in CRISPRi screens from four distinct cell lines. This work highlights the utility of utilizing multiple genome-wide approaches to identify novel genes in rare diseases and other conditions.

INTRODUCTION

Recessive dystrophic epidermolysis bullosa (RDEB) is a heritable blistering disease caused by mutations in the *COL7A1* gene, which encodes type VII collagen (C7). C7 is involved in multiple aspects of skin biology, including (1) anchoring the epidermis to the dermis, (2) mediating re-epithelialization and maturation of granulation tissue during wound healing, and (3) establishing front-to-rear polarity in keratinocytes (Sakai 1986, Shimizu 1996, Nystrom 2013, Dayal 2013). RDEB is characterized by extreme skin fragility and repeated cycles of wounding and blistering that eventually lead to scarring, fibrosis, and aggressive cutaneous squamous cell carcinoma (cSCC) (Fine 2014). RDEB-associated cSCC (henceforth RDEBSCC) usually develops in areas of chronic wounding, and patients often develop multiple primary tumors (Tomita 2003, Fine 2009).

The risk of developing RDEBSCC rises dramatically as patients age, with a cumulative risk of over 80% by age 45 (Fine 2009). RDEBSCC also accounts for more than two thirds of all patient deaths, largely due to the high rate of metastasis (Fine 2009). The preferred first-line treatment for RDEBSCCs is wide local excision, but amputation may be recommended when the former is not possible (Mellerio 2016). Radiotherapy and chemotherapy have been used in some contexts but are highly damaging to the already fragile skin of RDEB patients (Mellerio 2016). There have been instances of RDEB patients with SCC responding favorably to inhibitors of epidermal growth factor receptor (EGFR) and programmed cell death protein 1 (PD-1), but these cases are patient-specific, and the response is often short-lived (Arnold 2009, Kim 2013, Diociaiuti 2019, Medek 2019, Has 2020c, Khaddour 2020, Reimer 2020). The multikinase inhibitor rigosertib was recently shown to induce apoptosis in ten different RDEBSCC samples *in vitro* and in RDEBSCC xenografts with low toxicity for non-cancerous cells (Atanasova 2019b). These results have led to the authorization of two early phase clinical trials to evaluate the use of rigosertib in patients (NCT03786237 and NCT04177498). Early detection is crucial for successful excision/treatment, but RDEBSCCs are difficult to diagnose because they occur in areas of chronic wounds and can be mistaken for granulation tissue or ulceration (Mellerio 2016). Unfortunately, successful excision/treatment of a primary RDEBSCC does not preclude the development of additional tumors, so these are temporary measures at best.

To improve diagnosis and prevent/treat RDEBSCC, it is crucial to elucidate the mechanisms of RDEBSCC development and progression. Numerous studies have demonstrated that the RDEB skin microenvironment is conducive to SCC development, which is characterized by chronic inflammation and progressively worsening fibrosis due to impaired wound healing. Previous studies have shown that RDEB skin and blood serum have higher levels of proinflammatory cytokines, such as IL-1β, IL-6, TNF-α, and IFN-γ (Petrof 2013, Odorisio 2014, Esposito 2016, Cianfarani 2017). TGF-β signaling, a main driver of fibrosis, is also elevated in the skin of humans and mice with RDEB (Fritsch 2008, Ng 2012, Kuttner 2013, Nystrom 2013, 2015, 2018; Odorisio 2014, Martins 2016, Mittapalli 2016, Guerra 2017, Zhang 2018, Atanasova 2019b, Chacon-Solano 2019, Cianfarani 2019, Condorelli 2019a, 2019b; Liu 2019).

Characterization of 27 RDEBSCCs using RNA, whole-genome, and whole-exome sequencing found that the copy number variants (CNVs) and driver/tumor suppressor gene mutations in RDEBSCCs largely resembled those seen in sporadic/UV-induced SCC (UVSCC), head and neck SCC (HNSCC), and lung SCC (LSCC) (Cho 2018). RDEBSCCs had lower mutational burdens than UVSCC and the mutation profiles of RDEBSCCs were characterized by high rates of mutations from the APOBEC (apolipoprotein B mRNA-editing enzyme catalytic polypeptide-like) family of cytosine deaminases rather than UV radiation (Cho 2018). When the mutation signature and gene expression profiles were compared with other SCC types, RDEBSCCs showed the greatest similarity with the basal and mesenchymal subtypes of HNSCC rather than UVSCC (Cho 2018). Although these studies provided substantial insight into the contributions of the microenvironment and the mutational landscape of RDEBSCC, there are still many unanswered questions regarding the development and progression of RDEBSCC, highlighting the need for further investigations.

In this study, we characterized the gene expression profiles of nine HLA-matched sibling pairs of wild-type and RDEB keratinocytes (WTKs & RDEBKs) and six RDEBSCC cell lines to identify clinically relevant differences related to cancer formation, progression, and metastasis. Then, we used genome-wide CRISPR activation (CRISPRa) and inhibition (CRISPRi) screens to identify novel drivers and inhibitors of proliferation in keratinocytes and RDEBSCC cells. We identified three genes (*QPRT*, *SEMA5A*, and *TAFA3*) that were significantly differentially expressed in one or more RNA-seq comparisons and were also found to drive (*SEMA5A*) or inhibit (*QPRT* and *TAFA3*) proliferation in keratinocytes. To our knowledge, none of these genes have been investigated in the context of RDEB (or RDEBSCC) and therefore warrant further investigation.

RESULTS

RNA-seq of wild-type, RDEB, and RDEBSCC keratinocytes

Due to its propensity for local recurrence and metastasis, RDEBSCC is nearly impossible to treat, even when tumors are identified early enough to be excised. To investigate disease progression and SCC development in RDEB, we used RNA-seq to analyze gene expression and identify differentially expressed genes (DEGs) in keratinocytes from nine RDEB patients (RDEBK) and their healthy, HLA-matched siblings (WTK), as well as six cell lines derived from RDEBSCC tumors (**Figure 1**). Reads were mapped to the GRCh38/hg38 reference genome using HISAT2 (Kim 2019) and data filtering, normalization, and differential gene expression tests were performed using the Bioconductor package edgeR (Robinson & Smyth 2007, 2008; Robinson, McCarthy, & Smyth 2010; Robinson & Oshlack 2010; McCarthy, Chen, & Smyth 2012; Chen, Lun, & Smyth 2014, 2016; Dai 2014; Zhou, Lindsay, & Robinson 2014; Lun, Chen, & Smyth 2016).

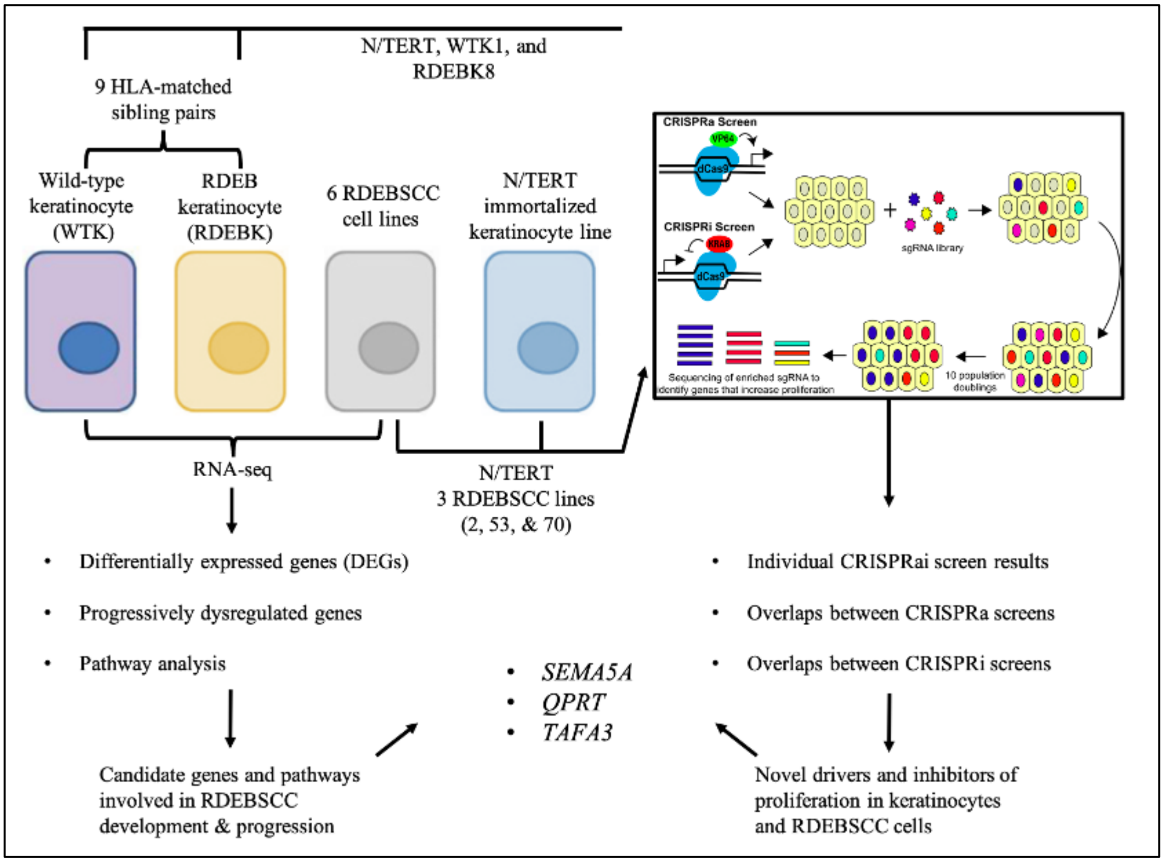

Figure 1: Overview of methodology and data analysis.

We used edgeR to perform differential gene expression tests between RDEBKs and WTKs that also factored in differences between the pairs, which is similar to a paired t-test. There were 63 genes that were significantly differentially expressed ($q<0.05$; q = FDR-corrected p-value) between RDEBKs and WTKs, with 42 increased (>1.25-fold) and 21 decreased (< -1.25-fold) in RDEBKs relative to WTKs (**Figure 2A, Table S1**). To identify any enriched functions and/or pathways among these DEGs, we used the Molecular Signatures Database in the Gene Set Enrichment Analysis (GSEA) tool from the BROAD Institute (Subramanian 2005, Liberzon 2011, 2015). There were 12 DEGs that overlapped with the Gene Ontology (GO) term "biological adhesion": *COL1A1*, *CNTNAP4*, *EDIL3*, *HYAL1*, *IL1B*, three protocadherins (*PCDH18*, *PCDH19*, and *PCDHGA2*), *SEMA5A*, *SGCE*, and *TMEM47*. To determine whether any upstream regulators, diseases, or functions were predicted to be activated or inhibited based on the list of

DEGs, we used Ingenuity Pathway Analysis (IPA, QIAGEN). To maximize the usefulness of the approach, we broadened our list of genes to include those that had a p-value < 0.05 (before correcting for multiple testing) and whose expression changed at least 1.25-fold, giving us a list of 640 genes (**Figure 2B**). Based on the gene expression differences of these 640 genes, there were 38 upstream regulators (genes, RNAs, and proteins) predicted to be activated (Z > 2.0) and 25 predicted to be inhibited (Z < -2.0) in RDEBKs (**Tables S2-3**). The activated upstream regulators included terms related to TGF-β signaling, including TGFB1 (Z=3.257, p=1.79E-17), SMAD4 (Z=2.505, p=9.94E-04), TGFBR1 (Z=2.198, p=1.58E-05), and the TGF-β group (Z=2.028, p=2.48E-07). Interestingly, miR-29b-3p, which is inhibited by TGFB/SMAD and has been shown to inhibit *COL7A1*, was predicted to be inhibited (Z=-2.913, p=2.30E-06), further supporting activation of TGF-β signaling (**Table S3**, Vanden Oever 2016). Transcription factors that promote epithelial-to-mesenchymal transition (EMT) were also predicted to be activated, including TWIST1 (Z=2.849, p=1.02E-08), TWIST2 (Z= 2.213, p=2.62E-03), and FOXC2 (Z=2.219, p=1.93E-02, logFC=2.92), and these are regulated by TGF-β (**Table S2**).

There were 12 diseases and functions predicted to be activated (Z>2.0, p<0.05) and 4 predicted to be inhibited (Z<-2.0, p<0.05) in RDEBKs based on our gene list (**Table S4**). The top disease/function by activation Z-score was "fibrosis" (Z=2.984, p=4.37E-07). Fibrosis is a major complication for people with RDEB that gets progressively more severe due to impaired wound healing and chronic inflammation (Condorelli 2019a). Activation of fibrosis is also supported by our upstream regulator data, as TGF-β is a prominent driver of fibrosis (Condorelli 2019a). The other activated diseases/functions included three in the "cell death and survival" category (cell survival, cell viability, and cell viability of neurons) and six related to cancer or precancerous lesions (renal lesion, genitourinary tumor, differentiation of neuroblastoma, mammary tumor, progression of tumor, and growth of solid tumor), suggesting that RDEBKs have altered expression of genes related to proliferation and/or cell death. Taken together, these results suggest that RDEBKs may have a more "mesenchymal" gene expression profile than WTKs due to strong activation of TGF-β signaling leading to activation of pro-EMT and pro-fibrotic signaling cascades.

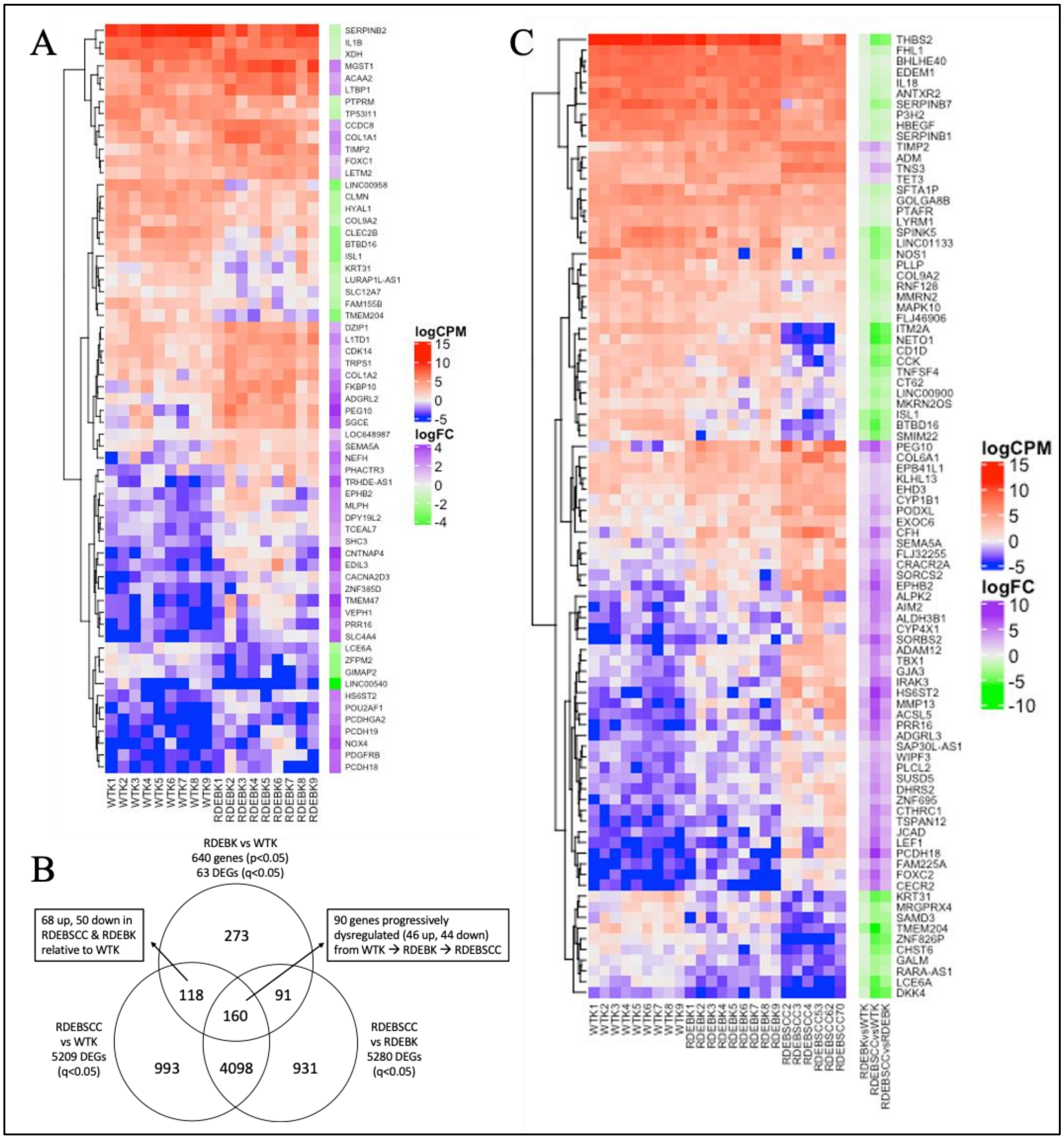

Figure 2: A. Heatmap of the 63 significantly (q<0.05) differentially expressed genes (DEGs) between RDEBKs and WTKs after adjusting for differences across pairs. **B.** Venn diagram showing the number of DEGs overlapping between each comparison. For RDEBK vs WTK, the 640 genes used for pathway analysis were used to calculate overlaps. **C.** Heatmap of the 90 genes that were progressively increased or decreased from WTK to RDEBK to RDEBSCC.

Once we analyzed the differences between RDEBKs and WTKs, the next step in our analysis was to incorporate the gene expression data from the RDEBSCC cell lines. There were 5209 significantly differentially expressed genes ($q < 0.05$) between RDEBSCCs and WTKs, including 2783 increased (FC >1.25) and 2426 decreased (FC < 1.25) in RDEBSCCs relative to WTKs (**Figure 2B**). There were 5280 DEGs between RDEBSCCs and RDEBKs, including 2604 increased and 2676 decreased in RDEBSCC relative to RDEBK (**Figure 2B**). There were 4258 genes that were differentially expressed in RDEBSCC relative to both WTK and RDEBK (**Figure 2B**). For genes that were differentially expressed in both RDEBSCC vs WTK and RDEBSCC vs RDEBK, the direction of expression change (increased or decreased) was always consistent: 2198 were increased and 2060 were decreased in RDEBSCC relative to both WTKs and RDEBKs. Next, we cross-referenced these gene lists with the list of 640 DEGs between RDEBKs and WTKs to look for overlaps. There were 160 genes that were differentially expressed in all three comparisons (**Figure 2B**). Of these 160, there were 46 genes whose expression progressively increased and 44 whose expression progressively decreased from WTK to RDEBK to RDEBSCC (**Figure 2B-C, Table S5**). There were also 118 genes that were differentially expressed in RDEBK vs WTK and RDEBSCC vs WTK (but not RDEBSCC vs RDEBK), including 68 that were increased and 50 that were decreased in both RDEBSCCs and RDEBKs relative to WTKs (**Figure 2B**).

There were numerous genes that encode peptidases and peptidase inhibitors in the list of progressively dysregulated genes, including three increased (*ADAM12*, *MMP13*, *TIMP2*) and three decreased (*SERPINB1*, *SERPINB7*, *SPINK5*). Previous work has shown that MMP13 is strongly expressed in RDEBSCCs, but not in benign hyperkeratotic lesions, and progressively decreases from the tumor through the transitional region (Kivisaari 2008, Hata 2015). ADAM12 was also elevated in the RDEBSCC reported by Hata *et al.* (2015). Absent in melanoma 2 (*AIM2*), which encodes an inflammasome protein, was also progressively upregulated in our data and has been previously shown to increase with cutaneous SCC (cSCC) development (Farshchian

2017). This group also showed that inhibition of AIM2 in cSCC cells inhibited production of MMP1 and MMP13 and inhibited growth and vascularization of cSCC xenografts, suggesting that there is some connection between AIM2 and MMP13 and that these genes could have significant potential as biomarkers and/or therapeutic targets for RDEBSCC (Farshchian 2017).

CRISPRa and CRISPRi screens for drivers and inhibitors of proliferation

After using RNA-seq to identify differentially expressed genes between wild-type, RDEB, and RDEBSCC keratinocytes, we sought to complement this dataset by using more interventional methods to identify genes and pathways that are involved in RDEB disease progression and RDEBSCC development. CRISPR activation and inhibition (CRISPRa, CRISPRi) screens have successfully identified drivers and inhibitors of proliferation (Sanson 2018), mechanisms of drug resistance (Konerman 2015), stem cell differentiation factors (Xiong 2017, Liu 2018, Yang 2019), etc. in a wide variety of cell types. CRISPRa (Calabrese Set A, Addgene ID=92379) and CRISPRi (Dolcetto Set B, Addgene ID=92386) sgRNA plasmid libraries were purchased from Addgene. Libraries were expanded by transforming *E. coli* and isolating the plasmid DNA (pDNA). To verify library composition and determine the relative abundance of each sgRNA, we PCR-amplified the variable region of the plasmid (containing the sgRNA sequence) from pDNA using primers containing Illumina adapter sequences, then sequenced the PCR products on an Illumina MiniSeq. Libraries were packaged into a lentiviral vector for delivery into cells.

For each screen, the cell line of interest was first transduced with a lentiviral construct containing dCas9-VP64 for CRISPRa screen or dCas9-KRAB for CRISPRi screen and an antibiotic resistance gene (blasticidin) to enable selection. Next, we transduced cells stably expressing dCas9-VP64 (or dCas9-KRAB) with the lentiviral sgRNA library specific for either the activation or inhibition screens (Sanson 2018). See materials and methods for cell culture protocols. Once the screens were completed, we harvested the cells, isolated genomic DNA, PCR-amplified the sgRNA region of the sgRNA construct and sequenced the PCR products. The abundance of each sgRNA was calculated as the number of reads corresponding to the sgRNA per million sgRNA reads (counts per million, CPM). sgRNAs with screen CPM values less than 5.0 were removed. We calculated a fold change for each sgRNA by comparing the screen CPM value to the initial CPM value, then calculated Z-scores based on logFC values. sgRNAs with a Z-score greater than 1.75 were considered enriched.

<u>CRISPRi screens for inhibitors of proliferation in keratinocytes and RDEBSCC cells</u>

To identify inhibitors of proliferation in keratinocytes that could also be used to inhibit RDEBSCC growth, we performed CRISPRi screens in the immortalized keratinocyte cell line, N/TERT, as well as three RDEBSCC cell lines (2, 53, and 70) from our RNA-seq data transduced with dCas9-KRAB. There were 1474 enriched sgRNAs ($Z > 1.75$) in the N/TERT CRISPRi screen, including 58 genes with two enriched sgRNAs and 11 genes with three enriched sgRNAs (**Table 1**). There were numerous well-established inhibitors of proliferation in keratinocytes among the genes with multiple enriched sgRNAs, including TP53 (FC= 12.93, 11.67, 11.32) and TP53 binding protein 1 (*TP53BP1*; logFC= 2.53, 2.10, 2.03); several members of the TGF-β signaling pathway, including *TGFB1* (FC= 2.08, 1.86), *TGFBR1* (FC= 8.96, 8.82, 5.08), *TGFBR2* (FC= 11.28, 9.49, 6.24), and *SMAD4* (FC= 8.92, 3.56, 3.50); integrin αV (*ITGAV*, FC= 2.96, 2.72) and β6 (*ITGB6*, FC= 3.17, 2.74), which can activate TGF-β in the ECM during wound healing; ubiquitin-specific peptidase 28 (*USP28*; FC= 5.53, 2.94, 2.77), a deubiquitinase that initiates DNA damage-induced apoptosis; death-associated protein kinase 3 (*DAPK3*; FC= 2.96, 2.57, 2.51), and *ROCK1* (FC= 2.45, 2.00) and *ROCK2* (FC= 1.94, 1.84). The enrichment of these known inhibitors of proliferation in keratinocytes suggests that our CRISPRi screens were robust enough to identify true inhibitors of proliferation.

Next, we examined the results of the RDEBSCC CRISPRi screens (**Table 1**). There were 1466 enriched sgRNAs in the RDEBSCC2 CRISPRi screen, including 46 genes with two enriched sgRNAs and three genes with three enriched sgRNAs. There were 1147 enriched sgRNAs in the RDEBSCC53 CRISPRi screen, including 32 genes with two enriched sgRNAs and six genes with three enriched sgRNAs. There were 1635 enriched sgRNAs in the RDEBSCC70 CRISPRi screen, including 57 genes with two enriched sgRNAs and four genes with three enriched sgRNAs. The RDEBSCC CRISPRi screens did not show enrichment of many of the major inhibitors of proliferation in keratinocytes, likely due to the high rate of mutations and chromosomal abnormalities in RDEBSCCs. For example, none of the sgRNAs for *TP53* were enriched in RDEBSCC2 or RDEBSCC70 while all three were enriched in RDEBSCC53, and none of the sgRNAs for *TP53BP1* were enriched in any of the three RDEBSCC screens.

Table 1: Summary of CRISPRi proliferation screen results.

Cell Line	Enriched sgRNAs	Genes with 2 enriched sgRNAs	Genes with 3 enriched sgRNAs
N/TERT	1474	58	11
RDEBSCC2	1466	46	3
RDEBSCC53	1147	32	6
RDEBSCC70	1635	57	4

We used competition assays to validate the results of the CRISPRi screens. dCas9-KRAB N/TERTs were transduced with a lentiviral construct expressing the sgRNA of interest and GFP (sgRNA-GFP). If the sgRNA targeted gene is an inhibitor of proliferation, transduced (GFP+) cells should proliferate at a higher rate and the percentage of GFP+ cells should increase over time compared to transduction with a non-targeting (NT) sgRNA-GFP (**Figure 3A**). A small group of sgRNAs targeting established inhibitors of proliferation (TGFBR1, TGFBR2, and TP53) in keratinocytes to serve as positive controls for the competition assays. After 10 days, the percentage of GFP+ cells significantly increased in cells transduced with sgRNAs targeting TGFBR1, TGFBR2, and TP53 relative to cells transduced with NT sgRNA (**Figure 3B**). These results show that the competition assay is a suitable method for validating the results of CRISPRi (and CRISPRa) screens.

To identify top candidate genes, we looked for sgRNAs that were enriched in multiple screens. Consistent enrichment of an sgRNA in proliferation-based screens performed in distinct cell lines is a strong indicator that the gene being inhibited by that sgRNA is a true inhibitor of proliferation. Out of 57,011 sgRNAs, only 73 sgRNAs were enriched in all three RDEBSCC CRISPRi screens, and 53 of these sgRNAs were also enriched in the N/TERT CRISPRi screen (**Figure 3C**). All three sgRNAs targeting TAFA chemokine family member 3 (*TAFA3*) were enriched ($Z > 1.75$) in all four CRISPRi screens. Interestingly, *TAFA3* was the only gene with more than one enriched sgRNA in all four screens, making it a top candidate for further investigation. *TAFA3* encodes a small, chemokine-like protein that is generally expressed in the brain.

In addition to *TAFA3*, we chose four other genes with sgRNAs enriched in all four screens for validation with competition assays: C-C motif chemokine ligand 3 (*CCL3)*, protein tyrosine kinase 2β (*PTK2B*), quinolinic acid phosphoribosyltransferase (*QPRT*), and signal transducer and activator of transcription 2 (*STAT2*). *CCL3* encodes macrophage inflammatory protein 1α (MIP-1α), a cytokine that is predominantly produced by CD8+ T cells, but keratinocytes have been shown to produce CCL3 when co-cultured with T cells (Rauschenberger 2019). Interestingly, MIP-1α was found to have the highest degree of homology with the TAFA chemokines when the TAFA family was initially described (Tom Tang 2004). *PTK2B* encodes focal adhesion kinase 2 (FAK2), a non-receptor protein tyrosine kinase that is involved in regulating adhesion, proliferation, migration, and invasion (Shen 2018). *PTK2B* is overexpressed in a variety of different cancers, but there is some evidence that it can act as a tumor suppressor in certain contexts (Shen 2018). *QPRT* encodes an enzyme in the tryptophan-nicotinamide pathway that catalyzes the conversion of quinolinic acid into nicotinic acid mononucleotide, a precursor to NAD+ (Shibata 2018). *QPRT* had two sgRNAs enriched in the N/TERT, RDEBSCC2, and RDEBSCC53 screens, but one sgRNA narrowly missed the cutoff in the RDEBSCC70 screen ($Z=1.59$). *STAT2* encodes a component of the JAK-STAT signaling pathway, a main regulator of the inflammatory response (and other processes). STAT2, together with STAT1 and IRF9, form the interferon-stimulated gene factor 3 (ISGF3) transcription factor complex that mediates canonical type I interferon signaling (Thomas 2015, Owen 2019). STAT2 activates transcription of genes involved in immunoregulation, antigen presentation, and NK cell function, and is generally considered to be a tumor suppressor, suggesting it could also inhibit proliferation in keratinocytes (Thomas 2015, Owen 2019).

To determine whether inhibition of each of these five candidate genes could increase proliferation in keratinocytes, we performed competition assays. After 8 days, the percentage of GFP+ cells significantly increased in N/TERT cultures transduced with sgRNAs for *TAFA3* (all three sgRNAs tested), *PTK2B, QPRT,* and *STAT2* relative to a non-targeting sgRNA control, but no significant changes were detected for *CCL3* (**Figure 3D**). We also looked at the expression of each of these genes in the RNA-seq data to determine whether any of these genes were differentially expressed between WTKs, RDEBKs, and RDEBSCCs. *PTK2B, QPRT, STAT2,* and *TAFA3* were expressed at varying levels across all three cell types, but *CCL3* expression was not detected in any RNA-seq samples. *PTK2B* and *STAT2* were not differentially expressed in any of the comparisons. *TAFA3* was significantly increased in RDEBSCCs relative to RDEBKs, but not WTKs (logFC = 1.67). *QPRT* was significantly decreased in RDEBSCCs relative to both WTKs and RDEBKs (logFC= -4.46, -4.75). Taken together, these results suggest that inhibition of *TAFA3, PTK2B, QPRT,* and/or *STAT2* increases proliferation in non-cancerous keratinocytes, and *QPRT* may also inhibit proliferation of RDEBSCC cells.

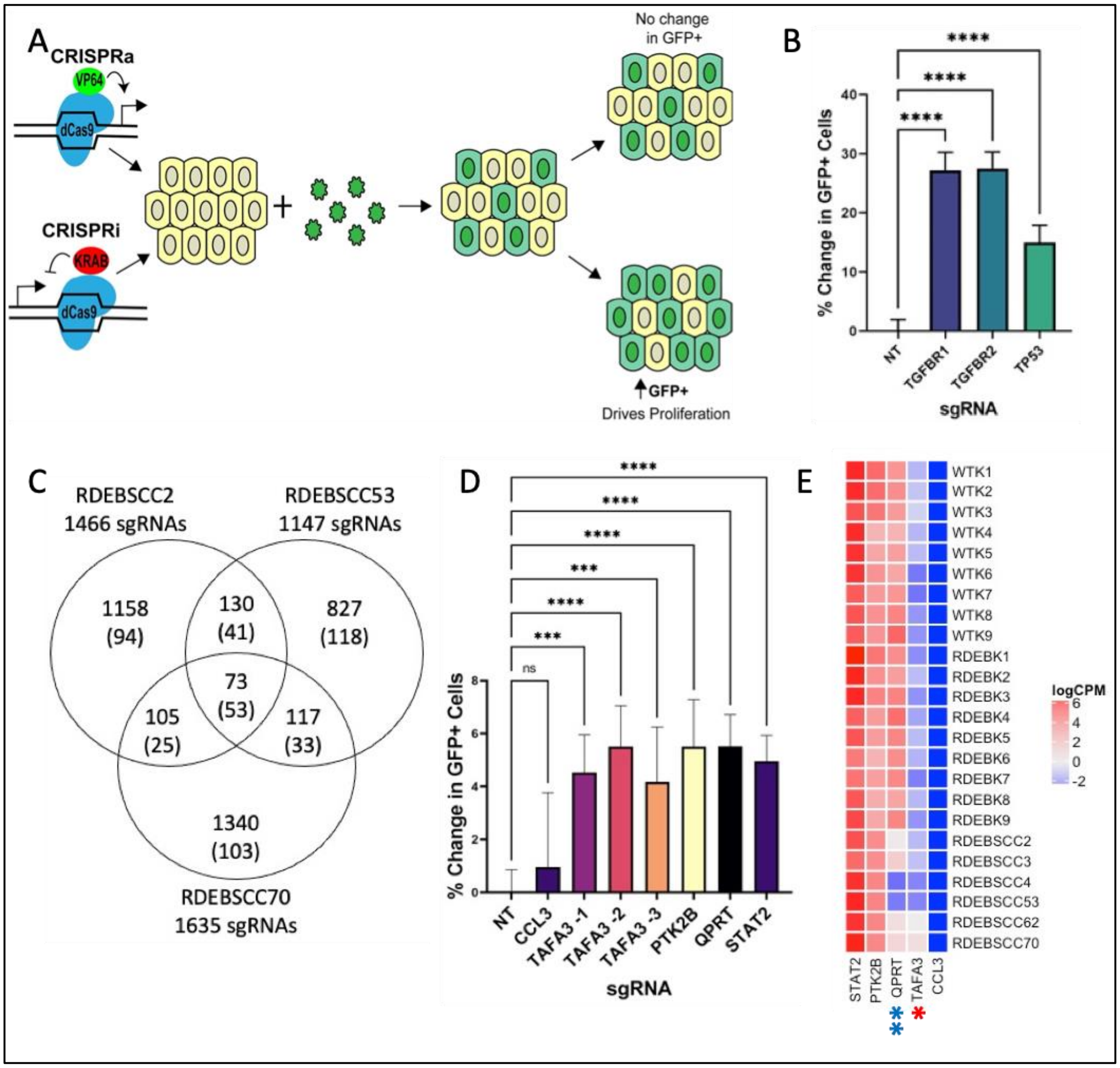

Figure 3: Competition assays for CRISPRi candidates. **A.** Overview of competition assay. **B.** Validation of competition assay methodology using known inhibitors of proliferation in keratinocytes (**** = p<0.0001). **C.** Venn diagram showing the number of overlapping sgRNAs across the RDEBSCC CRISPRi screens. Numbers in parentheses refer to the number of sgRNAs that overlapped with the N/TERT CRISPRi screen. **D.** Competition assays for candidate genes identified in CRISPRi proliferation screens (*** p<0.001, **** p<0.0001). **E.** Heatmap of logCPM values for CRISPRi candidate genes in RNA-seq data. Number of asterisks indicate the number of comparisons in which the gene is differentially expressed, colors refer to direction of expression change with disease state (red = increased, blue = decreased relative to WTK).

CRISPRa screens for drivers of proliferation in keratinocytes

We performed CRISPRa proliferation screens in N/TERT keratinocytes and two keratinocyte lines that we created by immortalizing patient keratinocytes (WTK1 and RDEBK8 in our RNA-seq data) transduced with dCas9-VP64. By performing screens using wild-type (WTK) and RDEB keratinocytes (RDEBK), we aimed to (1) identify drivers of proliferation in keratinocytes, (2) determine whether drivers of proliferation in WTKs also increased proliferation in RDEBKs, (3) identify drivers of proliferation that are unique to RDEBKs, and (4) cross-reference screen results with our RNA-seq and CRISPRi data as it relates to disease progression and SCC development in RDEB.

CRISPRa screen results can be found in **Table 2**. There were 1814 enriched sgRNAs (Z>1.75) in the N/TERT CRISPRa screen, including 64 genes that had two enriched sgRNAs. There were 715 enriched sgRNAs (Z>1.75) in the RDEBK8 CRISPRa screen, including 19 genes with two enriched sgRNAs, and one gene with three enriched sgRNAs. We used a different method for the WTK1 CRISPRa screen because there were much fewer sgRNAs detected (2528 in WTK1 vs 52459 and 36201 in N/TERT and RDEBK8, respectively) and sgRNAs with sufficient read counts (CPM>5.0) to be included (1412 vs 43304 and 30016). The WTK1 CRISPRa screen had a higher sequencing depth (30.4 million reads vs 24.3 and 24.5 million reads) and similar percentage of mapped reads (83.75% of reads mapped to sgRNAs vs 80.88% and 83.79%), suggesting that these differences were not due to lack of sequencing or poor-quality sequencing data. The low number of sgRNAs impacted the Z-score calculation such that a Z-score of 1.75 in the WTK1 screen corresponded to a >100-fold change in sgRNA abundance. Instead, all sgRNAs with a FC >2.0 were considered enriched, yielding 767 enriched sgRNAs and 14 genes with two enriched sgRNAs. Next, we looked for sgRNAs that were enriched in more than one screen. There were no sgRNAs enriched in all three screens, but there were 15 sgRNAs enriched in NTERT and WTK1, 29 sgRNAs enriched in NTERT and RDEBK8, and 15 sgRNAs enriched in WTK1 and RDEBK8 (**Figure 4A**).

We chose sgRNAs targeting 12 genes across the three CRISPRa screens to use for competition assays in N/TERTs (CRISPRa Table 2). There were two genes, DENN domain-containing 4B (*DENND4B*) and transmembrane immune signaling adaptor (*TYROBP)*, that had two enriched sgRNAs in both WTK1 and RDEBK8, and *DENND4B* was the only gene with enrichment of all three sgRNAs across any of the three screens (RDEBK8). Our lab recently showed that CRISPRa-mediated upregulation of *TYROBP* and *DENND4B* resulted in increased production of C7 protein in both wild-type and RDEB keratinocytes, so we sought to determine whether these genes also affect proliferation (Thompson & Pickett-Leonard 2021, in prep.). We also chose follistatin like 1 (*FSTL1*) and integrin subunit β3 (*ITGB3*) from the WTK1-RDEBK8 sgRNAs for further investigation. FSTL1 can promote fibrosis, inflammation, and tumor growth and/or metastasis in some cancers, including head and neck squamous cell carcinoma (HNSCC) (Sundaram 2017, Mattiotti 2018). *ITGB3* encodes the β subunit of integrin avβ3, a dermal integrin that can bind ECM proteins such as fibronectin, fibrin, and vitronectin to facilitate adhesion and migration of fibroblasts.

Table 2: Summary of CRISPRa proliferation screen results.

Cell Line	Enriched sgRNAs	Genes with 2 enriched sgRNAs	Genes with 3 enriched sgRNAs
N/TERT	1814	64	0
WTK1	767	14	0
RDEBK8	715	19	1

We chose two genes from the 15 sgRNAs enriched in N/TERT and WTK1: integrin subunit β1 (*ITGB1*), and semaphorin 5A (*SEMA5A*). ITGB1 plays a major role in the epidermis, where it heterodimerizes with ITGA2 and ITGA3 to form the main epidermal integrins. ITGB1 also heterodimerizes with ITGA5 and ITGA9, which are mainly expressed in the dermis, but are expressed in the epidermis during wound healing. SEMA5A has been shown to promote migration and invasion in melanoma cells, is positively regulated at both the mRNA and protein level by the anti-apoptotic protein Bcl-2 and has been implicated in the pathogenesis of autoimmune diseases through its association with IL-17RA (D’Aguanno 2018, Lobna 2021). The other candidate genes include ADAM metallopeptidase domain 2 (*ADAM2*), chromodomain Y like 2 (*CDYL2*), colony stimulating factor 3 receptor (*CSF3R*), germinal center associated signaling and motility (*GCSAM*), Kelch domain containing 8A (*KLHDC8A*), and keratin 33B (*KRT33B*). There were two enriched sgRNAs for both *ADAM2* and *KRT33B* in the WTK1 screen and two enriched sgRNAs for *CSF3R* and *KLHDC8A* in the RDEBK8 screen. *CDYL2* is an epigenetic regulator that has been shown to promote migration, invasion, and EMT in breast cancer (Siouda 2020). *GCSAM* was one of the most highly enriched sgRNAs in the N/TERT CRISPRa screen.

As with the CRISPRi candidate genes, we performed competition assays to determine whether CRISPRa-mediated upregulation of these genes could increase proliferation in keratinocytes. N/TERTs stably expressing dCas9-VP64 were transduced with a sgRNA-GFP lentiviral construct containing an sgRNA targeting the gene of interest. After 8 days, the percentage of GFP+ cells significantly increased in dCas9-VP64 N/TERTs transduced with sgRNAs for all 12 candidate genes relative to a non-targeting (NT) sgRNA control (**Figure 4B**). We also checked the expression of these genes in the RNA-seq data (**Figure 4C**). *ADAM2* was the only gene not detected in any sample, but *CSF3R*, *KLHDC8A*, *KRT33B*, and *TYROBP* were only detected in a few samples each (and at very low levels). The other seven genes were expressed in all samples. *CDYL2*, *DENND4B*, *GCSAM*, and *ITGB3* were not differentially expressed in any of the three comparisons. *FSTL1* expression was slightly increased ($p<0.05$) in RDEBKs relative to WTKs (logFC= 0.74). *ITGB1* expression was significantly decreased in RDEBSCCs relative to both WTKs and RDEBKs (logFC= -0.82, -0.89). *SEMA5A* was significantly increased in RDEBKs relative to WTKs (logFC= 2.20) and in RDEBSCCs relative to both WTKs and RDEBKs (logFC= 3.50, 1.50). Taken together, these results suggest that upregulation of the twelve candidate genes results in increased proliferation in keratinocytes and that *SEMA5A* may also drive proliferation of RDEBSCC cells.

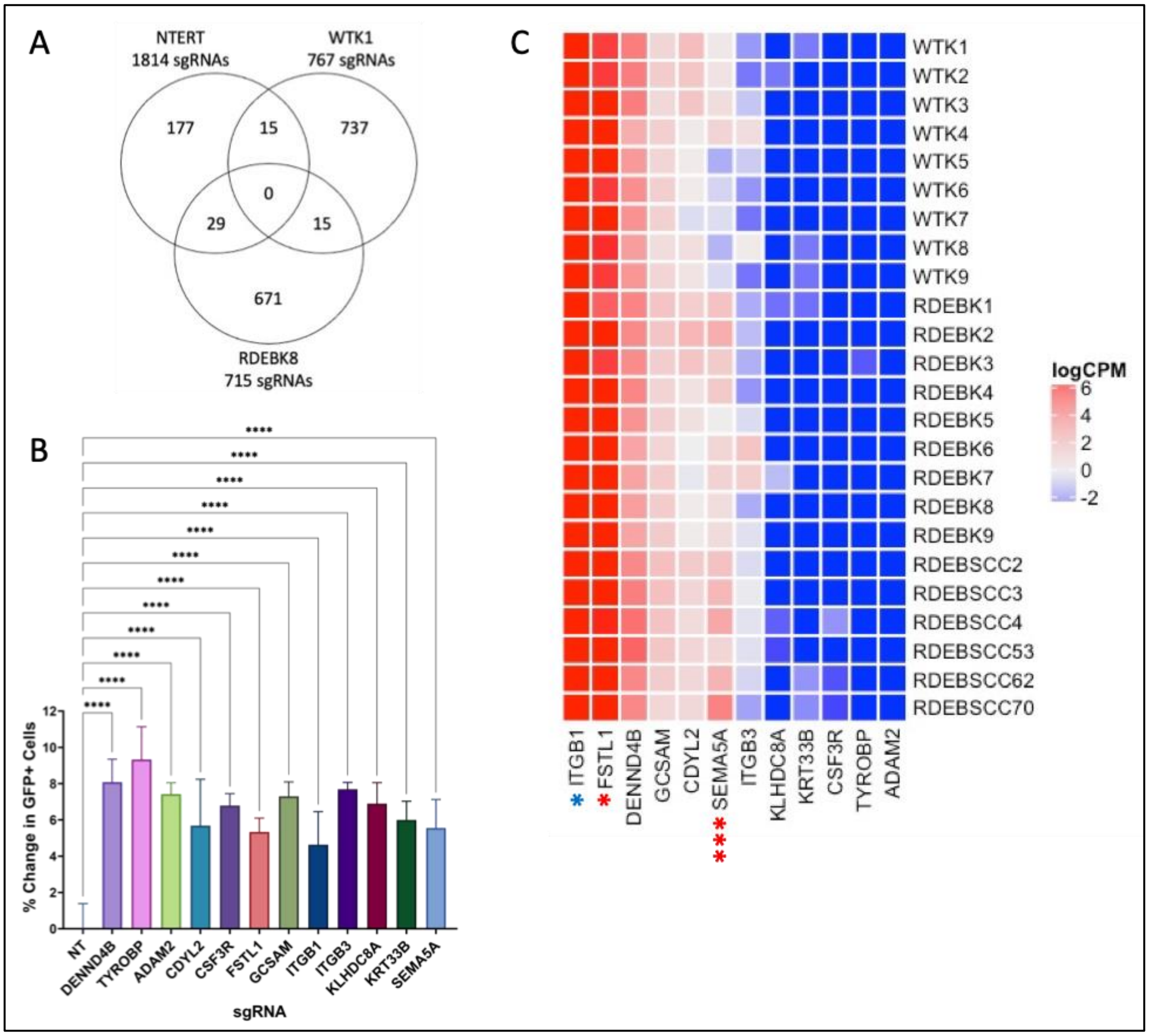

Figure 4: CRISPRa screen results. **A.** Venn diagram showing the number of sgRNAs that overlapped between the three CRISPRa screens. **B.** Competition assay results for the 12 candidate genes selected from across the three CRISPRa screens (**** = p<0.0001). **C.** Heatmap of logCPM values for CRISPRa candidate genes in RNA-seq data. Number of asterisks indicate the number of comparisons in which the gene is differentially expressed, colors refer to direction of expression change with disease state (red = increased, blue = decreased).

DISCUSSION

Cutaneous squamous cell carcinoma (cSCC) accounts for as many as two thirds of all deaths among people with RDEB due to its rapid development and metastasis (Fine 2009). RDEBSCC has a much lower average age of onset (~35 years) than UVSCC or HNSCC (>60 years), generally develops in areas of chronic wounding, and patients frequently develop multiple (median per patient = 3-3.5) primary tumors (Fine 2009, Montaudie 2016). Contrary to the hyper-aggressive nature of these tumors, RDEBSCCs often appear well-differentiated, acquire similar driver mutations and copy number alterations to UVSCC and HNSCC, and have a lower overall mutational burden than UVSCC (Montaudie 2016, Cho 2018, Sans-DeSanNicolas 2018). Genomic characterization of RDEBSCCs also showed that ~42% of all mutations (and ~67% of driver mutations) were caused by APOBEC cytidine deaminases and only 38% were UV-induced, compared with <2% and ~78% of UVSCC mutations, respectively (Cho 2018). Previous work has shown that the RDEB skin microenvironment is conducive to SCC development due to a combination of chronic inflammation, progressively worsening fibrosis, high keratinocyte turnover, and increased immune signaling as a result of impaired wound healing (Fritsch 2008, Martins 2009, 2016; Knaup 2011, Ng 2012, Kuttner 2013, Nystrom 2013, 2015, 2018; Petrof 2013, van der Kooi-Pol 2013, Dayal 2014, 2021; Odorisio 2014, Annicchiarico 2015, Hoste 2015, Esposito 2016, Mittapalli 2016, Cianfarani 2017, 2019; Guerra 2017, Liao 2018, Atanasova 2019a, Chacon-Solano 2019, Condorelli 2019b, Filoni 2020, Phillips 2020, Beilin 2021, Lincoln 2021). The five-year survival rate of RDEBSCC is essentially zero and there are currently no effective therapeutics for treating RDEBSCC, but clinical trials are in development for the multikinase inhibitor rigosertib, which was shown to induce apoptosis in ten different RDEBSCC lines and RDEBSCC xenografts in mice (Fine 2009, Atanasova 2019b, Has 2020c).

Early diagnosis of RDEBSCCs is crucial due to their rapid progression and metastasis. Since they generally develop in areas of chronic wounding and cells appear well-differentiated, RDEBSCCs frequently resemble granulation tissue or ulceration, especially during the early stages of development, making early diagnosis difficult (Fine 2009, Mellerio 2016). Identification of genes/proteins that start to progressively increase or decrease in the early stages of RDEBSCC development could be useful for developing a new diagnostic tool for identifying RDEBSCCs before they are readily visible. To this end, we sought to identify new candidate genes using a combination of RNA-sequencing and genome-wide CRISPRa and CRISPRi screens in wild-type, RDEB, and RDEBSCC keratinocytes. We identified 63 significantly differentially expressed genes between wild-type and RDEB keratinocytes across nine pairs of HLA-matched siblings (**Figure 2A**). To expand the list of potential candidates, we also included genes that had an unadjusted p-value < 0.05 and a fold change of at least 1.25-fold up or down, resulting in 640 genes. When we compared this list of 640 genes to the lists of significantly differentially expressed genes between RDEBSCCs vs WTKs and RDEBSCCs vs RDEBKs, there were 46 genes whose expression became progressively increased and 44 that progressively decreased from WTKs to RDEBKs to RDEBSCCs (**Figure 2B-C**).

To identify novel inhibitors of proliferation in keratinocytes and RDEBSCC cells, we performed genome-wide CRISPRi screens on N/TERT immortalized keratinocytes and three of the six RDEBSCC cell lines (2, 53, 70). There were 53 sgRNAs (out of >57,000) that were enriched in all four screens relative to the starting material. Only one gene, TAFA chemokine-like family member 3 (*TAFA3*), had all three sgRNAs enriched across the four screens. We used competition assays to validate *TAFA3* and four other candidate genes, C-C motif chemokine ligand 3 (*CCL3)*, protein tyrosine kinase 2β (*PTK2B*), quinolinic acid phosphoribosyltransferase (*QPRT*), and signal transducer and activator of transcription 2 (*STAT2*). sgRNA-mediated inhibition of *TAFA3*, *PTK2B*, *QPRT*, and *STAT2*, but not *CCL3*, all significantly increased cell proliferation. *PTK2B* and *STAT2* were not differentially expressed across any of the three cell types in the RNA-seq data, and *TAFA3* was moderately (but significantly) increased in RDEBSCC cells relative to RDEBKs. *QPRT* was significantly decreased in RDEBSCCs relative to both WTKs (logFC = -4.46) and RDEBKs (logFC = -4.74), thus supporting the results of the CRISPRi screen and competition assays.

QPRT mediates the conversion of quinolinic acid (QA) into nicotinamide mononucleotide (NMN), which is then converted into nicotinamide adenine dinucleotide (NAD+) by NMN adenyltransferases as part of the kynurenine pathway (KP). It is interesting that QPRT inhibition increased proliferation in N/TERTs and RDEBSCCs, because (1) QA, the substrate of QPRT, is highly cytotoxic when it accumulates, and (2) NMN, the product of QPRT, is directly converted into NAD+, which is required for a wide variety of cellular processes, suggesting that QPRT would promote proliferation rather than inhibit it (Sheipouri 2015, Roberti 2021). A previous study showed that UVB radiation and UVB + IFN-γ, but not IFN-γ alone, reduced expression of QPRT (Sheipouri 2015). Decreased expression of QPRT in response to UVB and IFN-γ was coupled with increased expression of nicotinic acid phosphoribosyl-transferase (NAPT) and nicotinamide phosphoribosyltransferase (NAMT), the two main enzymes in the NAD+ salvage pathway. The NAD+ salvage pathway is much more efficient at generating NAD+ than the KP, and UVB and IFN-γ are known to deplete NAD+ and cause DNA damage, cell death, and inflammation in the skin, so it is possible that cells preferentially use the NAD+ salvage pathway to generate NAD+ when stressed.

Two genes encoding enzymes upstream of QPRT in the KP, *KYNU* and *HAAO*, also had sgRNAs enriched in some of the CRISPRi screens. *KYNU*, which encodes kynureninase (KYNU), had one enriched sgRNA in the N/TERT and RDEBSCC70 CRISPRi screens and was increased in RDEBKs relative to WTKs (logFC = 2.102). *HAAO*, which encodes 3-hydroxyanthranilate-3,4-dioxygenase (3-HAO), had one enriched sgRNA in the RDEBSCC2 and RDEBSCC53 CRISPRi screens. KYNU catalyzes the conversion of kynurenine and 3-hydroxykynurenine to anthranilic acid (AA) and hydroxyanthranilic acid (3-HAA), respectively.

3-HAO catalyzes the conversion of 3-HAA to alpha-amino-beta-carboxy-muconate semialdehyde (ACMS), an unstable intermediate that undergoes spontaneous cyclization to form QA (Sheipouri 2015, Novak Kujundzic 2021). Both AA and 3-HAA can generate free radicals, which can damage cells, inhibit proliferation, and increase cell death, so inhibition of KYNU and/or 3-HAO could increase proliferation by preventing excessive generation of these metabolites (Sheipouri 2015). Complete inhibition of either (or both) of these genes would also be harmful, however, because 3-HAA is required for QPRT-mediated generation of NMN that leads to NAD+ synthesis (Sheipouri 2015). Further research of the effects of KP manipulation in keratinocytes and fibroblasts is needed to fully elucidate the biological significance of these results.

To identify novel drivers of proliferation in wild-type and RDEB keratinocytes, we performed genome-wide CRISPRa screens on N/TERTs and two keratinocyte lines that were immortalized in our lab, WTK1 and RDEBK8. There were no sgRNAs that were enriched in all three screens, but there were 15 overlapping sgRNAs between NTERT and WTK1, 29 between NTERT and RDEBK8, and 15 between WTK1 and RDEBK8. We chose twelve candidate genes to validate with competition assays, and dCas9-VP64/sgRNA-mediated upregulation of each of the twelve significantly increased proliferation relative to the untransduced cells. Two of the candidate genes, DENN domain containing 4B (*DENND4B*) and transmembrane immune signaling adaptor (*TYROBP*), were also identified as top candidates in the C7-CRISPRa screen. DENND4B is a Rab guanine nucleotide exchange factor (GEF) that may be involved in vesicle-mediated transport, but very little research has been done on this gene or protein. *TYROBP* is mainly expressed in lymphoid and myeloid immune cells, such as natural killer cells, monocytes (dendritic cells and macrophages), neutrophils, and B cells, but not in keratinocytes, and this is reflected in the RNA-seq data (Tomasello 2005). It is possible that TYROBP-expressing immune cells, such as neutrophils or macrophages, could stimulate keratinocyte proliferation in the context of wound healing via mechanisms that involve TYROBP, but this would require significant additional research to evaluate. Like *TYROBP*, four of the other twelve candidate genes (*ADAM2, CSF3R*, *KLHDC8A*, and *KRT33B*) were either not expressed or detected at very low levels in the RNA-seq data. *DENND4B*, as well as *CDYL2*, *GCSAM*, and *ITGB3*, were expressed in all samples, but were not differentially expressed in the RNA-seq data (**Figure 4C**).

Follistatin like 1 (*FSTL1*) was slightly increased in RDEBKs relative to WTKs ($p < 0.05$, logFC = 0.74) and integrin subunit β3 (*ITGB1*) was slightly, but significantly, decreased in RDEBSCCs relative to both WTKs and RDEBKs (logFC = -0.82, -0.89) (**Figure 4C**). Previous research has found that FSTL1 increases, promotes, or is associated with a variety of pro-tumorigenic characteristics, including immune infiltration, chemoresistance, stemness, migration, invasion, etc. (Sundaram 2017, Yang 2017, Mattiotti 2018, Cheng 2019, Jin 2020, Li 2020, Zhang 2020). While it is possible that FSTL1 could have a pro-tumorigenic role in RDEBSCC, it was not significantly upregulated, even when compared to WTKs. Interestingly, one study showed that FSTL1 mediated increased chemoresistance and stemness in breast cancer by activating Wnt/beta-catenin via ITGB3, suggesting that the two interact (Cheng 2019). ITGB3 forms heterodimers with ITGAV and ITGA2B and serves as a receptor for numerous ECM proteins, such as fibronectin, laminin, thrombospondin, and vitronectin (among others).

Semaphorin 5A (*SEMA5A*) expression significantly increased from WTKs to RDEBKs ($q < 0.05$, logFC = 2.20) to RDEBSCCs ($q < 0.05$, logFC = 3.50, 1.50), suggesting that it could be correlated with disease progression in RDEB (**Figure 4C**). Semaphorins help regulate neuron growth and proliferation but are also aberrantly expressed in a variety of cancers (Lu 2012). One study found that decreased SEMA5A was associated with poor survival in women with non-small cell lung cancer, but SEMA5A usually exhibits pro-tumorigenic characteristics (Lu 2010, 2012). SEMA5A and plexin-B3 (receptor for SEMA5A) promoted migration, invasion, proliferation, angiogenesis, and metastasis and reduced apoptosis in pancreatic, gastric, and endometrial cancers (Sadanandam 2010, 2012; Lu 2012, Saxena 2018, Dziobek 2019, Chen 2020). Further investigation will be needed to determine whether SEMA5A could be useful as a biomarker and what role(s) it plays in RDEB disease progression and RDEBSCC development, but its enrichment in completely independent experiments suggest that it could be useful.

MATERIALS AND METHODS

Cell Culture: WTK, RDEBK, and RDEBSCC cells were maintained in keratinocyte complete media (KCM): EpiLife medium +60µM calcium/EpiLife Defined Growth Supplement (EDGS, ThermoFisher). Cell culture flasks were pre-coated using a Coating Matrix kit (recombinant human type I collagen, ThermoFisher) according to manufacturer instructions. Cells were passaged or harvested using trypsin once they reached 75-85% confluence. Mutation information for RDEBK and RDEBSCC cells can be found in **Table S6**.

RNA Isolation: RNA was isolated using the RNeasy micro kit (QIAGEN). RNA was submitted for Agilent eukaryotic RNA quality analysis to generate a RIN score and RiboGreen quantitation to obtain accurate concentrations before library preparation. All RNA used for library preparation had RIN scores greater than 8.5.

RNA-seq Library Preparation and Sequencing: Library preparation was performed using the TruSeq Stranded mRNA LT kit (Illumina) according to manufacturer instructions. Libraries were submitted to the University of Minnesota Genomics Center for quality control before sequencing. Insert size was determined using an Agilent Bioanalyzer, library concentrations were determined using PicoGreen quantitation, and amplification ability was determined using KAPA QC. RNA-sequencing was performed on an Illumina HiSeq 2500 in High-Output mode or an Illumina MiniSeq to generate 75 base paired-end reads.

RNA-seq Data Pre-processing and Analysis: Raw read counts were obtained through pre-processing of RNA-seq data using the rnaseq-pipeline developed by John Garbe at the University of Minnesota Informatics Institute (https://bitbucket.org/jgarbe/gopher-pipelines/). Raw read counts were imported into RStudio, and downstream analysis was performed using the edgeR package in RStudio (Robinson, McCarthy, and Smyth, 2010). Briefly, lowly expressed genes were filtered out, normalization factors and dispersion were calculated, and a negative binomial model was fit to the data. Differential gene expression tests were performed for each pairwise comparison using the QL F-test method ($q<0.05$, FC1.25).

Competition assay: Oligonucleotides for sgRNA plasmid construction were ordered from IDT and cloned into the sgRNA and GFP expression lentiviral plasmid (LGR; Addgene 65656) as previously described (Shalem 2014) and sequence confirmed. Lentivirus expressing sgRNA and GFP (sgRNA-GFP) was generated and N/TERT_dCas9-VP64 (CRISPRa) or N/TERT_dCas9-KRAB (CRISPRi) cells were transduced with sgRNA-GFP lentivirus using LentiBlast Premium (OZ Biosciences) according to manufacturer's directions. Media was changed after 24 hours, and cells were passaged 48 hours post-transduction. Half of the cells were collected for the Day 0 time point and the remaining cells were grown and passaged at 75% confluency until the experiment end time point (Day 8 or Day 10). Cells were fixed with 4% PFA at each time point and the fraction of GFP+ cells was determined by FACS analysis. The percentage of GFP+ cells at Day 8/10 was subtracted from the percentage of GFP+ cells at Day 0 to obtain the percent change in GFP+ cells. Values were normalized to the non-targeting sgRNA.

SUPPLEMENTARY FIGURES

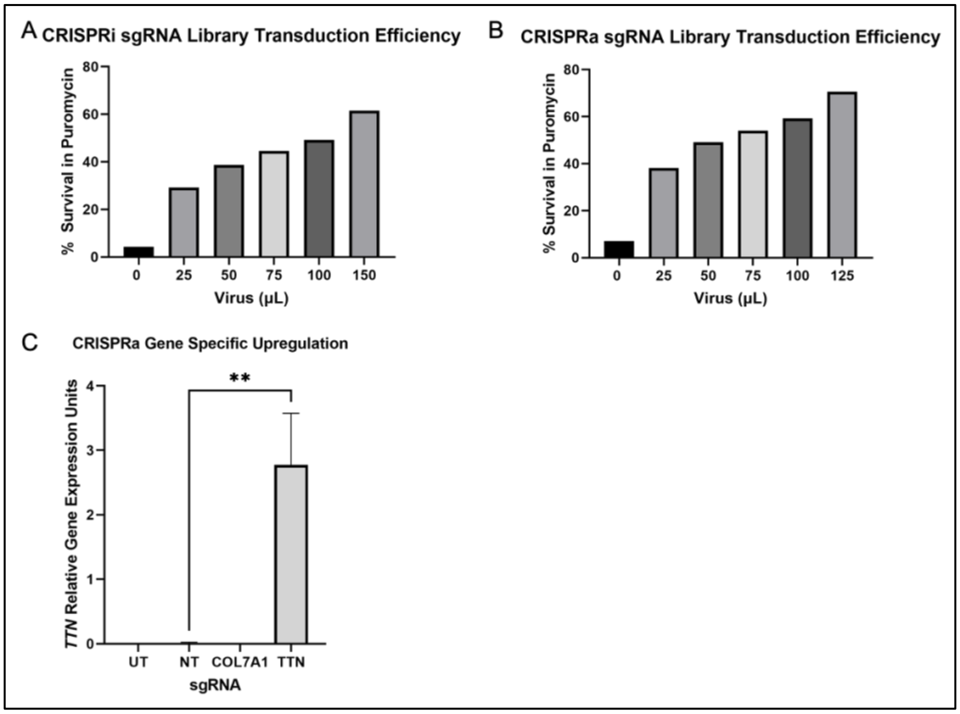

Figure S1: Transduction efficiency for **A.** CRISPRi and **B.** CRISPRa libraries. **C.** Testing the dCas9-VP64 system to ensure that gene-specific upregulation can be achieved.

SUPPLEMENTARY TABLES

Table S1: Significantly differentially expressed genes between RDEBKs and WTKs.

Gene	logFC	q-value	Description
AC025171.1	1.168	4.02E-02	novel transcript, sense overlapping to ANXA2R;
ACAA2	1.657	4.45E-03	acetyl-CoA acyltransferase 2
ADGRL2	3.596	5.85E-06	adhesion G protein-coupled receptor L2
BTBD16	-2.551	8.25E-06	BTB domain containing 16
CACNA2D3	2.266	2.29E-02	calcium voltage-gated channel auxiliary subunit α2δ3
CCDC8	1.699	1.42E-02	coiled-coil domain containing 8
CDK14	1.823	2.77E-02	cyclin dependent kinase 14
CLEC2B	-2.505	1.47E-02	C-type lectin domain family 2 member B
CLMN	-1.766	1.77E-03	calmin
CNTNAP4	4.253	8.37E-03	contactin associated protein like 4
COL1A1	2.446	4.02E-02	collagen type I α1 chain
COL1A2	2.501	7.45E-03	collagen type I α2 chain
COL9A2	-1.238	4.46E-02	collagen type IX α2 chain
DPY19L2	2.337	1.30E-02	dpy-19 like 2
DZIP1	1.537	4.46E-02	DAZ interacting zinc finger protein 1
EDIL3	3.590	2.29E-02	EGF like repeats and discoidin domains 3
EPHB2	2.662	8.37E-03	EPH receptor B2
FAM155B	-1.764	2.29E-02	family with sequence similarity 155 member B
FKBP10	3.068	1.67E-02	FKBP prolyl isomerase 10
FOXC1	1.024	1.47E-02	forkhead box C1
GIMAP2	-2.578	1.88E-02	GTPase, IMAP family member 2
HS6ST2	2.625	2.29E-02	heparan sulfate 6-O-sulfotransferase 2
HYAL1	-1.846	1.71E-02	hyaluronidase 1
IL1B	-1.057	4.02E-02	interleukin 1β
ISL1	-2.680	9.51E-03	ISL LIM homeobox 1
KRT31	-1.727	2.77E-02	keratin 31
L1TD1	2.434	7.46E-05	LINE1 type transposase domain containing 1
LCE6A	-1.908	1.20E-02	late cornified envelope 6A
LETM2	1.298	3.83E-02	leucine zipper & EF-hand containing transmembrane 2
LINC00540	-4.338	1.67E-02	long intergenic non-protein coding RNA 540
LINC00958	-2.911	2.31E-02	long intergenic non-protein coding RNA 958
LTBP1	1.991	4.02E-02	latent TGF-β binding protein 1
LURAP1L-AS1	-1.275	1.20E-02	LURAP1L antisense RNA 1
MGST1	2.619	8.25E-06	microsomal glutathione S-transferase 1

MLPH	2.511	7.45E-03	melanophilin
NEFH	3.087	4.20E-02	neurofilament heavy
NOX4	3.725	7.45E-03	NADPH oxidase 4
PCDH18	3.158	2.29E-02	protocadherin 18
PCDH19	3.269	1.82E-03	protocadherin 19
PCDHGA2	2.721	2.31E-02	protocadherin γ subfamily A, 2
PDGFRB	3.058	2.29E-02	platelet derived growth factor receptor β
PEG10	4.314	1.77E-03	paternally expressed 10
PHACTR3	2.474	9.73E-05	phosphatase and actin regulator 3
POU2AF1	2.345	4.02E-02	POU class 2 homeobox associating factor 1
PRR16	2.785	1.36E-02	proline rich 16
PTPRM	-1.142	3.83E-02	protein tyrosine phosphatase receptor type M
SEMA5A	2.201	1.04E-05	semaphorin 5A
SERPINB2	-1.317	4.46E-02	serpin family B member 2
SGCE	3.431	2.31E-02	sarcoglycan ε (epsilon)
SHC3	1.586	2.29E-02	SHC adaptor protein 3
SLC12A7	-1.357	5.00E-02	solute carrier family 12 member 7
SLC4A4	3.315	2.29E-02	solute carrier family 4 member 4
TCEAL7	1.956	1.36E-02	transcription elongation factor A like 7
TIMP2	2.097	1.20E-02	TIMP metallopeptidase inhibitor 2
TMEM204	-2.799	7.40E-03	transmembrane protein 204
TMEM47	4.324	7.37E-04	transmembrane protein 47
TP53I11	-1.570	5.00E-02	tumor protein p53 inducible protein 11
TRHDE-AS1	3.664	4.16E-02	TRHDE antisense RNA 1
TRPS1	1.650	3.21E-02	transcriptional repressor GATA binding 1
VEPH1	3.478	2.29E-02	ventricular zone expressed PH domain containing 1
XDH	-0.927	1.40E-02	xanthine dehydrogenase
ZFPM2	-2.448	2.45E-02	zinc finger protein, FOG family member 2
ZNF385D	2.689	7.40E-03	zinc finger protein 385D

Table S2: Upstream regulators that had significant overlap p-values ($p < 0.05$) and were predicted to be activated ($Z > 2.0$) in RDEBKs relative to WTKs by Ingenuity Pathway Analysis (IPA) based on the list of 640 differentially expressed genes between RDEBKs and WTKs.

Upstream Regulator	Activation Z-score	p-value of overlap	DEGs downstream	Consistent with Activation
AGT	3.646	5.01E-15	66	42
PTH	3.532	1.09E-05	16	13
TGFB1	3.257	1.79E-17	111	58
ESR1*	2.927	2.90E-09	74	37
MRTFB	2.896	1.12E-04	14	11
TWIST1	2.849	1.02E-08	20	15
SOX9	2.720	1.63E-05	12	10
TEAD1	2.714	1.93E-06	11	10
TEAD3	2.714	6.12E-08	11	10
TEAD2	2.714	4.94E-08	11	10
TCF7L2	2.712	3.03E-02	17	10
MYB	2.655	2.16E-03	12	9
COLQ	2.530	9.21E-06	10	9
SMAD4	2.505	9.94E-04	17	9
EP300	2.480	1.89E-02	19	8
CGA	2.433	1.69E-02	7	6
NFATC1	2.433	4.34E-04	10	6
ADRB2	2.425	3.70E-04	7	6
HSF1	2.400	3.77E-02	11	6
MYC	2.362	1.18E-06	60	34
HMGA1	2.357	2.56E-07	19	14
GATA6	2.332	4.40E-02	10	8
PI3K	2.256	2.79E-06	23	13
WT1	2.240	1.23E-04	18	11
RNF31	2.236	1.13E-02	6	5
CALR	2.224	7.92E-03	5	5
BCAP31	2.224	5.30E-04	5	5
FOXC2*	2.219	1.93E-02	5	5
TWIST2	2.213	2.62E-03	5	5
FGFR1	2.210	2.96E-04	10	9
CG	2.207	5.05E-10	38	21
TGFBR1	2.198	1.58E-05	11	9
KDM3A	2.183	4.09E-03	5	5
TRH	2.177	2.32E-03	5	5
SMARCB1	2.157	3.99E-02	9	7
S100A8	2.111	2.72E-04	14	10

CTNNB1	2.089	1.25E-08	55	20
TGF-β	2.028	2.48E-07	25	16

Table S3: Upstream regulators that had significant overlap p-values ($p < 0.05$) and were predicted to be inhibited ($Z < -2.0$) in RDEBKs relative to WTKs by Ingenuity Pathway Analysis (IPA) based on the list of 640 differentially expressed genes between RDEBKs and WTKs.

Upstream Regulator	Activation Z-score	p-value of overlap	Downstream Genes	Consistent with Activation
OGA	-3.421	1.41E-07	31	24
miR-29b-3p	-2.913	2.30E-06	12	11
GRIN3A	-2.828	8.71E-03	8	8
let-7a-5p	-2.682	9.54E-06	17	14
KRAS	-2.584	7.13E-06	42	14
mir-1	-2.538	6.66E-04	10	9
TGM2	-2.514	2.20E-03	14	11
IKZF3	-2.449	9.33E-03	6	6
JAK1	-2.425	8.73E-03	6	6
HRAS	-2.388	1.85E-11	50	19
miR-338-3p	-2.333	2.13E-07	9	8
miR-30c-5p	-2.255	1.92E-05	14	11
miR-450a-5p	-2.236	2.05E-03	7	5
SPDEF	-2.236	1.83E-03	5	5
MDM2	-2.226	6.71E-03	7	5
mir-133	-2.219	3.27E-02	5	5
α-catenin	-2.199	4.51E-07	15	12
EZH2	-2.166	2.68E-03	20	10
PSMB11	-2.145	3.08E-04	11	9
ACE2	-2.126	2.28E-04	6	5
PPARGC1A	-2.124	3.56E-06	26	19
miR-335-3p	-2.121	3.30E-07	8	7
ATG7	-2.120	1.53E-02	6	5
Immunoglobulin	-2.092	2.31E-03	32	17
PIK3R1	-2.041	3.37E-04	9	7

Table S4: Diseases and functions predicted to be activated or inhibited by IPA based on the list of 640 differentially expressed genes between RDEBKs and WTKs.

Diseases or Functions Annotation	Activation Z-score	p-value of overlap	# Genes
Fibrosis	2.984	4.37E-07	58
Cell survival	2.654	8.02E-13	121
Renal lesion	2.526	8.02E-15	116
Genitourinary tumor	2.481	2.39E-21	433
Cell viability	2.467	7.69E-11	111
Differentiation of neuroblastoma cell lines	2.376	1.26E-06	10
Remodeling of blood vessel	2.359	2.51E-10	17
Mammary tumor	2.270	4.44E-13	186
Progression of tumor	2.251	4.68E-10	34
Growth of solid tumor	2.138	1.32E-07	37
Differentiation of connective tissue cells	2.138	1.90E-07	52
Cell viability of neurons	2.074	3.82E-08	27
Cell death of endothelial cells	-2.202	1.25E-06	22
Glucose metabolism disorder	-2.361	2.71E-16	128
Organismal death	-3.680	7.38E-09	154
Morbidity or mortality	-3.706	2.70E-09	157

Table S5: Genes that progressively increased or decreased in expression from wild-type keratinocytes to RDEB keratinocytes to RDEBSCC cells. Bold text indicates genes that were significantly differentially expressed in RDEBK vs WTK (q<0.05).

Gene	RDEBK vs WTK		SCC vs WTK		SCC vs RDEBK		Gene Description
	logFC	p-value	logFC	q-value	logFC	q-value	
ACSL5	2.06	6.64E-04	6.58	2.58E-05	3.81	1.21E-03	acyl-CoA synthetase long chain 5
ADAM12	1.42	3.34E-02	4.66	6.80E-06	3.26	1.67E-04	ADAM metallopeptidase domain 12
ADGRL3	1.88	7.72E-03	4.36	5.71E-04	2.46	2.04E-02	adhesion G protein-coupled receptor L3
ADM	0.63	4.01E-02	1.46	3.33E-04	0.72	4.50E-02	adrenomedullin
AIM2	1.74	4.40E-03	4.78	5.69E-05	3.50	7.02E-04	absent in melanoma 2
ALDH3B1	1.63	9.05E-03	4.70	7.65E-05	2.80	3.80E-03	aldehyde dehydrogenase 3 family member B1
ALPK2	2.27	3.54E-04	4.90	3.17E-03	3.70	1.49E-02	α kinase 2
ANTXR2	-0.64	1.21E-02	-2.03	8.77E-05	-1.35	2.64E-03	ANTXR cell adhesion 2
BHLHE40	-0.36	3.21E-02	-0.94	2.18E-04	-0.59	8.80E-03	basic helix-loop-helix family member e40

BTBD16	**-2.55**	**1.41E-09**	**-5.05**	**2.49E-05**	**-2.64**	**3.19E-03**	**BTBD containing 16**
CCK	-1.03	1.52E-02	-4.54	1.98E-04	-3.87	6.92E-04	cholecystokinin
CD1D	-0.55	2.92E-02	-3.74	1.05E-04	-3.17	4.02E-04	CD1d molecule
CECR2	2.25	6.86E-03	5.05	3.68E-04	2.33	2.56E-02	CECR2 histone acetyl-lysine reader
CFH	1.67	4.66E-02	5.31	1.52E-04	2.96	8.84E-03	complement factor H
CHST6	-0.87	4.79E-02	-4.01	4.60E-04	-3.36	1.73E-03	carbohydrate sulfotransferase6
COL6A1	1.16	2.28E-02	3.69	1.59E-04	2.55	2.97E-03	collagen type VI α1
COL9A2	**-1.24**	**1.86E-04**	**-2.60**	**4.86E-05**	**-1.28**	**1.16E-02**	**collagen type IX α2**
CRACR2A	1.36	1.02E-02	4.04	1.17E-05	2.60	6.18E-04	calcium release activated channel regulator 2A
CT62	-0.91	1.53E-02	-2.25	4.83E-03	-1.60	3.10E-02	cancer/testis assoc. 62
CTHRC1	1.42	4.21E-02	4.72	2.18E-05	3.17	5.50E-04	collagen triple helix repeat containing 1
CYP1B1	1.15	3.98E-02	2.90	3.00E-04	1.35	4.68E-02	cytochrome P450 family 1 subfamily B member 1
CYP4X1	1.99	1.45E-03	3.76	2.12E-03	2.26	3.50E-02	cytochrome P450 family 4 subfamily X member 1
DHRS2	1.67	2.67E-03	4.31	1.33E-05	2.47	1.42E-03	dehydrogenase/reductase2
DKK4	-1.15	4.38E-02	-5.16	1.94E-04	-4.45	8.04E-04	dickkopf WNT signaling pathway inhibitor 4
EDEM1	-0.38	4.01E-02	-1.35	4.52E-05	-1.02	6.40E-04	ER degradation enhancing α-mannosidase like 1
EHD3	0.64	4.97E-02	1.72	3.80E-03	1.34	1.87E-02	EH domain containing 3
EPB41L1	0.58	2.96E-02	1.69	3.23E-04	1.10	9.62E-03	erythrocyte membrane protein band 4.1 like 1
EPHB2	**2.66**	**1.03E-05**	**6.55**	**1.24E-06**	**3.45**	**2.55E-04**	**EPH receptor B2**
EXOC6	1.24	9.61E-04	2.57	3.98E-05	1.09	2.82E-02	exocyst complex component 6
FAM225A	1.67	4.23E-02	4.20	3.37E-04	2.29	1.45E-02	family with sequence similarity 225 member A
FHL1	-0.70	1.39E-02	-1.95	2.42E-04	-1.44	2.81E-03	4.5 LIM domains 1
FLJ32255	1.32	4.80E-03	2.62	9.95E-05	1.14	3.87E-02	lnc-ANXA2R-1
FLJ46906	-0.87	4.70E-02	-2.10	1.04E-03	-1.22	3.15E-02	uncharacterized LOC441172; lncRNA
FOXC2	2.92	4.12E-02	5.90	1.98E-04	2.72	1.68E-02	forkhead box C2
GALM	-0.76	2.88E-02	-2.89	4.10E-04	-2.27	2.72E-03	galactose mutarotase
GJA3	1.34	7.43E-03	3.99	6.65E-05	2.33	4.65E-03	gap junction α3
GOLGA8B	-0.49	4.45E-02	-1.39	5.10E-04	-0.91	1.12E-02	golgin A8 member B
HBEGF	-0.53	3.00E-02	-1.87	6.69E-04	-1.49	3.86E-03	heparin binding EGF like growth factor

HS6ST2	**2.63**	**5.88E-05**	**7.41**	**8.51E-07**	**4.98**	**1.89E-05**	**heparan sulfate 6-O-sulfotransferase 2**
IL18	-0.54	2.77E-02	-1.64	4.21E-03	-1.20	2.57E-02	interleukin 18
IRAK3	0.95	4.90E-02	5.60	2.23E-06	4.56	1.43E-05	interleukin 1 receptor associated kinase 3
ISL1	-2.68	1.24E-05	-3.91	4.87E-03	-2.52	4.16E-02	ISL LIM homeobox 1
ITM2A	-1.29	1.31E-02	-5.28	7.14E-04	-4.30	2.67E-03	integral membrane 2A
JCAD	1.80	1.92E-02	4.97	1.75E-04	2.93	5.88E-03	junctional cadherin 5 associated; KIAA1462
KLHL13	0.71	1.40E-02	1.77	7.92E-05	1.11	4.59E-03	kelch like member 13
KRT31	**-1.73**	**9.03E-05**	**-4.83**	**1.95E-03**	**-4.01**	**5.88E-03**	**keratin 31**
LCE6A	**-1.91**	**1.74E-05**	**-4.93**	**5.53E-05**	**-2.92**	**3.97E-03**	**late cornified envelope 6A**
LEF1	2.17	2.61E-02	5.79	4.77E-04	2.60	3.44E-02	lymphoid enhancer binding factor 1
LINC00900	-1.13	2.03E-02	-3.10	3.29E-04	-2.02	7.14E-03	long intergenic non-protein coding RNA 900
LINC01133	-1.19	8.93E-03	-3.81	7.62E-05	-2.87	7.58E-04	long intergenic non-protein coding RNA 1133
LYRM1	-0.44	4.94E-02	-1.22	2.96E-04	-0.80	8.44E-03	LYR motif containing 1
MAPK10	-0.71	2.34E-02	-1.51	7.27E-04	-0.82	3.69E-02	mitogen-activated protein kinase 10
MKRN2OS	-0.79	4.23E-02	-2.28	3.88E-04	-1.59	5.88E-03	MKRN2 opposite strand
MMP13	3.09	3.02E-04	6.33	5.08E-05	3.27	4.64E-03	matrix metallopeptidase 13
MMRN2	-0.87	3.22E-02	-2.09	6.64E-04	-1.32	1.56E-02	multimerin 2
MRGPRX4	-1.02	3.08E-02	-3.08	2.47E-03	-1.77	5.00E-02	MAS related GPR family member X4
NETO1	-0.91	1.63E-02	-5.50	4.02E-04	-4.72	1.16E-03	neuropilin & tolloid like 1
NOS1	-1.28	2.63E-02	-3.72	6.04E-03	-2.56	3.67E-02	nitric oxide synthase 1
P3H2	-0.69	2.66E-02	-1.62	3.99E-03	-1.08	3.86E-02	prolyl 3-hydroxylase 2
PCDH18	**3.16**	**5.92E-05**	**7.77**	**2.62E-05**	**4.19**	**1.20E-03**	**protocadherin 18**
PEG10	**4.31**	**1.09E-06**	**6.11**	**1.10E-04**	**2.92**	**1.49E-02**	**paternally expressed 10**
PLCL2	1.47	1.15E-02	3.46	4.69E-04	1.98	1.97E-02	phospholipase C like 2
PLLP	-1.31	2.40E-04	-2.16	1.45E-03	-1.18	4.90E-02	plasmolipin
PODXL	1.01	4.63E-02	3.59	5.45E-05	2.21	3.18E-03	podocalyxin like
PRR16	**2.79**	**2.23E-05**	**5.43**	**1.35E-04**	**2.72**	**1.21E-02**	**proline rich 16**
PTAFR	-0.49	4.29E-02	-1.01	1.30E-03	-0.58	4.34E-02	platelet activating factor receptor
RARA-AS1	-1.26	2.64E-03	-2.74	1.21E-03	-1.73	2.37E-02	RARA antisense RNA 1
RNF128	-0.92	1.15E-02	-2.81	3.45E-03	-1.91	2.87E-02	ring finger protein 128
SAMD3	-1.04	3.87E-02	-3.10	2.08E-02	-2.78	3.40E-02	sterile α motif domain containing 3

SAP30L-AS1	0.82	4.67E-02	2.39	3.19E-04	1.44	1.34E-02	SAP30L antisense RNA 1 (head-to-head)
SEMA5A	**2.20**	**2.85E-09**	**3.50**	**1.76E-04**	**1.50**	**4.88E-02**	**semaphorin 5A**
SERPINB1	-0.74	7.89E-03	-1.59	8.85E-04	-1.04	1.60E-02	serpin family B member 1
SERPINB7	-0.75	4.07E-02	-3.34	1.46E-03	-2.64	6.70E-03	serpin family B member 7
SFTA1P	-0.92	1.81E-02	-2.09	5.25E-03	-1.61	2.34E-02	surfactant associated 1, lncRNA
SMIM22	-1.79	1.26E-02	-4.14	4.48E-04	-2.36	1.60E-02	small integral membrane protein 22
SORBS2	3.17	2.24E-02	6.19	2.91E-04	3.73	6.38E-03	sorbin & SH3 domain 2
SORCS2	1.75	2.75E-02	5.23	1.77E-05	2.87	2.05E-03	sortilin related VPS10 containing receptor 2
SPINK5	-1.92	1.83E-02	-3.97	8.96E-04	-2.69	1.01E-02	serine peptidase inhibitor Kazal type 5
SUSD5	1.27	1.63E-02	3.78	1.33E-05	2.37	8.24E-04	sushi domain containing 5
TBX1	1.45	2.12E-02	3.91	1.59E-04	1.69	4.12E-02	T-box transcription 1
TET3	0.45	2.73E-02	1.48	1.96E-03	0.93	3.57E-02	tet methylcytosine dioxygenase 3
THBS2	-0.77	4.76E-04	-4.54	3.51E-05	-3.87	1.33E-04	thrombospondin 2
TIMP2	**2.10**	**1.68E-05**	**3.35**	**4.56E-05**	**1.50**	**2.12E-02**	**TIMP metallopeptidase inhibitor 2**
TMEM204	**-2.80**	**6.09E-06**	**-5.78**	**2.51E-05**	**-3.43**	**1.38E-03**	**transmembrane protein 204**
TNFSF4	-1.19	2.79E-02	-3.11	1.20E-03	-2.42	6.52E-03	TNF superfamily 4
TNS3	0.60	3.96E-02	3.15	1.80E-08	2.54	4.08E-07	tensin 3
TSPAN12	1.83	2.08E-02	4.25	2.20E-04	2.21	1.64E-02	tetraspanin 12
WIPF3	0.97	4.05E-02	2.97	2.07E-04	2.12	3.10E-03	WAS/WASL interacting protein family member 3
ZNF695	1.31	2.32E-02	3.00	4.35E-04	1.89	1.18E-02	zinc finger protein 695
ZNF826P	-0.82	1.54E-02	-4.89	2.93E-04	-4.10	1.11E-03	zinc finger protein 826, pseudogene

Table S6: Mutation information for all RDEB samples used.

Sample	Allele 1	Allele 2
RDEBK1	c.3140-1G>A	c.3140-1G>A
RDEBK2	c.4048-1G>C (IVS34-1G>C)	c.553C>T (p.Arg185*)
RDEBK3	c.6751-1G>T	c.3840delC (p.Gly1281Valfs*44)
RDEBK4	c.4078G>T (p.Gly1360*)	c.8075delG (p.Gly2692Alafs*94)
RDEBK5	c.6751-2A>G (IVS85-2A>G)	c.3840delC (p.Gly1281ValfsX44)
RDEBK6	c.5287C>T (p.Arg1763*)	c.2388G>A (p.Trp796*)
RDEBK7	c.2005C>T (p.Arg669*)	c.2005C>T (p.Arg669*)
RDEBK8	c.4738_4740delinsA (p.Val1580ThrFS*28)	c.425A>G (p.Lys142Arg)
RDEBK9	c.5888G>A (p.Trp1963*)	c.5888G>A (p.Trp1963*)
RDEBSCC2	c.6269delC (p.P2090LfsX116	c.8253_8254delAG (p.R2751SfsX38)
RDEBSCC3	c.1573C>T (p.R525X)	c.1732C>T (p.R578X)
RDEBSCC4	c.8244insC	c.8244insC
RDEBSCC53	c.2005C>T (p.R669X)	c.2005C>T (p.R669X)
RDEBSCC62	c.682+1G>A	c.7474C>T (p.R2492X)
RDEBSCC70	c.425A>G (p.K142R)	c.425A>G (p.K142R)

CHAPTER 4

DISCUSSION AND FUTURE DIRECTIONS

Dystrophic epidermolysis bullosa (DEB) has a wide range of clinical manifestations that become progressively worse with age, making it one of the most physically and mentally debilitating genetic disorders for affected individuals and their families. DEB patients can experience repeated blistering and wounding, pain (chronic and acute), itch, risk of infection (local and systemic), malnutrition/nutritional problems, anemia, respiratory problems, time-consuming wound care regimens, difficulty performing everyday tasks, and problems with their teeth, mouth, nails, hair, scalp, and eyes, among others. On top of all these challenges, people with DEB (especially those with more severe cases) must live with the ever-present and constantly-increasing risk of developing squamous cell carcinoma. Concerns about cSCC were also reflected in responses to a recent survey of people with EB and caregivers of people with EB: when asked what they considered to be the most important factors for future EB therapeutics, "reducing the risk of skin cancer" (77.8% of patients and 86% of caregivers) was the top response, followed by reducing wound number/severity, reducing pain, improving wound healing, and reducing infections (Bruckner 2020).

The overall goal of my graduate research was to identify new ways to improve the lives of individuals with DEB by improving our understanding of DEB progression. This work has led to the identification of multiple genes and a compound that can promote C7 production in keratinocytes, which could be used as the basis of new targeted therapies for improving DEB symptoms. I have also identified drivers and inhibitors of proliferation in keratinocytes, inhibitors of proliferation in RDEBSCCs, and genes that become progressively upregulated or downregulated with disease progression (from wild-type to RDEB to RDEBSCC), which could be used to develop new diagnostic tools and/or preventative treatments for RDEBSCC. These results are also relevant outside of DEB, as they have implications for cell-cell and cell-matrix interactions in the epidermis; protein processing, trafficking, and secretion (especially large proteins like C7); and various cancer-related processes, including cancer development, the cell-

cell and cell-matrix interactions of cancer cells in the microenvironment, and mechanisms of epithelial-to-mesenchymal transition and metastasis.

The most direct (and likely the most effective) way to improve DEB symptoms is to increase the amount of C7 at the dermal-epidermal junction. Many different strategies for increasing C7 production have been investigated, including (1) transplantation of allogeneic C7-producing cells, (2) transplantation of patient cells that have been modified to express functional C7 using gene therapy or gene editing techniques, (3) injection of recombinant C7 protein, and (4) compounds that induce exon skipping or readthrough of premature termination codons to enable production of a slightly truncated C7 protein. Some therapies have shown promising results for treating DEB, including gene therapy approaches using grafts of modified patient keratinocytes (Siprashvili 2016, Eichstadt 2019), bone marrow transplantation in pediatric RDEB patients (Wagner 2010, Tolar 2013), and gentamicin in RDEB patients with nonsense mutations (Woodley 2017). Continued research and optimization of these approaches will likely lead to the regulatory approval of a DEB therapeutic at some point, but it is uncertain how long this will take, highlighting the need for continued exploration of potential treatments for DEB.

To identify new strategies for increasing C7 in the skin, we developed a keratinocyte C7 reporter cell line and used this reporter line to perform a genome-wide CRISPRa screen for positive regulators of C7 production. By using FACS to isolate the top 10% of tdTomato-expressing cells and using high-throughput sequencing to identify which sgRNAs were enriched in this population, we were able to identify numerous candidate genes and pathways for increasing C7. The list of enriched sgRNAs was used to perform pathway analysis, and the results of that analysis were used to create a list of 25 compounds for a targeted drug screen. Only four of these 25 compounds significantly increased tdTomato fluorescence and *COL7A1* expression: dasatinib, kaempferol, and two of the four bilberry anthocyanins, cyanidin-3-O-glucoside, and peonidin-3-O-glucoside. In RDEB keratinocytes, however, kaempferol was the only compound that significantly increased *COL7A1* gene expression, C7 production, and tdTomato fluorescence.

It is not clear why the other three compounds did not increase C7 production in RDEB keratinocytes, but could be due to differences in gene expression, signaling pathway activity, uptake of the compound, or some other mechanism that impacted the sensitivity of RDEB keratinocytes to these compounds.

Data processing and analysis

To get our list of enriched sgRNAs, we needed to identify the sgRNAs that were present in each population, calculate the relative abundance of each sgRNA in each population, and calculate the difference between these relative abundance values across populations. First, we used Cutadapt to sort the reads based on the presence of the five-base sequence (CACCG) that directly preceded the sgRNA sequence in the sgRNA construct. Reads that did not contain this sequence (<1%) were discarded. We also enabled the adapter trimming function of Cutadapt, which automatically removes "adapter sequences" (CACCG) and any preceding bases from the reads such that the first 20 bases of each read represented the sgRNA sequence. Next, we used Cutadapt to trim the reads such that only the first 20 bases remained. The file containing the 20-base reads was loaded into Matlab for further processing. In Matlab, the first step of "mapping" the reads was to determine the total number of unique 20-base sequences in the file and the number of reads corresponding to each of those unique sequences. To identify which sgRNAs were represented, we cross-referenced the list of unique sequences with the list of sgRNAs in the CRISPRa library. Since the sgRNAs were identified using an intersect function, only exact matches were considered. It is possible that some reads with a mismatch or uncalled bases (designated as "N") could have been confidently assigned to a specific sgRNA, but we achieved high mapping efficiency (>73.5% in all populations) without tolerating mismatches, so we decided to stick with the more stringent method. We calculated the relative abundance (counts per million sgRNA reads, CPM) of each sgRNA using the following formula: CPM = (read total for sgRNA + 1) / (total sgRNA reads) * (10^6).

We sequenced the library plasmid DNA before performing any screens to determine library diversity and establish baseline abundance values for each sgRNA. We obtained ~39 million total pDNA reads and ~83% mapped to sgRNA sequences, resulting in ~33.2 million sgRNA reads. We detected (at least one read) 57,681 sgRNAs out of 57,762 total (~99.86%) and the distribution of relative abundances appeared normal. For the tdTomato-high population, there were ~21 million total reads, and ~16.1 million sgRNA reads (76.4% mapping efficiency) across 53,854 different sgRNAs. As in other types of sequencing data, we removed sgRNAs with CPM values less than five, resulting in 48,333 sgRNAs. We also performed limited sequencing of the tdTomato-mid and tdTomato-low populations. For the tdTomato-mid population, there were ~13.1 million total reads and ~10.4 million sgRNA reads (79.5% mapping efficiency) across 53,854 sgRNAs. For the tdTomato-low population, there were ~13.4 million total reads and ~9.9 million sgRNA reads (73.7% mapping efficiency) across 52,798 sgRNAs.

To determine which sgRNAs were enriched in the tdTomato-high population relative to the starting material (pDNA), we calculated the logFC value for each sgRNA, then we calculated Z-scores based on the logFC values. sgRNAs with a Z-score of at least 1.75 (FC ~ 2.49, logFC ~ 1.31) were considered enriched. There were 1544 enriched sgRNAs, including 75 genes that had two enriched sgRNAs and one gene that had all three sgRNAs enriched. We chose this cutoff to strike a balance between maximizing the capture of true positives while maintaining a reasonable threshold for false positives. If we tightened the Z-score cutoff to 2.00, 2.25, 2.50, 2.75, or 3.0, the number of enriched sgRNAs would be reduced to 820, 383, 197, 104, or 56, respectively. Increasing the stringency of the Z-score cutoff would reduce our false discovery rate, but it would also remove hundreds of potentially viable candidate genes, so we opted to use a slightly more relaxed cutoff. It is possible that repeating the pathway analysis with the list of 820 and/or 383 sgRNAs could have impacted our choice of compounds for the targeted drug screen. If we relaxed the Z-score cutoff to 1.50, the number of enriched sgRNAs would increase to 2804. Even though our total number of true positives would increase, the false discovery rate would also increase, and the pathway analysis would be less informative and less powerful.

In our initial submission to the Journal of Investigative Dermatology, one of the reviewers suggested that the tdTomato-low and/or tdTomato-mid populations would be better comparisons for the tdTomato-high population than the pDNA. The Z-score cutoff we used for the log2 fold changes for tdTomato-high relative to pDNA corresponded to a ~2.5-fold increase, so we identified the sgRNAs with a fold change of at least 2.5 between tdTomato-high and the tdTomato-low and tdTomato-mid populations. There were 7112 and 3679 sgRNAs with fold changes of at least 2.5 in tdTomato-high relative to tdTomato-low and tdTomato-mid, respectively. There were 1258 sgRNAs with a fold change of at least 2.5 relative to both tdTomato-low and tdTomato-mid. We then compared these lists of sgRNAs to our initial list of 1544 enriched sgRNAs. There were 226 sgRNAs that were not detected in tdTomato-mid and/or tdTomato-low. Of the 1318 remaining sgRNAs that were enriched in tdTomato-high vs pDNA, we found 652, 740, and 396 sgRNAs that were also enriched relative to tdTomato-low, tdTomato-mid, or both, respectively. To determine whether the sgRNA FC values for tdTomato-low or tdTomato-mid more closely resembled the FC values for the pDNA, we created plots of FC values for the 45,764 sgRNAs that were detected in all three tdTomato populations and our list of 1318 enriched sgRNAs. When the FC values of all 45,764 sgRNAs were considered, the R^2 values were 0.0243 for tdTomato-low vs pDNA and 0.2488 for tdTomato-mid vs pDNA. When only the FC values of the 1318 enriched sgRNAs were considered, the R^2 values were 0.0028 for tdTomato-low vs pDNA and 0.0591 for tdTomato-mid vs pDNA.

The relatively low level of overlap could potentially be explained by differences in sgRNA distribution between the pDNA and the lentiviral vector, suggesting that the tdTomato-low and tdTomato-mid populations could have been used to further narrow down the list of enriched sgRNAs (and candidate genes). It is worth noting, however, that the *COL7A1* sgRNA that was highly enriched relative to the pDNA (FC = 15.31) was not enriched relative to tdTomato-low (FC = 0.88) but was enriched relative to tdTomato-mid (FC = 12.73). Our numerous validation experiments consistently showed that tdTomato fluorescence was directly proportional to *COL7A1* expression and C7 protein levels, so it is extremely unlikely that these cells were producing high levels of C7 without showing high tdTomato fluorescence. A more likely explanation for this result is that some cells were not expressing high levels of tdTomato/C7 when FACS was performed despite being transduced with an sgRNA corresponding to a true driver of C7 production. This suggests that enriched sgRNAs are not necessarily false positives just because the sgRNA isn't enriched relative to the low population.

Kaempferol as a treatment for DEB

Kaempferol is a plant flavonoid found in many different foods, including apples, grapes, several types of berries, broccoli, kale, spinach, potatoes, green tea, some legumes, and numerous plant species. This compound has been shown to promote apoptosis and inhibit proliferation, migration, invasion, fibrosis, and inflammation in a variety of tissues and cell types, including the skin (Chen & Chen 2013). Due to this wide range of effects, there are multiple mechanisms by which kaempferol could increase C7 production. Kaempferol has been shown to inhibit the expression and/or activity of numerous proinflammatory proteins that affect *COL7A1* expression, including TGF-β, TNF-α, NF-κB, and IL-1β (Kowalski 2005, Cortes 2007, Lee 2009, Chen & Chen 2013, Liu 2019, Perera 2019, Sekiguchi 2019, Lee & Jeong 2021). Although TGF-β is a strong promoter of *COL7A1* expression in both keratinocytes and fibroblasts, it also drives chronic inflammation and fibrosis in DEB skin, so kaempferol would not be suitable for use in DEB if it increased C7 production through TGF-β. IL-1β, TNF-α, and NF-κB, which is activated by TNF-α and binds to the TNF-α response element in the *COL7A1* promoter, decreased *COL7A1* expression in keratinocytes, but increased *COL7A1* expression in fibroblasts (Kon 2005). Interestingly, keratinocyte *COL7A1* expression was substantially increased when cells were treated with TGF-β in addition to one or both of TNF-α and IL-1β, suggesting that their effects on *COL7A1* are more context-dependent (Takeda 2005). TNF-α also increases expression of c-Jun and JunB, two of the proteins that can form the AP-1 transcription factor. As a transcription factor, AP-1 promotes *COL7A1* expression by binding to *COL7A1* promoter, but the individual components, c-Jun and JunB, can each bind SMAD3 and prevent it from binding to DNA, inhibiting TGF-β/Smad-driven *COL7A1* expression (Verrecchia 2000, 2001a, 2001b). AP-1 is positively regulated by TNF-α and PI3K/AKT, which are inhibited by kaempferol, and MAPK/ERK, which is activated by kaempferol, so the overall effect of kaempferol on AP-1 likely depends on the relative expression of these pathways in the treated cells.

Another potential mechanism by which kaempferol could increase C7 production is through the Sp1 transcription factor, which is known to promote *COL7A1* expression. The *COL7A1* promoter contains numerous Sp1 binding sites, including five within the 600 bases directly upstream of the transcription start site (Naso 2003). There were also two sgRNAs for Sp1 enriched in our screen. Previous studies have described both positive (Wei 2014, Ochiai 2016) and negative (Zhou 2018) effects of kaempferol on Sp1 activity, suggesting that the effect of kaempferol on Sp1 expression is likely context-dependent.

DEB skin is characterized by chronic inflammation and fibrosis that facilitate disease progression and eventually lead to RDEBSCC development. Recent studies have illustrated the potential therapeutic benefits of kaempferol in the skin using mouse/rat models of dermatological conditions. Topical application of kaempferol was found to significantly improve healing of incisional and excisional wounds in diabetic and non-diabetic rats, with treated rat wounds showing higher rates of re-epithelialization, hydroxyproline levels, and tensile strength (Ozay 2019). Numerous studies have found that kaempferol exhibits substantial anti-fibrotic and anti-inflammatory activity. Kaempferol reduced oxidative stress, production of proinflammatory cytokines and mediators of fibrosis, immune infiltrate, and apoptosis in lesional skin of mice with bleomycin-induced fibrosis (Sekiguchi 2019). A separate study showed that kaempferol inhibited oxidative stress and fibrosis through suppression of hypoxia-associated ATP/IL-6 signaling in mice with bleomycin-induced fibrosis and in fibroblasts from patients with systemic sclerosis

(Perera 2019). In a mouse model of psoriasis, kaempferol treatment resulted in reduced immune cell infiltration, T cell proliferation, and expression of proinflammatory proteins such as IL-6, IL-17A, TNF-α, and NF-κB in lesional skin (Liu 2019). In a mouse model of atopic dermatitis (AD), mice that received kaempferol had a substantially attenuated AD phenotype, including reduced skin thickness, lymph node size, mast cell invasion, serum IgE levels, and expression of inflammatory cytokines (Lee & Jeong 2021). These effects were found to be caused by inhibition of multidrug resistance-associated protein 1 (MRP-1), an ATP-binding cassette protein that is crucial for T cell activation, activation-related signaling, and subsequent apoptosis (Lee & Jeong 2021). Inhibition of MRP-1 inhibited phosphorylation of JNK, leading to inhibition of c-Jun activation (and AP-1 activity); and of the TAK1 and IKKα kinases, which led to reduced NF-κB activation and IL-2 expression (Lee & Jeong 2021). Overall, these studies have demonstrated that kaempferol reduces inflammation and fibrosis and promotes wound healing in the skin with very low toxicity. This suggests that kaempferol may be able to facilitate wound healing and skin integrity in people with DEB through C7-dependent and C7-independent mechanisms.

In addition to its potent anti-fibrotic and anti-inflammatory characteristics, kaempferol also exhibits potent anti-cancer activity, suggesting that it could potentially be useful in treating RDEBSCC. Kaempferol has been shown to inhibit proliferation, migration, invasion, angiogenesis, lipogenesis, glucose uptake, and oxidative phosphorylation and increase growth arrest, apoptosis, and oxidative stress in a variety of cancer types (Chen & Chen 2013). A recent study found that the multikinase inhibitor rigosertib was able to induce apoptosis in ten RDEBSCC cell lines and inhibit growth of RDEBSCCs in murine xenografts with low toxicity, which led to the authorization of an early phase clinical trial for rigosertib in patients with RDEBSCC (Atanasova 2019b). Rigosertib was initially investigated as an inhibitor of polo-like kinase 1 (PLK1) but has also been shown to activate the oxidative stress response via AP-1 and inhibit activation of PI3K/AKT, RAS-mediated activation of MAPK/ERK, and stabilization of microtubules (Watt 2011, Chapman 2012, Prasad 2016, Athuluri-Divakar 2016, Jost 2017, Atanasova 2019b). Kaempferol has been shown to inhibit PLK1 and PI3K/AKT and increase AP-1 production via MAPK/ERK signaling, suggesting that it could also induce apoptosis of RDEBSCC cells (Kang 2009, Chen & Chen 2013, Kim 2020).

BIBLIOGRAPHY

1. Has, C., Bauer, J.W., Bodemer, C., Bolling, M.C., Bruckner-Tuderman, L., Diem, A., Fine, J. -D., Heagerty, A., Hovnanian, A., Marinkovich, M.P., et al. (2020a). Consensus reclassification of inherited epidermolysis bullosa and other disorders with skin fragility. Br. J. Dermatol. *183*, 614–627.
2. Kero, M. (1984). Occurrence of epidermolysis bullosa in Finland. Acta Derm Venereol *64*, 57–62.
3. Inaba, Y., Kitamura, K., Ogawa, H., Manabe, M., and Sasai, Y. (1989). [A study on the estimation of prevalence of epidermolysis bullosa in Japan]. Nihon Hifuka Gakkai Zasshi *99*, 1021–1026.
4. Pavičić, Ž., Kmet-Vižintin, P., Kansky, A., and Dobrić, I. (1990). Occurrence of Hereditary Bullous Epidermolyses in Croatia. Pediatr Dermatol *7*, 108–110.
5. McKenna, K.E., Walsh, M.Y., and Bingham, E.A. (1992). Epidermolysis bullosa in Northern Ireland. Br J Dermatol *127*, 318–321.
6. Abahussein, A.A., Al-Zayir, A.A., Mostafa, W.Z., and Okoro, A.N. (1993). Epidermolysis bullosa in the eastern province of Saudi Arabia. Int J Dermatol *32*, 579–581.
7. Horn, H.M., Priestley, G.C., Eady, R. a. J., and Tidman, M.J. (1997). The prevalence of epidermolysis bullosa in Scotland. British Journal of Dermatology *136*, 560–564.
8. Fine, J.-D., Eady, R.A.J., Bauer, E.A., Briggaman, R.A., Bruckner-Tuderman, L., Christiano, A., Heagerty, A., Hintner, H., Jonkman, M.F., McGrath, J., et al. (2000). Revised classification system for inherited epidermolysis bullosa. Journal of the American Academy of Dermatology *42*, 1051–1066.
9. Tadini, G., Gualandri, L., Colombi, M., Paradisi, M., Angelo, C., Zambruno, G., Castiglia, L., Annicchiarico, G., Hasheem, M.E., Barlati, S., et al. (2005). II registre italiano delle epidermolisi bollose ereditarie. Giornale italiano di dermatologia e venereologia : organo ufficiale, Societa italiana di dermatologia e sifilografia *140*, 359–372.
10. Abu Sa'd, J., Indelman, M., Pfendner, E., Falik-Zaccai, T.C., Mizrachi-Koren, M., Shalev, S., Amitai, D.B., Raas-Rothshild, A., Adir-Shani, A., Borochowitz, Z.-U., et al. (2006). Molecular Epidemiology of Hereditary Epidermolysis Bullosa in a Middle Eastern Population. Journal of Investigative Dermatology *126*, 777–781.
11. Kho, Y.C., Rhodes, L.M., Robertson, S.J., Su, J., Varigos, G., Robertson, I., Hogan, P., Orchard, D., and Murrell, D.F. (2010). Epidemiology of Epidermolysis Bullosa in the Antipodes: The Australasian Epidermolysis Bullosa Registry With a Focus on Herlitz Junctional Epidermolysis Bullosa. Arch Dermatol *146*.
12. Hernandez-Martín, A., Aranegui, B., Escámez, M.J., de Lucas, R., Vicente, A., Rodríguez-Díaz, E., Bernabeu-Wittel, J., Gonzalez-Hermosa, R., García-Patos, V., Ginarte, M., et al. (2013). Prevalence of Dystrophic Epidermolysis Bullosa in Spain: A Population-Based Study Using the 3-Source Capture–Recapture Method. Evidence of a Need for Improvement in Care. Actas Dermo-Sifiliográficas *104*, 890–896.
13. Dănescu, S., Has, C., Senila, S., Ungureanu, L., and Cosgarea, R. (2015). Epidemiology of inherited epidermolysis bullosa in Romania and genotype-phenotype correlations in patients with dystrophic epidermolysis bullosa. J Eur Acad Dermatol Venereol *29*, 899–903.
14. Fine, J.-D. (2016). Epidemiology of Inherited Epidermolysis Bullosa Based on Incidence and Prevalence Estimates From the National Epidermolysis Bullosa Registry. JAMA Dermatol *152*, 1231.
15. Baardman, R., Yenamandra, V.K., Duipmans, J.C., Pasmooij, A.M.G., Jonkman, M.F., Akker, P.C., and Bolling, M.C. (2020). Novel insights into the epidemiology of epidermolysis bullosa (EB) from the Dutch EB Registry: EB more common than previously assumed? J Eur Acad Dermatol Venereol *35*, 995–1006.

16. Fine, J.-D., Bruckner-Tuderman, L., Eady, R.A.J., Bauer, E.A., Bauer, J.W., Has, C., Heagerty, A., Hintner, H., Hovnanian, A., Jonkman, M.F., et al. (2014). Inherited epidermolysis bullosa: Updated recommendations on diagnosis and classification. Journal of the American Academy of Dermatology *70*, 1103–1126.
17. Has, C., Liu, L., Bolling, M.C., Charlesworth, A.V., El Hachem, M., Escámez, M.J., Fuentes, I., Büchel, S., Hiremagalore, R., Pohla-Gubo, G., et al. (2020b). Clinical practice guidelines for laboratory diagnosis of epidermolysis bullosa. Br J Dermatol *182*, 574–592.
18. Theocharidis, G., and Connelly, J.T. (2019). Minor collagens of the skin with not so minor functions. J. Anat. *235*, 418–429.
19. Parente, M.G., Chung, L.C., Ryynanen, J., Woodley, D.T., Wynn, K.C., Bauer, E.A., Mattei, M.G., Chu, M.L., and Uitto, J. (1991). Human type VII collagen: cDNA cloning and chromosomal mapping of the gene. Proceedings of the National Academy of Sciences *88*, 6931–6935.
20. Greenspan, Ds., Byers, Mg., Eddy, Rl., Hoffman, Gg., and Shows, Tb. (1993). Localization of the human collagen gene COL7A1 to 3p21.3 by fluorescence in situ hybridization. Cytogenetics Cell Genet *62*, 35–36.
21. Christiano, A.M., Greenspan, D.S., Lee, S., and Uitto, J. (1994a). Cloning of human type VII collagen. Complete primary sequence of the alpha 1(VII) chain and identification of intragenic polymorphisms. Journal of Biological Chemistry *269*, 20256–20262.
22. Christiano, A.M., Hoffman, G.G., Chung-Honet, L.C., Lee, S., Cheng, W., Uitto, J., and Greenspan, D.S. (1994b). Structural Organization of the Human Type VII Collagen Gene (COL7A1), Composed of More Exons Than Any Previously Characterized Gene. Genomics *21*, 169–179.
23. Morris, N.P., Keene, D.R., Glanville, R.W., Bentz, H., and Burgeson, R.E. (1986). The tissue form of type VII collagen is an antiparallel dimer. Journal of Biological Chemistry *261*, 5638–5644.
24. Burgeson, R.E. (1993). Type VII Collagen, Anchoring Fibrils, and Epidermolysis Bullosa. Journal of Investigative Dermatology *101*, 252–255.
25. Bruckner-Tuderman, L., Nilssen, O., Zimmermann, D.R., Dours-Zimmermann, M.T., Kalinke, D.U., Gedde-Dahl, T., and Winberg, J.O. (1995). Immunohistochemical and mutation analyses demonstrate that procollagen VII is processed to collagen VII through removal of the NC-2 domain. Journal of Cell Biology *131*, 551–559.
26. Sakai, L.Y., Keene, D.R., Morris, N.P., and Burgeson, R.E. (1986). Type VII collagen is a major structural component of anchoring fibrils. Journal of Cell Biology *103*, 1577–1586.
27. Bruckner-Tuderman, L., Höpfner, B., and Hammami-Hauasli, N. (1999). Biology of anchoring fibrils: lessons from dystrophic epidermolysis bullosa. Matrix Biology *18*, 43–54.
28. Chung, H.J., and Uitto, J. (2010). Type VII Collagen: The Anchoring Fibril Protein at Fault in Dystrophic Epidermolysis Bullosa. Dermatologic Clinics *28*, 93–105.
29. Burgeson, R.E., Morris, N.P., Murray, L.W., Duncan, K.G., Keene, D.R., and Sakai, L.Y. (1985). The Structure of Type VII Collagen. Annals of the New York Academy of Sciences *460*, 47–57.
30. Burgeson, R.E., Lunstrum, G.P., Rokosova, B., Rimberg, C.S., Rosenbaum, L.M., and Keene, D.R. (1990). The Structure and Function of Type VII Collagen. Ann NY Acad Sci *580*, 32–43.
31. Christiano, A.M., Rosenbaum, L.M., Chung-Honet, L.C., Parente, M.G., Woodley, D.T., Pan, T.-C., Zhang, R.Z., Chu, M.-L., Burgeson, R.E., and Uitto, J. (1992). The large non-collagenous domain (NC-1) of type VII collagen is amino-terminal and chimeric. Homology to cartilage matrix protein, the type III domains of fibronectin and the A domains of von Willebrand factor. Hum Mol Genet *1*, 475–481.
32. Chen, M., Marinkovich, M.P., Veis, A., Cai, X., Rao, C.N., O'Toole, E.A., and Woodley, D.T. (1997). Interactions of the Amino-terminal Noncollagenous (NC1) Domain of Type

VII Collagen with Extracellular Matrix Components. Journal of Biological Chemistry *272*, 14516–14522.

33. Chen, M., Jones, J.C.R., O'Toole, E.A., Li, Y.-Y., Woodley, D.T., and Peter Marinkovich, M. (1999). NC1 Domain of Type VII Collagen Binds to the β3 Chain of Laminin 5 Via a Unique Subdomain Within the Fibronectin-Like Repeats. Journal of Investigative Dermatology *112*, 177–183.
34. Brittingham, R., Uitto, J., and Fertala, A. (2006). High-affinity binding of the NC1 domain of collagen VII to laminin 5 and collagen IV. Biochemical and Biophysical Research Communications *343*, 692–699.
35. Villone, D., Fritsch, A., Koch, M., Bruckner-Tuderman, L., Hansen, U., and Bruckner, P. (2008). Supramolecular Interactions in the Dermo-epidermal Junction Zone. Journal of Biological Chemistry *283*, 24506–24513.
36. Wegener, H., Leineweber, S., and Seeger, K. (2013). The vWFA2 domain of type VII collagen is responsible for collagen binding. Biochemical and Biophysical Research Communications *430*, 449–453.
37. Gebauer, J.M., Flachsenberg, F., Windler, C., Richer, B., Baumann, U., and Seeger, K. (2020). Structural and biophysical characterization of the type VII collagen vWFA2 subdomain leads to identification of two binding sites. FEBS Open Bio *10*, 580–592.
38. Aho, S., and Uitto, J. (1998). Two-hybrid Analysis Reveals Multiple Direct Interactions for Thrombospondin I. 12.
39. Atanasova, V.S., Russell, R.J., Webster, T.G., Cao, Q., Agarwal, P., Lim, Y.Z., Krishnan, S., Fuentes, I., Guttmann-Gruber, C., McGrath, J.A., et al. (2019). Thrombospondin-1 Is a Major Activator of TGF-β Signaling in Recessive Dystrophic Epidermolysis Bullosa Fibroblasts. Journal of Investigative Dermatology *139*, 1497-1505.e5.
40. Bentz, H., Morris, N.P., Murray, L.W., Sakai, L.Y., Hollister, D.W., and Burgeson, R.E. (1983). Isolation and partial characterization of a new human collagen with an extended triple-helical structural domain. Proceedings of the National Academy of Sciences *80*, 3168–3172.
41. Bächinger, H.P., Morris, N.P., Lunstrum, G.P., Keene, D.R., Rosenbaum, L.M., Compton, L.A., and Burgeson, R.E. (1990). The relationship of the biophysical and biochemical characteristics of type VII collagen to the function of anchoring fibrils. Journal of Biological Chemistry *265*, 10095–10101.
42. Colombo, M., Brittingham, R.J., Klement, J.F., Majsterek, I., Birk, D.E., Uitto, J., and Fertala, A. (2003). Procollagen VII Self-Assembly Depends on Site-Specific Interactions and Is Promoted by Cleavage of the NC2 Domain with Procollagen C-Proteinase. Biochemistry *42*, 11434–11442.
43. Rattenholl, A., Pappano, W.N., Koch, M., Keene, D.R., Kadler, K.E., Sasaki, T., Timpl, R., Burgeson, R.E., Greenspan, D.S., and Bruckner-Tuderman, L. (2002). Proteinases of the Bone Morphogenetic Protein-1 Family Convert Procollagen VII to Mature Anchoring Fibril Collagen. Journal of Biological Chemistry *277*, 26372–26378.
44. Mariath, L.M., Santin, J.T., Schuler-Faccini, L., and Kiszewski, A.E. (2020). Inherited epidermolysis bullosa: update on the clinical and genetic aspects. Anais Brasileiros de Dermatologia *95*, 551–569.
45. Varki, R., Sadowski, S., Uitto, J., and Pfendner, E. (2006). Epidermolysis bullosa. II. Type VII collagen mutations and phenotype-genotype correlations in the dystrophic subtypes. Journal of Medical Genetics *44*, 181–192.
46. Dang, N., and Murrell, D.F. (2008). Mutation analysis and characterization of COL7A1 mutations in dystrophic epidermolysis bullosa. Exp Dermatol *17*, 553–568.
47. Hammami-Hauasli, N., Schumann, H., Raghunath, M., Kilgus, O., Lüthi, U., Luger, T., and Bruckner-Tuderman, L. (1998). Some, but Not All, Glycine Substitution Mutations

inCOL7A1 Result in Intracellular Accumulation of Collagen VII, Loss of Anchoring Fibrils, and Skin Blistering. Journal of Biological Chemistry *273*, 19228–19234.

48. Sakuntabhai, A., Hammami-Hauasli, N., Bodemer, C., Rochat, A., Prost, C., Barrandon, Y., de Prost, Y., Lathrop, M., Wojnarowska, F., Bruckner-Tuderman, L., et al. (1998). Deletions within COL7A1 Exons Distant from Consensus Splice Sites Alter Splicing and Produce Shortened Polypeptides in Dominant Dystrophic Epidermolysis Bullosa. The American Journal of Human Genetics *63*, 737–748.
49. Mellerio, Salas-Alanis, Talamantes, Horn, Tidman, Ashton, Eady, and Mcgrath (1998). A recurrent glycine substitution mutation, G2043R, in the type VII collagen gene (COL7A1) in dominant dystrophic epidermolysis bullosa: GLYCINE MUTATION, COLLAGEN VII AND DEB. British Journal of Dermatology *139*, 730–737.
50. Mecklenbeck, S., Hammami-Hauasli, N., Höpfner, B., Schumann, H., Kramer, A., Bruckner-Tuderman, L., and Küster, W. (1999). Clustering of COL7A1 Mutations in Exon 73: Implications for Mutation Analysis in Dystrophic Epidermolysis Bullosa. Journal of Investigative Dermatology *112*, 398–400.
51. Christiano, A.M., Morricone, A., Paradisi, M., Angelo, C., Mazzanti, C., Cavalieri, R., and Uitto, J. (1995). A Glycine-to-Arginine Substitution in the Triple-Helical Domain of Type VII Collagen in a Family with Dominant Dystrophic Epidermolysis Bullosa. Journal of Investigative Dermatology *104*, 438–440.
52. Christiano, A.M., McGrath, J.A., Tan, K.C., and Uitto, J. (1996). Glycine substitutions in the triple-helical region of type VII collagen result in a spectrum of dystrophic epidermolysis bullosa phenotypes and patterns of inheritance. Am J Hum Genet *58*, 671–681.
53. Cserhalmi-Friedman, P.B., Karpati, S., Horvath, A., and Christiano, A.M. (1997). Identification of the glycine-to-arginine substitution G2043R in type VII collagen in a family with dominant dystrophic epidermolysis bullosa from Hungary. Exp Dermatol *6*, 303–307.
54. Winberg, J. (1997). Modulation of disease severity of dystrophic epidermolysis bullosa by a splice site mutation in combination with a missense mutation in the COL7A1 gene. Human Molecular Genetics *6*, 1125–1135.
55. Almaani, N., McGrath, J., Liu, L., Dopping-Hepenstal, P., Lai-Cheong, J., Wong, A., Nanda, A., Moss, C., Martinéz, A., and Mellerio, J. (2011). Identical Glycine Substitution Mutations in Type VII Collagen May Underlie Both Dominant and Recessive Forms of Dystrophic Epidermolysis Bullosa. Acta Derm Venerol *91*, 262–266.
56. Turczynski, S., Titeux, M., Pironon, N., Cohn, H.I., Murrell, D.F., and Hovnanian, A. (2016). Marked intrafamilial phenotypic heterogeneity in dystrophic epidermolysis bullosa caused by inheritance of a mild dominant glycine substitution and a novel deep intronic recessive *COL7A1* mutation. Br J Dermatol *174*, 1122–1125.
57. Gardella, R., Belletti, L., Barlati, S., and Colombi, M. (1996). Identification of Two Splicing Mutations in the Collagen Type VII Gene (COL7A1) of a Patient Affected by the Localisata Variant of Recessive Dystrophic Epidermolysis Bullosa. Am. J. Hum. Genet. 9.
58. Gardella, R., Castiglia, D., Posteraro, P., Bernardini, S., Zoppi, N., Paradisi, M., Tadini, G., Barlati, S., McGrath, J.A., Zambruno, G., et al. (2002). Genotype–Phenotype Correlation in Italian Patients with Dystrophic Epidermolysis Bullosa. Journal of Investigative Dermatology *119*, 1456–1462.
59. Järvikallio, A., Pulkkinen, L., and Uitto, J. (1997). Molecular basis of dystrophic epidermolysis bullosa: Mutations in the type VII collagen gene (COL7A1). Human Mutation *10*, 338–347.
60. Kern, J.S., Kohlhase, J., Bruckner-Tuderman, L., and Has, C. (2006). Expanding the COL7A1 Mutation Database: Novel and Recurrent Mutations and Unusual Genotype – Phenotype Constellations in 41 Patients with Dystrophic Epidermolysis Bullosa. Journal of Investigative Dermatology *126*, 1006–1012.

61. van den Akker, P.C., van Essen, A.J., Kraak, M.M.J., Meijer, R., Nijenhuis, M., Meijer, G., Hofstra, R.M.W., Pas, H.H., Scheffer, H., and Jonkman, M.F. (2009). Long-term follow-up of patients with recessive dystrophic epidermolysis bullosa in the Netherlands: Expansion of the mutation database and unusual phenotype–genotype correlations. Journal of Dermatological Science *56*, 9–18.
62. Mariath, L.M., Santin, J.T., Frantz, J.A., Doriqui, M.J.R., Kiszewski, A.E., and Schuler-Faccini, L. (2019). An overview of the genetic basis of epidermolysis bullosa in Brazil: discovery of novel and recurrent disease-causing variants. Clin Genet *96*, 189–198.
63. Hovnanian, A., Rochat, A., Bodemer, C., Petit, E., Rivers, C.A., Prost, C., Fraitag, S., Christiano, A.M., Uitto, J., Lathrop, M., et al. (1997). Characterization of 18 New Mutations in COL7A1 in Recessive Dystrophic Epidermolysis Bullosa Provides Evidence for Distinct Molecular Mechanisms Underlying Defective Anchoring Fibril Formation. Am. J. Hum. Genet. 12.
64. Terracina, M., Posteraro, P., Zambruno, G., Castiglia, D., Schubert, M., Sonego, G., Atzori, F., and Bruckner-Tuderman, L. (1998). Compound Heterozygosity for a Recessive Glycine Substitution and a Splice Site Mutation in the COL7A1 Gene Causes an Unusually Mild Form of Localized Recessive Dystrophic Epidermolysis Bullosa. Journal of Investigative Dermatology *111*, 744–750.
65. Toyonaga, E., Nishie, W., Komine, M., Murata, S., Shinkuma, S., Natsuga, K., Nakamura, H., Ohtsuki, M., and Shimizu, H. (2015). Skipped exon in COL7A1 determines the clinical phenotypes of dystrophic epidermolysis bullosa. Br J Dermatol *172*, 1141–1144.
66. McGrath, J.A., Schofield, O.M.V., and Eady, R.A.J. (1994). Epidermolysis bullosa pruriginosa: dystrophic epidermolysis bullosa with distinctive clinicopathological features. Br J Dermatol *130*, 617–625.
67. Fine, J.-D. (2010). Inherited epidermolysis bullosa. 17.
68. Christiano, A.M., Fine, J.-D., and Uitto, J. (1997). Genetic Basis of Dominantly Inherited Transient Bullous Dermolysis of the Newborn: A Splice Site Mutation in the Type VII Collagen Gene. Journal of Investigative Dermatology *109*, 811–814.
69. Fassihi, H., Diba, V.C., Wessagowit, V., Dopping-Hepenstal, P.J.C., Jones, C.A., Burrows, N.P., and McGrath, J.A. (2005). Transient bullous dermolysis of the newborn in three generations. Br J Dermatol *153*, 1058–1063.
70. Shi, B.-J., Zhu, X.-J., Liu, Y., Hao, J., Yan, G.-F., Wang, S.-P., Wang, X.-Y., and Diao, Q.-C. (2015). Transient bullous dermolysis of the newborn: a novel *de novo* mutation in the *COL7A1* gene. Int J Dermatol *54*, 438–442.
71. Chiaverini, C., Charlesworth, A.V., Youssef, M., Cuny, J.-F., Rabia, S.H., Lacour, J.-P., and Meneguzzi, G. (2010). Inversa Dystrophic Epidermolysis Bullosa Is Caused by Missense Mutations at Specific Positions of the Collagenic Domain of Collagen Type VII. Journal of Investigative Dermatology *130*, 2508–2511.
72. van den Akker, P.C., Mellerio, J.E., Martinez, A.E., Liu, L., Meijer, R., Dopping-Hepenstal, P.J.C., van Essen, A.J., Scheffer, H., Hofstra, R.M.W., McGrath, J.A., et al. (2011). The inversa type of recessive dystrophic epidermolysis bullosa is caused by specific arginine and glycine substitutions in type VII collagen. Journal of Medical Genetics *48*, 160–167.
73. Care for Blisters | debra of America. https://www.debra.org/how/care-blisters
74. El Hachem, M., Zambruno, G., Bourdon-Lanoy, E., Ciasulli, A., Buisson, C., Hadj-Rabia, S., Diociaiuti, A., Gouveia, C.F., Hernández-Martín, A., de Lucas Laguna, R., et al. (2014). Multicenter consensus recommendations for skin care in inherited epidermolysis bullosa. Orphanet J Rare Dis *9*, 76.
75. Rashidghamat, E., and McGrath, J.A. (2017). Novel and emerging therapies in the treatment of recessive dystrophic epidermolysis bullosa. Interactable & Rare Diseases Research *6*, 6–20.

76. Wiegand, C., Schönfelder, U., Abel, M., Ruth, P., Kaatz, M., and Hipler, U.-C. (2010). Protease and pro-inflammatory cytokine concentrations are elevated in chronic compared to acute wounds and can be modulated by collagen type I in vitro. Arch Dermatol Res *302*, 419–428.
77. Gorell, E.S., Leung, T.H., Khuu, P., and Lane, A.T. (2015). Purified Type I Collagen Wound Matrix Improves Chronic Wound Healing in Patients with Recessive Dystrophic Epidermolysis Bullosa. Pediatr Dermatol *32*, 220–225.
78. Bruckner, A.L., Losow, M., Wisk, J., Patel, N., Reha, A., Lagast, H., Gault, J., Gershkowitz, J., Kopelan, B., Hund, M., et al. (2020). The challenges of living with and managing epidermolysis bullosa: insights from patients and caregivers. Orphanet J Rare Dis *15*, 1.
79. Stanley, J.R., Rubinstein, N., and Klaus-Kovtun, V. (1985). Epidermolysis Bullosa Acquisita Antigen Is Synthesized by Both Human Keratinocytes and Human Dermal Fibroblasts. Journal of Investigative Dermatology *85*, 542–545.
80. Bruckner-Tuderman, L., Schnyder, U.W., Winterhalter, K.H., and Bruckner, P. (1987). Tissue form of type VII collagen from human skin and dermal fibroblasts in culture. Eur J Biochem *165*, 607–611.
81. König, A., and Bruckner-Tuderman, L. (1992). Transforming Growth Factor-0 Stimulates Collagen VII Expression by Cutaneous Cells In Vitro. The Journal of Cell Biology *117*, 7.
82. Ryynänen, J., Sollberg, S., Parente, M.G., Chung, L.C., Christiano, A.M., and Uitto, J. (1992). Type VII collagen gene expression by cultured human cells and in fetal skin. Abundant mRNA and protein levels in epidermal keratinocytes. J. Clin. Invest. *89*, 163–168.
83. Goto, M., Sawamura, D., Ito, K., Abe, M., Nishie, W., Sakai, K., Shibaki, A., Akiyama, M., and Shimizu, H. (2006). Fibroblasts Show More Potential as Target Cells than Keratinocytes in COL7A1 Gene Therapy of Dystrophic Epidermolysis Bullosa. Journal of Investigative Dermatology *126*, 766–772.
84. Woodley, D.T., Atha, T., Huang, Y., Chen, M., Krueger, G.G., Jorgensen, C.M., Fairley, J.A., Chan, L., and Keene, D.R. (2003). Normal and Gene-Corrected Dystrophic Epidermolysis Bullosa Fibroblasts Alone Can Produce Type VII Collagen at the Basement Membrane Zone. Journal of Investigative Dermatology *121*, 1021–1028.
85. Fritsch, A., Loeckermann, S., Kern, J.S., Braun, A., Bösl, M.R., Bley, T.A., Schumann, H., von Elverfeldt, D., Paul, D., Erlacher, M., et al. (2008). A hypomorphic mouse model of dystrophic epidermolysis bullosa reveals mechanisms of disease and response to fibroblast therapy. J. Clin. Invest. *118*, 1669–1679.
86. Kern, J.S., Loeckermann, S., Fritsch, A., Hausser, I., Roth, W., Magin, T.M., Mack, C., Müller, M.L., Paul, O., Ruther, P., et al. (2009). Mechanisms of Fibroblast Cell Therapy for Dystrophic Epidermolysis Bullosa: High Stability of Collagen VII Favors Long-term Skin Integrity. Molecular Therapy *17*, 1605–1615.
87. McGuire, J., Birchall, N., Cuono, C., Moellmann, G., Kuklinska, E., and Langdon, R. (1987). Successful Engraftment of Allogeneic Keratinocyte Cultures in Recessive Dystrophic Epidermolysis-Bullosa. J. Invest. Dermatol. *88*, 506–506.
88. Wong, T., Gammon, L., Liu, L., Mellerio, J.E., Dopping-Hepenstal, P.J.C., Pacy, J., Elia, G., Jeffery, R., Leigh, I.M., Navsaria, H., et al. (2008). Potential of Fibroblast Cell Therapy for Recessive Dystrophic Epidermolysis Bullosa. Journal of Investigative Dermatology *128*, 2179–2189.
89. Natsuga, K., Sawamura, D., Goto, M., Homma, E., Goto-Ohguchi, Y., Aoyagi, S., Akiyama, M., Kuroyanagi, Y., and Shimizu, H. (2010). Response of Intractable Skin Ulcers in Recessive Dystrophic Epidermolysis Bullosa Patients to an Allogeneic Cultured Dermal Substitute. Acta Derm Venerol *90*, 165–169.
90. Nagy, N., Almaani, N., Tanaka, A., Lai-Cheong, J.E., Techanukul, T., Mellerio, J.E., and McGrath, J.A. (2011). HB-EGF Induces COL7A1 Expression in Keratinocytes and

Fibroblasts: Possible Mechanism Underlying Allogeneic Fibroblast Therapy in Recessive Dystrophic Epidermolysis Bullosa. Journal of Investigative Dermatology *131*, 1771–1774.

91. Petrof, G., Martinez-Queipo, M., Mellerio, J.E., Kemp, P., and McGrath, J.A. (2013). Fibroblast cell therapy enhances initial healing in recessive dystrophic epidermolysis bullosa wounds: results of a randomized, vehicle-controlled trial. Br J Dermatol *169*, 1025–1033.
92. Venugopal, S.S., Yan, W., Frew, J.W., Cohn, H.I., Rhodes, L.M., Tran, K., Melbourne, W., Nelson, J.A., Sturm, M., Fogarty, J., et al. (2013). A phase II randomized vehicle-controlled trial of intradermal allogeneic fibroblasts for recessive dystrophic epidermolysis bullosa. Journal of the American Academy of Dermatology *69*, 898-908.e7.
93. Moravvej, H., Abdollahimajd, F., Naseh, M.H., Piravar, Z., Abolhasani, E., Mozafari, N., and Niknejad, H. (2018). Cultured allogeneic fibroblast injection vs. fibroblasts cultured on amniotic membrane scaffold for dystrophic epidermolysis bullosa treatment. Br J Dermatol *179*, 72–79.
94. Russo, B., Brembilla, N.C., and Chizzolini, C. (2020). Interplay Between Keratinocytes and Fibroblasts: A Systematic Review Providing a New Angle for Understanding Skin Fibrotic Disorders. Front. Immunol. *11*, 648.
95. Falabella, A.F., Valencia, I.C., Eaglstein, W.H., and Schachner, L.A. (2000). Tissue-Engineered Skin (Apligraf) in the Healing of Patients With Epidermolysis Bullosa Wounds. Arch Dermatol *136*.
96. Fivenson, D.P., Scherschun, L., Choucair, M., KuKuruga, D., Young, J., and Shwayder, T. (2003a). Graftskin therapy in epidermolysis bullosa. Journal of the American Academy of Dermatology *48*, 886–892.
97. Fivenson, D.P., Scherschun, L., and Cohen, L.V. (2003b). Apligraf in the Treatment of Severe Mitten Deformity Associated with Recessive Dystrophic Epidermolysis Bullosa. Plastic and Reconstructive Surgery *112*, 584–588.
98. Phillips, J., and Rockwell, W.B. (2003). Surgical Treatment of Recessive Dystrophic Epidermolysis Bullosa in the Hand: Use of Tissue-Engineered Skin (Apligraf): Annals of Plastic Surgery *50*, 441–442.
99. Martínez Pardo, M.E., Reyes Frías, M.L., Ramos Durón, L.E., Gutiérrez Salgado, E., Gómez, J.C., Marín, M.A., and Luna Zaragoza, D. (1999). Clinical application of amniotic membranes on a patient with epidermolysis bullosa. Ann Transplant *4*, 68–73.
100. Department of Nanomedicine and Tissue Engineering, Shaheed Beheshti Medical University, Tehran, Iran., Niknejad, H., Peirovi, H., Jorjani, M., Ahmadiani, A., Ghanavi, J., and Seifalian, A. (2008). Properties of the amniotic membrane for potential use in tissue engineering. ECM *7*, 88–99.
101. Lo, V., Lara-Corrales, I., Stuparich, A., and Pope, E. (2010). Amniotic membrane grafting in patients with epidermolysis bullosa with chronic wounds. Journal of the American Academy of Dermatology *62*, 1038–1044.
102. Gibbons, G.W. (2015). Grafix®, a Cryopreserved Placental Membrane, for the Treatment of Chronic/Stalled Wounds. Advances in Wound Care *4*, 534–544.
103. Nevala-Plagemann, C., Lee, C., and Tolar, J. (2015). Placenta-based therapies for the treatment of epidermolysis bullosa. Cytotherapy *17*, 786–795.
104. Marinkovich, M.P., and Tang, J.Y. (2019). Gene Therapy for Epidermolysis Bullosa. Journal of Investigative Dermatology *139*, 1221–1226.
105. Jiang, W., Bu, D., Yang, Y., and Zhu, X. (2002a). A Novel Splice Site Mutation in Collagen Type VII Gene in a Chinese Family with Dominant Dystrophic Epidermolysis Bullosa Pruriginosa. Acta Dermato-Venereologica *82*, 187–191.
106. Peister, A., Mellad, J.A., Larson, B.L., Hall, B.M., Gibson, L.F., and Prockop, D.J. (2004). Adult stem cells from bone marrow (MSCs) isolated from different strains of inbred mice vary in surface epitopes, rates of proliferation, and differentiation potential. Blood *103*, 1662–1668.

107. Kunter, U., Rong, S., Djuric, Z., Boor, P., Müller-Newen, G., Yu, D., and Floege, J. (2006). Transplanted Mesenchymal Stem Cells Accelerate Glomerular Healing in Experimental Glomerulonephritis. JASN *17*, 2202–2212.
108. Ortiz, L.A., DuTreil, M., Fattman, C., Pandey, A.C., Torres, G., Go, K., and Phinney, D.G. (2007). Interleukin 1 receptor antagonist mediates the anti-inflammatory and antifibrotic effect of mesenchymal stem cells during lung injury. Proceedings of the National Academy of Sciences *104*, 11002–11007.
109. Phinney, D.G., and Prockop, D.J. (2007). Concise Review: Mesenchymal Stem/Multipotent Stromal Cells: The State of Transdifferentiation and Modes of Tissue Repair—Current Views. STEM CELLS *25*, 2896–2902.
110. Tögel, F., and Westenfelder, C. (2007). Adult bone marrow–derived stem cells for organ regeneration and repair. Developmental Dynamics *236*, 3321–3331.
111. Tolar, J., Wang, X., Braunlin, E., McElmurry, R.T., Nakamura, Y., Bell, S., Xia, L., Zhang, J., Hu, Q., Panoskaltsis-Mortari, A., et al. (2007). The host immune response is essential for the beneficial effect of adult stem cells after myocardial ischemia. Exp Hematology *35*, 682–690.
112. Tolar, J., Ishida-Yamamoto, A., Riddle, M., McElmurry, R.T., Osborn, M., Xia, L., Lund, T., Slattery, C., Uitto, J., Christiano, A.M., et al. (2009). Amelioration of epidermolysis bullosa by transfer of wild-type bone marrow cells. Blood *113*, 1167–1174.
113. Wagner, J.E., Ishida-Yamamoto, A., McGrath, J.A., Hordinsky, M., Keene, D.R., Woodley, D.T., Chen, M., Riddle, M.J., Osborn, M.J., Lund, T., et al. (2010). Bone Marrow Transplantation for Recessive Dystrophic Epidermolysis Bullosa. N Engl J Med *363*, 629–639.
114. Tolar, J., and Wagner, J.E. (2013). Allogeneic blood and bone marrow cells for the treatment of severe epidermolysis bullosa: repair of the extracellular matrix. Lancet *382*, 1214–1223.
115. Conget, P.A., and Minguell, J.J. (1999). Phenotypical and functional properties of human bone marrow mesenchymal progenitor cells. J Cell Physiol *181*, 67–73.
116. Conget, P., Rodriguez, F., Kramer, S., Allers, C., Simon, V., Palisson, F., Gonzalez, S., and Yubero, M.J. (2010). Replenishment of type VII collagen and re-epithelialization of chronically ulcerated skin after intradermal administration of allogeneic mesenchymal stromal cells in two patients with recessive dystrophic epidermolysis bullosa. Cytotherapy *12*, 429–431.
117. Le Blanc, K., and Ringdén, O. (2005). Immunobiology of human mesenchymal stem cells and future use in hematopoietic stem cell transplantation. Biol Blood Marrow Transplant *11*, 321–334.
118. Caplan, A.I., and Dennis, J.E. (2006). Mesenchymal stem cells as trophic mediators. J Cell Biochem *98*, 1076–1084.
119. Li, Y., Ye, Z., Yang, W., Zhang, Q., and Zeng, J. (2021). An Update on the Potential of Mesenchymal Stem Cell Therapy for Cutaneous Diseases. Stem Cells International *2021*, 1–18.
120. El-Darouti, M., Fawzy, M., Amin, I., Abdel Hay, R., Hegazy, R., Gabr, H., and El Maadawi, Z. (2016). Treatment of dystrophic epidermolysis bullosa with bone marrow non-hematopoietic stem cells: a randomized controlled trial: Stem cells in dystrophic epidermolysis bullosa. Dermatologic Therapy *29*, 96–100.
121. Petrof, G., Lwin, S.M., Martinez-Queipo, M., Abdul-Wahab, A., Tso, S., Mellerio, J.E., Slaper-Cortenbach, I., Boelens, J.J., Tolar, J., Veys, P., et al. (2015). Potential of Systemic Allogeneic Mesenchymal Stromal Cell Therapy for Children with Recessive Dystrophic Epidermolysis Bullosa. Journal of Investigative Dermatology *135*, 2319–2321.
122. Has, C., South, A., and Uitto, J. (2020c). Molecular Therapeutics in Development for Epidermolysis Bullosa: Update 2020. Mol Diagn Ther *24*, 299–309.

123. Siprashvili, Z., Nguyen, N.T., Gorell, E.S., Loutit, K., Khuu, P., Furukawa, L.K., Lorenz, H.P., Leung, T.H., Keene, D.R., Rieger, K.E., et al. (2016). Safety and Wound Outcomes Following Genetically Corrected Autologous Epidermal Grafts in Patients with Recessive Dystrophic Epidermolysis Bullosa. JAMA *316*, 1808.
124. Eichstadt, S., Barriga, M., Ponakala, A., Teng, C., Nguyen, N.T., Siprashvili, Z., Nazaroff, J., Gorell, E.S., Chiou, A.S., Taylor, L., et al. (2019). Phase 1/2a clinical trial of gene-corrected autologous cell therapy for recessive dystrophic epidermolysis bullosa. JCI Insight *4*, e130554.
125. Lwin, S.M., Syed, F., Di, W.-L., Kadiyirire, T., Liu, L., Guy, A., Petrova, A., Abdul-Wahab, A., Reid, F., Phillips, R., et al. (2019). Safety and early efficacy outcomes for lentiviral fibroblast gene therapy in recessive dystrophic epidermolysis bullosa. JCI Insight *4*, e126243.
126. Mavilio, F., Pellegrini, G., Ferrari, S., Di Nunzio, F., Di Iorio, E., Recchia, A., Maruggi, G., Ferrari, G., Provasi, E., Bonini, C., et al. (2006). Correction of junctional epidermolysis bullosa by transplantation of genetically modified epidermal stem cells. Nat Med *12*, 1397–1402.
127. Sun, N., and Zhao, H. (2013). Transcription activator-like effector nucleases (TALENs): A highly efficient and versatile tool for genome editing. Biotechnol. Bioeng. *110*, 1811–1821.
128. Bogdanove, A.J., and Voytas, D.F. (2011). TAL Effectors: Customizable Proteins for DNA Targeting. Science *333*, 1843–1846.
129. Osborn, M.J., Starker, C.G., McElroy, A.N., Webber, B.R., Riddle, M.J., Xia, L., DeFeo, A.P., Gabriel, R., Schmidt, M., Von Kalle, C., et al. (2013). TALEN-based Gene Correction for Epidermolysis Bullosa. Molecular Therapy *21*, 1151–1159.
130. Chamorro, C., Mencía, A., Almarza, D., Duarte, B., Büning, H., Sallach, J., Hausser, I., Del Río, M., Larcher, F., and Murillas, R. (2016). Gene Editing for the Efficient Correction of a Recurrent COL7A1 Mutation in Recessive Dystrophic Epidermolysis Bullosa Keratinocytes. Molecular Therapy - Nucleic Acids *5*, e307.
131. Mencía, Á., Chamorro, C., Bonafont, J., Duarte, B., Holguin, A., Illera, N., Llames, S.G., Escámez, M.J., Hausser, I., Del Río, M., et al. (2018). Deletion of a Pathogenic Mutation-Containing Exon of COL7A1 Allows Clonal Gene Editing Correction of RDEB Patient Epidermal Stem Cells. Molecular Therapy - Nucleic Acids *11*, 68–78.
132. Shinkuma, S., Guo, Z., and Christiano, A.M. (2016). Site-specific genome editing for correction of induced pluripotent stem cells derived from dominant dystrophic epidermolysis bullosa. Proc Natl Acad Sci USA *113*, 5676–5681.
133. Nidhi, S., Anand, U., Oleksak, P., Tripathi, P., Lal, J.A., Thomas, G., Kuca, K., and Tripathi, V. (2021). Novel CRISPR–Cas Systems: An Updated Review of the Current Achievements, Applications, and Future Research Perspectives. IJMS *22*, 3327.
134. Webber, B.R., Osborn, M.J., McElroy, A.N., Twaroski, K., Lonetree, C., DeFeo, A.P., Xia, L., Eide, C., Lees, C.J., McElmurry, R.T., et al. (2016). CRISPR/Cas9-based genetic correction for recessive dystrophic epidermolysis bullosa. Npj Regen Med *1*, 16014.
135. Hainzl, S., Peking, P., Kocher, T., Murauer, E.M., Larcher, F., Del Rio, M., Duarte, B., Steiner, M., Klausegger, A., Bauer, J.W., et al. (2017). COL7A1 Editing via CRISPR/Cas9 in Recessive Dystrophic Epidermolysis Bullosa. Molecular Therapy *25*, 2573–2584.
136. Bonafont, J., Mencía, Á., García, M., Torres, R., Rodríguez, S., Carretero, M., Chacón-Solano, E., Modamio-Høybjør, S., Marinas, L., León, C., et al. (2019). Clinically Relevant Correction of Recessive Dystrophic Epidermolysis Bullosa by Dual sgRNA CRISPR/Cas9-Mediated Gene Editing. Molecular Therapy *27*, 986–998.
137. Izmiryan, A., Ganier, C., Bovolenta, M., Schmitt, A., Mavilio, F., and Hovnanian, A. (2018). Ex Vivo COL7A1 Correction for Recessive Dystrophic Epidermolysis Bullosa Using CRISPR/Cas9 and Homology-Directed Repair. Molecular Therapy - Nucleic Acids *12*, 554–567.

138. Takashima, S., Shinkuma, S., Fujita, Y., Nomura, T., Ujiie, H., Natsuga, K., Iwata, H., Nakamura, H., Vorobyev, A., Abe, R., et al. (2019). Efficient Gene Reframing Therapy for Recessive Dystrophic Epidermolysis Bullosa with CRISPR/Cas9. Journal of Investigative Dermatology *139*, 1711-1721.e4.
139. Jacków, J., Guo, Z., Hansen, C., Abaci, H.E., Doucet, Y.S., Shin, J.U., Hayashi, R., DeLorenzo, D., Kabata, Y., Shinkuma, S., et al. (2019). CRISPR/Cas9-based targeted genome editing for correction of recessive dystrophic epidermolysis bullosa using iPS cells. Proc Natl Acad Sci USA *116*, 26846–26852.
140. Kocher, T., Wagner, R.N., Klausegger, A., Guttmann-Gruber, C., Hainzl, S., Bauer, J.W., Reichelt, J., and Koller, U. (2019). Improved Double-Nicking Strategies for COL7A1-Editing by Homologous Recombination. Molecular Therapy - Nucleic Acids *18*, 496–507.
141. Kocher, T., March, O.P., Bischof, J., Liemberger, B., Hainzl, S., Klausegger, A., Hoog, A., Strunk, D., Bauer, J.W., and Koller, U. (2020). Predictable CRISPR/Cas9-Mediated COL7A1 Reframing for Dystrophic Epidermolysis Bullosa. Journal of Investigative Dermatology *140*, 1985-1993.e5.
142. Woodley, D.T., Keene, D.R., Atha, T., Huang, Y., Lipman, K., Li, W., and Chen, M. (2004). Injection of recombinant human type VII collagen restores collagen function in dystrophic epidermolysis bullosa. Nat Med *10*, 693–695.
143. Woodley, D.T., Wang, X., Amir, M., Hwang, B., Remington, J., Hou, Y., Uitto, J., Keene, D., and Chen, M. (2013). Intravenously Injected Recombinant Human Type VII Collagen Homes to Skin Wounds and Restores Skin Integrity of Dystrophic Epidermolysis Bullosa. Journal of Investigative Dermatology *133*, 1910–1913.
144. McGrath, J.A., Ashton, G.H.S., Mellerio, J.E., McMillan, J.R., Eady, R.A.J., Salas-Alanis, J.C., and Swensson, O. (1999). Moderation of Phenotypic Severity in Dystrophic and Junctional Forms of Epidermolysis Bullosa Through In-Frame Skipping of Exons Containing Non-Sense or Frameshift Mutations. Journal of Investigative Dermatology *113*, 314–321.
145. Schwieger-Briel, A., Weibel, L., Chmel, N., Leppert, J., Kernland-Lang, K., Grüninger, G., and Has, C. (2015). A COL7A1 variant leading to in-frame skipping of exon 15 attenuates disease severity in recessive dystrophic epidermolysis bullosa. Br J Dermatol *173*, 1308–1311.
146. Kowalewski, C., Bremer, J., Gostynski, A., Wertheim-Tysarowska, K., Wozniak, K., Bal, J., Jonkman, M.F., and Pasmooij, A.M.G. (2016). Amelioration of junctional epidermolysis bullosa due to exon skipping. Br J Dermatol *174*, 1375–1379.
147. Bremer, J., van der Heijden, E.H., Eichhorn, D.S., Meijer, R., Lemmink, H.H., Scheffer, H., Sinke, R.J., Jonkman, M.F., Pasmooij, A.M.G., and Van den Akker, P.C. (2019). Natural Exon Skipping Sets the Stage for Exon Skipping as Therapy for Dystrophic Epidermolysis Bullosa. Molecular Therapy - Nucleic Acids *18*, 465–475.
148. Bornert, O., Kühl, T., Bremer, J., van den Akker, P.C., Pasmooij, A.M., and Nyström, A. (2016). Analysis of the functional consequences of targeted exon deletion in COL7A1 reveals prospects for dystrophic epidermolysis bullosa therapy. Molecular Therapy *24*, 1302–1311.
149. Bremer, J., Bornert, O., Nyström, A., Gostynski, A., Jonkman, M.F., Aartsma-Rus, A., Akker, P.C. van den, and Pasmooij, A.M. (2016). Antisense Oligonucleotide-mediated Exon Skipping as a Systemic Therapeutic Approach for Recessive Dystrophic Epidermolysis Bullosa. Molecular Therapy - Nucleic Acids *5*.
150. McElroy, S.P., Nomura, T., Torrie, L.S., Warbrick, E., Gartner, U., Wood, G., and McLean, W.H.I. (2013). A Lack of Premature Termination Codon Read-Through Efficacy of PTC124 (Ataluren) in a Diverse Array of Reporter Assays. PLOS Biology *11*, e1001593.
151. Cogan, J., Weinstein, J., Wang, X., Hou, Y., Martin, S., South, A.P., Woodley, D.T., and Chen, M. (2014). Aminoglycosides Restore Full-length Type VII Collagen by Overcoming

Premature Termination Codons: Therapeutic Implications for Dystrophic Epidermolysis Bullosa. Molecular Therapy *22*, 1741–1752.
152. Atanasova, V.S., Jiang, Q., Prisco, M., Gruber, C., Piñón Hofbauer, J., Chen, M., Has, C., Bruckner-Tuderman, L., McGrath, J.A., Uitto, J., et al. (2017). Amlexanox Enhances Premature Termination Codon Read-Through in COL7A1 and Expression of Full-Length Type VII Collagen: Potential Therapy for Recessive Dystrophic Epidermolysis Bullosa. Journal of Investigative Dermatology *137*, 1842–1849.
153. Woodley, D.T., Cogan, J., Hou, Y., Lyu, C., Marinkovich, M.P., Keene, D., and Chen, M. (2017). Gentamicin induces functional type VII collagen in recessive dystrophic epidermolysis bullosa patients. Journal of Clinical Investigation *127*, 3028–3038.
154. Walker, P.D., and Shah, S.V. (1988). Evidence suggesting a role for hydroxyl radical in gentamicin-induced acute renal failure in rats. J Clin Invest *81*, 334–341.
155. Que, S.K.T., Zwald, F.O., and Schmults, C.D. (2018). Cutaneous squamous cell carcinoma. Journal of the American Academy of Dermatology *78*, 237–247.
156. Fania, L., Didona, D., Di Pietro, F.R., Verkhovskaia, S., Morese, R., Paolino, G., Donati, M., Ricci, F., Coco, V., Ricci, F., et al. (2021). Cutaneous Squamous Cell Carcinoma: From Pathophysiology to Novel Therapeutic Approaches. Biomedicines *9*, 171.
157. Katalinic, A., Kunze, U., and Schäfer, T. (2003). Epidemiology of cutaneous melanoma and non-melanoma skin cancer in Schleswig-Holstein, Germany: incidence, clinical subtypes, tumour stages and localization (epidemiology of skin cancer). Br J Dermatol *149*, 1200–1206.
158. Brewster, D.H., Bhatti, L.A., Inglis, J.H.C., Nairn, E.R., and Doherty, V.R. (2007). Recent trends in incidence of nonmelanoma skin cancers in the East of Scotland, 1992-2003. Br J Dermatol *156*, 1295–1300.
159. Andersson, E.M., Paoli, J., and Wastensson, G. (2011). Incidence of cutaneous squamous cell carcinoma in coastal and inland areas of Western Sweden. Cancer Epidemiol *35*, e69-74.
160. Muzic, J., Schmitt, A., Wright, A., Alnleml, D., Zubalr, A., Olazagasti Lourldo, J., Sosa Seda, I., Weaver, A., and Baum, C. (2017). Incidence and trends of basal cell carcinoma and cutaneous squamous cell carcinoma: A population-based study in Olmsted County, Minnesota, 2000-2010. Journal of the American Academy of Dermatology *76*, AB412.
161. Rogers, H.W., Weinstock, M.A., Feldman, S.R., and Coldiron, B.M. (2015). Incidence Estimate of Nonmelanoma Skin Cancer (Keratinocyte Carcinomas) in the US Population, 2012. JAMA Dermatol *151*, 1081.
162. Xiang, F., Lucas, R., Hales, S., and Neale, R. (2014). Incidence of Nonmelanoma Skin Cancer in Relation to Ambient UV Radiation in White Populations, 1978-2012: Empirical Relationships. JAMA Dermatol *150*, 1063.
163. Martincorena, I., Roshan, A., Gerstung, M., Ellis, P., Van Loo, P., McLaren, S., Wedge, D.C., Fullam, A., Alexandrov, L.B., Tubio, J.M., et al. (2015). High burden and pervasive positive selection of somatic mutations in normal human skin. Science *348*, 880–886.
164. Wikonkal, N.M., and Brash, D.E. (1999). Ultraviolet Radiation Induced Signature Mutations in Photocarcinogenesis. Journal of Investigative Dermatology Symposium Proceedings *4*, 6–10.
165. The Cancer Genome Atlas (TCGA) Research Network; Hammerman, P.S., Lawrence, M.S., Voet, D., Jing, R., Cibulskis, K., Sivachenko, A., Stojanov, P., McKenna, A., Lander, E.S., Gabriel, S., et al. (2012). Comprehensive genomic characterization of squamous cell lung cancers. Nature *489*, 519–525.
166. Pickering, C.R., Zhou, J.H., Lee, J.J., Drummond, J.A., Peng, S.A., Saade, R.E., Tsai, K.Y., Curry, J.L., Tetzlaff, M.T., Lai, S.Y., et al. (2014). Mutational Landscape of Aggressive Cutaneous Squamous Cell Carcinoma. Clin Cancer Res *20*, 6582–6592.

167. Cho, R.J., Alexandrov, L.B., den Breems, N.Y., Atanasova, V.S., Farshchian, M., Purdom, E., Nguyen, T.N., Coarfa, C., Rajapakshe, K., Prisco, M., et al. (2018). APOBEC mutation drives early-onset squamous cell carcinomas in recessive dystrophic epidermolysis bullosa. Sci. Transl. Med. *10*, eaas9668.
168. Brougham, N.D.L.S., Dennett, E.R., Cameron, R., and Tan, S.T. (2012). The incidence of metastasis from cutaneous squamous cell carcinoma and the impact of its risk factors: Cutaneous Squamous Cell Carcinoma Metastasis. J. Surg. Oncol. *106*, 811–815.
169. Skulsky, S.L., O'Sullivan, B., McArdle, O., Leader, M., Roche, M., Conlon, P.J., and O'Neill, J.P. (2017). Review of high-risk features of cutaneous squamous cell carcinoma and discrepancies between the American Joint Committee on Cancer and NCCN Clinical Practice Guidelines In Oncology. Head Neck *39*, 578–594.
170. Work Group, Invited Reviewers; Kim, J.Y.S., Kozlow, J.H., Mittal, B., Moyer, J., Olenecki, T., and Rodgers, P. (2018). Guidelines of care for the management of cutaneous squamous cell carcinoma. J Am Acad Dermatol *78*, 560–578.
171. Fine, J.-D., Johnson, L.B., Weiner, M., Li, K.-P., and Suchindran, C. (2009). Epidermolysis bullosa and the risk of life-threatening cancers: The National EB Registry experience, 1986-2006. Journal of the American Academy of Dermatology *60*, 203–211.
172. Montaudié, H., Chiaverini, C., Sbidian, E., Charlesworth, A., and Lacour, J.-P. (2016). Inherited epidermolysis bullosa and squamous cell carcinoma: a systematic review of 117 cases. Orphanet J Rare Dis *11*, 117.
173. Arnold, A.W., Bruckner-Tuderman, L., Zuger, C., and Itin, P.H. (2009). Cetuximab therapy of metastasizing cutaneous squamous cell carcinoma in a patient with severe recessive dystrophic epidermolysis bullosa. Dermatology *219*, 80–83.
174. Kim, M., Li, M., Intong, L.R.A., Tran, K., Melbourne, W., Marucci, D., Bucci, J., de Souza, P., Mallesara, G., and Murrell, D.F. (2013). Use of cetuximab as an adjuvant agent to radiotherapy and surgery in recessive dystrophic epidermolysis bullosa with squamous cell carcinoma. Br J Dermatol *169*, 208–210.
175. Diociaiuti, A., Steinke, H., Nyström, A., Schwieger-Briel, A., Meiss, F., Pfannenberg, C., Bruckner-Tuderman, L., Ruf, J., De Vito, R., El Hachem, M., et al. (2019). EGFR inhibition for metastasized cutaneous squamous cell carcinoma in dystrophic epidermolysis bullosa. Orphanet J Rare Dis *14*, 278.
176. Khaddour, K., Gorell, E.S., Dehdashti, F., Tang, J.Y., and Ansstas, G. (2020). Induced Remission of Metastatic Squamous Cell Carcinoma with an Immune Checkpoint Inhibitor in a Patient with Recessive Dystrophic Epidermolysis Bullosa. Case Rep Oncol *13*, 911–915.
177. Piccerillo, A., El Hachem, M., De Vito, R., De Luca, E.V., and Peris, K. (2020). Pembrolizumab for Treatment of a Patient With Multiple Cutaneous Squamous Cell Carcinomas and Recessive Dystrophic Epidermolysis Bullosa. JAMA Dermatol *156*, 708.
178. Reimer, A., Lu, S., He, Y., Bruckner-Tuderman, L., Technau-Hafsi, K., Meiss, F., Has, C., and Bubnoff, D. (2020). Combined anti-inflammatory and low-dose antiproliferative therapy for squamous cell carcinomas in recessive dystrophic epidermolysis bullosa. J Eur Acad Dermatol Venereol *34*.
179. Atanasova, V.S., Pourreyron, C., Farshchian, M., Lawler, M., Brown, C.A., Watt, S.A., Wright, S., Warkala, M., Guttmann-Gruber, C., Hofbauer, J.P., et al. (2019). Identification of Rigosertib for the Treatment of Recessive Dystrophic Epidermolysis Bullosa–Associated Squamous Cell Carcinoma. Clin Cancer Res *25*, 3384–3391.
180. Gumireddy, K., Reddy, M.V.R., Cosenza, S.C., Nathan, R.B., Baker, S.J., Papathi, N., Jiang, J., Holland, J., and Reddy, E.P. (2005). ON01910, a non-ATP-competitive small molecule inhibitor of Plk1, is a potent anticancer agent. Cancer Cell *7*, 275–286.
181. Weerdt, B.C.M. van de, and Medema, R.H. (2006). Polo-Like Kinases: A Team in Control of the Division. Cell Cycle *5*, 853–864.

182. Watt, S.A., Pourreyron, C., Purdie, K., Hogan, C., Cole, C.L., Foster, N., Pratt, N., Bourdon, J.-C., Appleyard, V., Murray, K., et al. (2011). Integrative mRNA profiling comparing cultured primary cells with clinical samples reveals PLK1 and C20orf20 as therapeutic targets in cutaneous squamous cell carcinoma. Oncogene *30*, 4666–4677.
183. Liu, Z., Sun, Q., and Wang, X. (2017). PLK1, A Potential Target for Cancer Therapy. Translational Oncology *10*, 22–32.
184. Ishiko, A., Masunaga, T., Ota, T., and Nishikawa, T. (2004). Does the position of the premature termination codon in COL7A1 correlate with the clinical severity in recessive dystrophic epidermolysis bullosa? Exp Dermatol *13*, 229–233.
185. Badiavas, E.V., Abedi, M., Butmarc, J., Falanga, V., and Quesenberry, P. (2003). Participation of bone marrow derived cells in cutaneous wound healing. J. Cell. Physiol. *196*, 245–250.
186. Kataoka, K., Medina, R.J., Kageyama, T., Miyazaki, M., Yoshino, T., Makino, T., and Huh, N. (2003). Participation of Adult Mouse Bone Marrow Cells in Reconstitution of Skin. The American Journal of Pathology *163*, 1227–1231.
187. Brittan, M., Braun, K.M., Reynolds, L.E., Conti, F.J., Reynolds, A.R., Poulsom, R., Alison, M.R., Wright, N.A., and Hodivala-Dilke, K.M. (2005). Bone marrow cells engraft within the epidermis and proliferation vivo with no evidence of cell fusion. J. Pathol. *205*, 1–13.
188. Woodley, D.T., Remington, J., Huang, Y., Hou, Y., Li, W., Keene, D.R., and Chen, M. (2007). Intravenously Injected Human Fibroblasts Home to Skin Wounds, Deliver Type VII Collagen, and Promote Wound Healing. Molecular Therapy *15*, 628–635.
189. Fujita, Y., Abe, R., Inokuma, D., Sasaki, M., Hoshina, D., Natsuga, K., Nishie, W., McMillan, J.R., Nakamura, H., Shimizu, T., et al. (2010). Bone marrow transplantation restores epidermal basement membrane protein expression and rescues epidermolysis bullosa model mice. Proceedings of the National Academy of Sciences *107*, 14345–14350.
190. Iinuma, S., Aikawa, E., Tamai, K., Fujita, R., Kikuchi, Y., Chino, T., Kikuta, J., McGrath, J.A., Uitto, J., Ishii, M., et al. (2015). Transplanted Bone Marrow–Derived Circulating PDGFRα $^{+}$ Cells Restore Type VII Collagen in Recessive Dystrophic Epidermolysis Bullosa Mouse Skin Graft. J.I. *194*, 1996–2003.
191. South, A.P., and Uitto, J. (2016). Type VII Collagen Replacement Therapy in Recessive Dystrophic Epidermolysis Bullosa—How Much, How Often? Journal of Investigative Dermatology *136*, 1079–1081.
192. Webber, B.R., O'Connor, K.T., McElmurry, R.T., Durgin, E.N., Eide, C.R., Lees, C.J., Riddle, M.J., Mathews, W.E., Frank, N.Y., Kluth, M.A., et al. (2017). Rapid generation of Col7a1−/− mouse model of recessive dystrophic epidermolysis bullosa and partial rescue via immunosuppressive dermal mesenchymal stem cells. Lab Invest *97*, 1218–1224.
193. Kampmann, M. (2018). CRISPRi and CRISPRa Screens in Mammalian Cells for Precision Biology and Medicine. ACS Chem. Biol. *13*, 406–416.
194. Lin, A., Giuliano, C.J., Palladino, A., John, K.M., Abramowicz, C., Yuan, M.L., Sausville, E.L., Lukow, D.A., Liu, L., Chait, A.R., et al. (2019). Off-target toxicity is a common mechanism of action of cancer drugs undergoing clinical trials. Sci Transl Med *11*, eaaw8412.
195. Sanson, K.R., Hanna, R.E., Hegde, M., Donovan, K.F., Strand, C., Sullender, M.E., Vaimberg, E.W., Goodale, A., Root, D.E., Piccioni, F., et al. (2018). Optimized libraries for CRISPR-Cas9 genetic screens with multiple modalities. Nat Commun *9*, 5416.
196. Lackner, D.H., Carré, A., Guzzardo, P.M., Banning, C., Mangena, R., Henley, T., Oberndorfer, S., Gapp, B.V., Nijman, S.M.B., Brummelkamp, T.R., et al. (2015). A generic strategy for CRISPR-Cas9-mediated gene tagging. Nat Commun *6*, 10237.
197. McDade, J.R., Waxmonsky, N.C., Swanson, L.E., and Fan, M. (2016). Practical Considerations for Using Pooled Lentiviral CRISPR Libraries. Curr Protoc Mol Biol *115*, 31.5.1-31.5.13.

198. Huttlin, E.L., Bruckner, R.J., Paulo, J.A., Cannon, J.R., Ting, L., Baltier, K., Colby, G., Gebreab, F., Gygi, M.P., Parzen, H., et al. (2017). Architecture of the human interactome defines protein communities and disease networks. Nature *545*, 505–509.
199. Tomasello, E., and Vivier, E. (2005). KARAP/DAP12/TYROBP: three names and a multiplicity of biological functions. Eur. J. Immunol. *35*, 1670–1677.
200. Dietrich, J., Cella, M., Seiffert, M., Bühring, H.-J., and Colonna, M. (2000). Cutting Edge: Signal-Regulatory Protein β1 Is a DAP12-Associated Activating Receptor Expressed in Myeloid Cells. J Immunol *164*, 9–12.
201. Hayashi, A., Ohnishi, H., Okazawa, H., Nakazawa, S., Ikeda, H., Motegi, S., Aoki, N., Kimura, S., Mikuni, M., and Matozaki, T. (2004). Positive Regulation of Phagocytosis by SIRPβ and Its Signaling Mechanism in Macrophages. Journal of Biological Chemistry *279*, 29450–29460.
202. Gaikwad, S., Larionov, S., Wang, Y., Dannenberg, H., Matozaki, T., Monsonego, A., Thal, D.R., and Neumann, H. (2009). Signal Regulatory Protein-β1. The American Journal of Pathology *175*, 2528–2539.
203. Breitenbach, J.S., Rinnerthaler, M., Trost, A., Weber, M., Klausegger, A., Gruber, C., Bruckner, D., Reitsamer, H.A., Bauer, J.W., and Breitenbach, M. (2015). Transcriptome and ultrastructural changes in dystrophic Epidermolysis bullosa resemble skin aging. Aging *7*, 389–411.
204. Esposito, S., Guez, S., Orenti, A., Tadini, G., Scuvera, G., Corti, L., Scala, A., Biganzoli, E., Berti, E., and Principi, N. (2016). Autoimmunity and Cytokine Imbalance in Inherited Epidermolysis Bullosa. IJMS *17*, 1625.
205. Cianfarani, F., Zambruno, G., Castiglia, D., and Odorisio, T. (2017). Pathomechanisms of Altered Wound Healing in Recessive Dystrophic Epidermolysis Bullosa. The American Journal of Pathology *187*, 1445–1453.
206. Chen, A.Y., and Chen, Y.C. (2013). A review of the dietary flavonoid, kaempferol on human health and cancer chemoprevention. Food Chemistry *138*, 2099–2107.
207. Wang, J., Fang, X., Ge, L., Cao, F., Zhao, L., Wang, Z., and Xiao, W. (2018). Antitumor, antioxidant and anti-inflammatory activities of kaempferol and its corresponding glycosides and the enzymatic preparation of kaempferol. PLoS One *13*, e0197563.
208. Liu, C., Liu, H., Lu, C., Deng, J., Yan, Y., Chen, H., Wang, Y., Liang, C. -L., Wei, J., Han, L., et al. (2019). Kaempferol attenuates imiquimod-induced psoriatic skin inflammation in a mouse model. Clin Exp Immunol *198*, 403–415.
209. Sekiguchi, A., Motegi, S., Fujiwara, C., Yamazaki, S., Inoue, Y., Uchiyama, A., Akai, R., Iwawaki, T., and Ishikawa, O. (2019). Inhibitory effect of kaempferol on skin fibrosis in systemic sclerosis by the suppression of oxidative stress. Journal of Dermatological Science *96*, 8–17.
210. Ambiga, S., Narayanan, R., Gowri, D., Sukumar, D., and Madhavan, S. (2007). Evaluation of wound healing capacity of flavonoids from Ipomoea carnea Jacq. Anc Sci Life *26*, 45–51.
211. Özay, Y., Güzel, S., Yumrutaş, Ö., Pehlivanoğlu, B., Erdoğdu, İ.H., Yildirim, Z., Türk, B.A., and Darcan, S. (2019). Wound Healing Effect of Kaempferol in Diabetic and Nondiabetic Rats. Journal of Surgical Research *233*, 284–296.
212. Concordet, J.-P., and Haeussler, M. (2018). CRISPOR: intuitive guide selection for CRISPR/Cas9 genome editing experiments and screens. Nucleic Acids Res *46*, W242–W245.
213. Piccioni, F., Younger, S.T., and Root, D.E. (2018). Pooled Lentiviral-Delivery Genetic Screens. Curr Protoc Mol Biol *121*, 32.1.1-32.1.21.
214. Martin, M. (2011). Cutadapt removes adapter sequences from high-throughput sequencing reads. EMBnet.Journal *17*, 10–12.

215. Murrell, D.F., Paller, A.S., Bodemer, C., Browning, J., Nikolic, M., Barth, J.A., Lagast, H., Krusinska, E., and Reha, A. (2020). Wound closure in epidermolysis bullosa: data from the vehicle arm of the phase 3 ESSENCE Study. Orphanet J Rare Dis *15*, 190.
216. Borges da Silva, H., Peng, C., Wang, H., Wanhainen, K.M., Ma, C., Lopez, S., Khoruts, A., Zhang, N., and Jameson, S.C. (2020). Sensing of ATP via the Purinergic Receptor P2RX7 Promotes CD8+ Trm Cell Generation by Enhancing Their Sensitivity to the Cytokine TGF-β. Immunity *53*, 158-171.e6.
217. Haure-Mirande, J.-V., Audrain, M., Fanutza, T., Kim, S.H., Klein, W.L., Glabe, C., Readhead, B., Dudley, J.T., Blitzer, R.D., Wang, M., et al. (2017). Deficiency of TYROBP, an adapter protein for TREM2 and CR3 receptors, is neuroprotective in a mouse model of early Alzheimer's pathology. Acta Neuropathol *134*, 769–788.
218. Reese, J.M., Bruinsma, E.S., Nelson, A.W., Chernukhin, I., Carroll, J.S., Li, Y., Subramaniam, M., Suman, V.J., Negron, V., Monroe, D.G., et al. (2018). ERβ-mediated induction of cystatins results in suppression of TGFβ signaling and inhibition of triple-negative breast cancer metastasis. Proc Natl Acad Sci USA *115*, E9580–E9589.
219. Lefterov, I., Schug, J., Mounier, A., Nam, K.N., Fitz, N.F., and Koldamova, R. (2015). RNA-sequencing reveals transcriptional up-regulation of Trem2 in response to bexarotene treatment. Neurobiology of Disease *82*, 132–140.
220. Zuo, Y., Huang, L., Enkhjargal, B., Xu, W., Umut, O., Travis, Z.D., Zhang, G., Tang, J., Liu, F., and Zhang, J.H. (2019). Activation of retinoid X receptor by bexarotene attenuates neuroinflammation via PPARγ/SIRT6/FoxO3a pathway after subarachnoid hemorrhage in rats. J Neuroinflammation *16*, 47.
221. Li, J., Zhao, R., Jiang, Y., Xu, Y., Zhao, H., Lyu, X., and Wu, T. (2020a). Bilberry anthocyanins improve neuroinflammation and cognitive dysfunction in APP/PSEN1 mice *via* the CD33/TREM2/TYROBP signaling pathway in microglia. Food Funct. *11*, 1572–1584.
222. Simard, M., Morin, S., Rioux, G., Séguin, R., Loing, E., and Pouliot, R. (2020). A Tissue-Engineered Human Psoriatic Skin Model to Investigate the Implication of cAMP in Psoriasis: Differential Impacts of Cholera Toxin and Isoproterenol on cAMP Levels of the Epidermis. IJMS *21*, 5215.
223. Warner, R.L., Bhagavathula, N., Nerusu, K., Hanosh, A., McClintock, S.D., Naik, M.K., Johnson, K.J., Ginsburg, I., and Varani, J. (2008). MDI 301, a nonirritating retinoid, improves abrasion wound healing in damaged/atrophic skin. Wound Repair and Regeneration *16*, 117–124.
224. Santini, M.P., Talora, C., Seki, T., Bolgan, L., and Dotto, G.P. (2001). Cross talk among calcineurin, Sp1/Sp3, and NFAT in control of p21WAF1/CIP1 expression in keratinocyte differentiation. Proceedings of the National Academy of Sciences *98*, 9575–9580.
225. Zhu, Y., Tchkonia, T., Pirtskhalava, T., Gower, A.C., Ding, H., Giorgadze, N., Palmer, A.K., Ikeno, Y., Hubbard, G.B., Lenburg, M., et al. (2015). The Achilles' heel of senescent cells: from transcriptome to senolytic drugs. Aging Cell *14*, 644–658.
226. Mavrogonatou, E., Pratsinis, H., and Kletsas, D. (2020). The role of senescence in cancer development. Seminars in Cancer Biology *62*, 182–191.
227. Sufaru, I.-G., Beikircher, G., Weinhaeusel, A., and Gruber, R. (2017). Inhibitors of DNA methylation support TGF-β1-induced *IL11* expression in gingival fibroblasts. J Periodontal Implant Sci *47*, 66.
228. Prodinger, C., Reichelt, J., Bauer, J.W., and Laimer, M. (2019). Epidermolysis bullosa: Advances in research and treatment. Exp Dermatol *28*, 1176–1189.
229. Fang, J., Cao, Z., Chen, Y.C., Reed, E., and Jiang, B.-H. (2004). 9-beta-D-arabinofuranosyl-2-fluoroadenine inhibits expression of vascular endothelial growth factor through hypoxia-inducible factor-1 in human ovarian cancer cells. Mol Pharmacol *66*, 178–186.

230. Xue, J., Bi, X., Wu, G., Meng, D., and Fang, J. (2007). Fludarabine reduces survivability of HepG2 cells through VEGF under hypoxia. Archives of Biochemistry and Biophysics *468*, 100–106.
231. Ehrlich, H.P., Griswold, T.R., and Rajaratnam, J. (1986). ATP-Induced Cell Contraction with Epidermolysis Bullosa Dystrophica Recessive and Normal Dermal Fibroblasts. Journal of Investigative Dermatology *86*, 96–100.
232. Malsy, M., Graf, B., and Almstedt, K. (2019). The active role of the transcription factor Sp1 in NFATc2-mediated gene regulation in pancreatic cancer. BMC Biochem *20*, 2.
233. Zajkowicz, A., Gdowicz-Kłosok, A., Krześniak, M., Janus, P., Łasut, B., and Rusin, M. (2018). The Alzheimer's disease-associated TREM2 gene is regulated by p53 tumor suppressor protein. Neuroscience Letters *681*, 62–67.
234. Nyström, A., Thriene, K., Mittapalli, V., Kern, J.S., Kiritsi, D., Dengjel, J., and Bruckner-Tuderman, L. (2015). Losartan ameliorates dystrophic epidermolysis bullosa and uncovers new disease mechanisms. EMBO Mol Med *7*, 1211–1228.
235. Luckett-Chastain, L.R., and Gallucci, R.M. (2009). Interleukin (IL)-6 modulates transforming growth factor-β expression in skin and dermal fibroblasts from IL-6-deficient mice. British Journal of Dermatology *161*, 237–248.
236. Beer, H.-D., Longaker, M.T., and Werner, S. (1997). Reduced Expression of PDGF and PDGF Receptors During Impaired Wound Healing. Journal of Investigative Dermatology *109*, 132–138.
237. Gope, R. (2002). The effect of epidermal growth factor & platelet-derived growth factors on wound healing process. Indian J Med Res *116*, 201–206.
238. Shimizu, H., McGrath, J.A., Christiano, A.M., Nishikawa, T., and Uitto, J. (1996). Molecular Basis of Recessive Dystrophic Epidermolysis Bullosa: Genotype/Phenotype Correlation in a Case of Moderate Clinical Severity. Journal of Investigative Dermatology *106*, 119–124.
239. Nyström, A., Velati, D., Mittapalli, V.R., Fritsch, A., Kern, J.S., and Bruckner-Tuderman, L. (2013). Collagen VII plays a dual role in wound healing. J. Clin. Invest. *123*, 3498–3509.
240. Dayal, J.H., Cole, C.L., Pourreyron, C., Watt, S.A., Lim, Y.Z., Salas-Alanis, J.C., Murrell, D.F., McGrath, J.A., Stieger, B., Jahoda, C., et al. (2013). Type VII collagen regulates tumour expression of organic anion transporting polypeptide OATP1B3, promotes front to rear polarity and increases structural organisation in 3D spheroid cultures of recessive dystrophic epidermolysis bullosa tumour keratinocytes. Journal of Cell Science jcs.128454.
241. Tomita, Y., Sato-Matsumura, K., Sawamura, D., Matsumura, T., and Shimizu, H. (2003). Simultaneous Occurrence of Three Squamous Cell Carcinomas in a Recessive Dystrophic Epidermolysis Bullosa Patient. Acta Dermato-Venereologica *83*, 225–226.
242. Mellerio, J.E., Robertson, S.J., Bernardis, C., Diem, A., Fine, J.D., George, R., Goldberg, D., Halmos, G.B., Harries, M., Jonkman, M.F., et al. (2016). Management of cutaneous squamous cell carcinoma in patients with epidermolysis bullosa: best clinical practice guidelines. Br J Dermatol *174*, 56–67.
243. Medek, K., Koelblinger, P., Koller, J., Diem, A., Ude-Schoder, K., Bauer, J.W., and Laimer, M. (2019). Wundheilungsstörungen während der antitumorösen Therapie mit Cetuximab bei schwerer generalisierter dystropher Epidermolysis bullosa. J Dtsch Dermatol Ges *17*, 448–450.
244. Odorisio, T., Di Salvio, M., Orecchia, A., Di Zenzo, G., Piccinni, E., Cianfarani, F., Travaglione, A., Uva, P., Bellei, B., Conti, A., et al. (2014). Monozygotic twins discordant for recessive dystrophic epidermolysis bullosa phenotype highlight the role of TGF-β signaling in modifying disease severity. Human Molecular Genetics *23*, 3907–3922.
245. Ng, Y.-Z., Pourreyron, C., Salas-Alanis, J.C., Dayal, J.H.S., Cepeda-Valdes, R., Yan, W., Wright, S., Chen, M., Fine, J.-D., Hogg, F.J., et al. (2012). Fibroblast-Derived Dermal

Matrix Drives Development of Aggressive Cutaneous Squamous Cell Carcinoma in Patients with Recessive Dystrophic Epidermolysis Bullosa. Cancer Res *72*, 3522–3534.
246. Küttner, V., Mack, C., Rigbolt, K.T., Kern, J.S., Schilling, O., Busch, H., Bruckner-Tuderman, L., and Dengjel, J. (2013). Global remodeling of cellular microenvironment due to loss of collagen VII. Mol Syst Biol *9*, 657.
247. Nyström, A., Bornert, O., Kühl, T., Gretzmeier, C., Thriene, K., Dengjel, J., Pfister-Wartha, A., Kiritsi, D., and Bruckner-Tuderman, L. (2018). Impaired lymphoid extracellular matrix impedes antibacterial immunity in epidermolysis bullosa. Proc Natl Acad Sci USA *115*, E705–E714.
248. Martins, V.L., Caley, M.P., Moore, K., Szentpetery, Z., Marsh, S.T., Murrell, D.F., Kim, M.H., Avari, M., McGrath, J.A., Cerio, R., et al. (2016). Suppression of TGF β and Angiogenesis by Type VII Collagen in Cutaneous SCC. JNCI.J *108*, djv293.
249. Mittapalli, V.R., Madl, J., Löffek, S., Kiritsi, D., Kern, J.S., Römer, W., Nyström, A., and Bruckner-Tuderman, L. (2016). Injury-Driven Stiffening of the Dermis Expedites Skin Carcinoma Progression. Cancer Res *76*, 940–951.
250. Guerra, L., Odorisio, T., Zambruno, G., and Castiglia, D. (2017). Stromal microenvironment in type VII collagen-deficient skin: The ground for squamous cell carcinoma development. Matrix Biol *63*, 1–10.
251. Zhang, W., Ge, Y., Cheng, Q., Zhang, Q., Fang, L., and Zheng, J. (2018). Decorin is a pivotal effector in the extracellular matrix and tumour microenvironment. Oncotarget *9*, 5480–5491.
252. Chacón-Solano, E., León, C., Díaz, F., García-García, F., García, M., Escámez, M.J., Guerrero-Aspizua, S., Conti, C.J., Mencía, Á., Martínez-Santamaría, L., et al. (2019). Fibroblast activation and abnormal extracellular matrix remodeling as common hallmarks in three cancer-prone genodermatoses. Br J Dermatol *181*, 512–522.
253. Cianfarani, F., De Domenico, E., Nyström, A., Mastroeni, S., Abeni, D., Baldini, E., Ulisse, S., Uva, P., Bruckner-Tuderman, L., Zambruno, G., et al. (2019). Decorin counteracts disease progression in mice with recessive dystrophic epidermolysis bullosa. Matrix Biology *81*, 3–16.
254. Kim, D., Paggi, J.M., Park, C., Bennett, C., and Salzberg, S.L. (2019). Graph-based genome alignment and genotyping with HISAT2 and HISAT-genotype. Nat Biotechnol *37*, 907–915.
255. Robinson, M.D., and Smyth, G.K. (2007). Moderated statistical tests for assessing differences in tag abundance. Bioinformatics *23*, 2881–2887.
256. Robinson, M.D., and Smyth, G.K. (2008). Small-sample estimation of negative binomial dispersion, with applications to SAGE data. Biostatistics *9*, 321–332.
257. Robinson, M.D., McCarthy, D.J., and Smyth, G.K. (2010). edgeR: a Bioconductor package for differential expression analysis of digital gene expression data. Bioinformatics *26*, 139–140.
258. Robinson, M.D., and Oshlack, A. (2010). A scaling normalization method for differential expression analysis of RNA-seq data. Genome Biol *11*, R25.
259. McCarthy, D.J., Chen, Y., and Smyth, G.K. (2012). Differential expression analysis of multifactor RNA-Seq experiments with respect to biological variation. Nucleic Acids Res *40*, 4288–4297.
260. Chen, Y., Lun, A.T.L., and Smyth, G.K. (2014). Differential Expression Analysis of Complex RNA-seq Experiments Using edgeR. In Statistical Analysis of Next Generation Sequencing Data, S. Datta, and D. Nettleton, eds. (Cham: Springer International Publishing), pp. 51–74.
261. Chen, Y., Lun, A.T.L., and Smyth, G.K. (2016). From reads to genes to pathways: differential expression analysis of RNA-Seq experiments using Rsubread and the edgeR quasi-likelihood pipeline. F1000Res *5*, 1438.

262. Dai, Z., Sheridan, J.M., Gearing, L.J., Moore, D.L., Su, S., Wormald, S., Wilcox, S., O'Connor, L., Dickins, R.A., Blewitt, M.E., et al. (2014). edgeR: a versatile tool for the analysis of shRNA-seq and CRISPR-Cas9 genetic screens. F1000Res *3*, 95.
263. Zhou, X., Lindsay, H., and Robinson, M.D. (2014). Robustly detecting differential expression in RNA sequencing data using observation weights. Nucleic Acids Res *42*, e91.
264. Lun, A.T.L., Chen, Y., and Smyth, G.K. (2016). It's DE-licious: A Recipe for Differential Expression Analyses of RNA-seq Experiments Using Quasi-Likelihood Methods in edgeR. Methods Mol Biol *1418*, 391–416.
265. Subramanian, A., Tamayo, P., Mootha, V.K., Mukherjee, S., Ebert, B.L., Gillette, M.A., Paulovich, A., Pomeroy, S.L., Golub, T.R., Lander, E.S., et al. (2005). Gene set enrichment analysis: A knowledge-based approach for interpreting genome-wide expression profiles. PNAS *102*, 15545–15550.
266. Liberzon, A., Subramanian, A., Pinchback, R., Thorvaldsdóttir, H., Tamayo, P., and Mesirov, J.P. (2011). Molecular signatures database (MSigDB) 3.0. Bioinformatics *27*, 1739–1740.
267. Liberzon, A., Birger, C., Thorvaldsdóttir, H., Ghandi, M., Mesirov, J.P., and Tamayo, P. (2015). The Molecular Signatures Database (MSigDB) hallmark gene set collection. Cell Syst *1*, 417–425.
268. Vanden Oever, M., Muldoon, D., Mathews, W., McElmurry, R., and Tolar, J. (2016). miR-29 Regulates Type VII Collagen in Recessive Dystrophic Epidermolysis Bullosa. Journal of Investigative Dermatology *136*, 2013–2021.
269. Condorelli, A.G., Logli, E., Cianfarani, F., Teson, M., Diociaiuti, A., El Hachem, M., Zambruno, G., Castiglia, D., and Odorisio, T. (2019a). MicroRNA-145-5p regulates fibrotic features of recessive dystrophic epidermolysis bullosa skin fibroblasts. Br J Dermatol *181*, 1017–1027.
270. Kivisaari, A.K., Kallajoki, M., Mirtti, T., McGrath, J.A., Bauer, J.W., Weber, F., Königová, R., Sawamura, D., Sato-Matsumura, K.C., Shimizu, H., et al. (2008). Transformation-specific matrix metalloproteinases (MMP)-7 and MMP-13 are expressed by tumour cells in epidermolysis bullosa-associated squamous cell carcinomas. Br J Dermatol *158*, 778–785.
271. Hata, H., Abe, R., Suto, A., Homma, E., Fujita, Y., Aoyagi, S., and Shimizu, H. (2015). MMP13 can be a useful differentiating marker between squamous cell carcinoma and benign hyperkeratotic lesions in recessive dystrophic epidermolysis bullosa. Br J Dermatol *172*, 769–773.
272. Farshchian, M., Nissinen, L., Siljamäki, E., Riihilä, P., Piipponen, M., Kivisaari, A., Kallajoki, M., Grénman, R., Peltonen, J., Peltonen, S., et al. (2017). Tumor cell-specific AIM2 regulates growth and invasion of cutaneous squamous cell carcinoma. Oncotarget *8*, 45825–45836.
273. Konermann, S., Brigham, M.D., Trevino, A.E., Joung, J., Abudayyeh, O.O., Barcena, C., Hsu, P.D., Habib, N., Gootenberg, J.S., Nishimasu, H., et al. (2015). Genome-scale transcriptional activation by an engineered CRISPR-Cas9 complex. Nature *517*, 583–588.
274. Xiong, K., Zhou, Y., Blichfeld, K.A., Hyttel, P., Bolund, L., Freude, K.K., and Luo, Y. (2017). RNA-Guided Activation of Pluripotency Genes in Human Fibroblasts. Cellular Reprogramming *19*, 189–198.
275. Liu, Y., Yu, C., Daley, T.P., Wang, F., Cao, W.S., Bhate, S., Lin, X., Still, C., Liu, H., Zhao, D., et al. (2018). CRISPR Activation Screens Systematically Identify Factors that Drive Neuronal Fate and Reprogramming. Cell Stem Cell *23*, 758-771.e8.
276. Yang, J., Rajan, S.S., Friedrich, M.J., Lan, G., Zou, X., Ponstingl, H., Garyfallos, D.A., Liu, P., Bradley, A., and Metzakopian, E. (2019). Genome-Scale CRISPRa Screen Identifies Novel Factors for Cellular Reprogramming. Stem Cell Reports *12*, 757–771.

277. Rauschenberger, T., Schmitt, V., Azeem, M., Klein-Hessling, S., Murti, K., Grän, F., Goebeler, M., Kerstan, A., Klein, M., Bopp, T., et al. (2019). T Cells Control Chemokine Secretion by Keratinocytes. Front. Immunol. *10*, 1917.
278. Tom Tang, Y., Emtage, P., Funk, W.D., Hu, T., Arterburn, M., Park, E.E.J., and Rupp, F. (2004). TAFA: a novel secreted family with conserved cysteine residues and restricted expression in the brain. Genomics *83*, 727–734.
279. Shen, T., and Guo, Q. (2018). Role of Pyk2 in Human Cancers. Med Sci Monit *24*, 8172–8182.
280. Shibata, K. (2018). Organ Co-Relationship in Tryptophan Metabolism and Factors That Govern the Biosynthesis of Nicotinamide from Tryptophan. Journal of Nutritional Science and Vitaminology *64*, 90–98.
281. Thomas, S.J., Snowden, J.A., Zeidler, M.P., and Danson, S.J. (2015). The role of JAK/STAT signalling in the pathogenesis, prognosis and treatment of solid tumours. Br J Cancer *113*, 365–371.
282. Owen, K.L., Brockwell, N.K., and Parker, B.S. (2019). JAK-STAT Signaling: A Double-Edged Sword of Immune Regulation and Cancer Progression. Cancers *11*, 2002.
283. Sundaram, G.M., Ismail, H.M., Bashir, M., Muhuri, M., Vaz, C., Nama, S., Ow, G.S., Vladimirovna, I.A., Ramalingam, R., Burke, B., et al. (2017). EGF hijacks miR-198/FSTL1 wound-healing switch and steers a two-pronged pathway toward metastasis. J Exp Med *214*, 2889–2900.
284. Mattiotti, A., Prakash, S., Barnett, P., and van den Hoff, M.J.B. (2018). Follistatin-like 1 in development and human diseases. Cell. Mol. Life Sci. *75*, 2339–2354.
285. D'Aguanno, S., Valentini, E., Tupone, M.G., Desideri, M., Di Martile, M., Spagnuolo, M., Buglioni, S., Ercolani, C., Falcone, I., De Dominici, M., et al. (2018). Semaphorin 5A drives melanoma progression: role of Bcl-2, miR-204 and c-Myb. J Exp Clin Cancer Res *37*, 278.
286. Lobna, M., Nasren, E., Adi, S., Jacob, B., Maria, G.-A.A., Marcus, M., and Zahava, V. (2021). The Expression of IL-17, in Chronic Spontaneous Urticaria Is Linked to Semaphorin5A. Biomolecules *11*, 373.
287. Siouda, M., Dujardin, A.D., Barbollat-Boutrand, L., Mendoza-Parra, M.A., Gibert, B., Ouzounova, M., Bouaoud, J., Tonon, L., Robert, M., Foy, J.-P., et al. (2020). CDYL2 Epigenetically Regulates MIR124 to Control NF-κB/STAT3-Dependent Breast Cancer Cell Plasticity. IScience *23*, 101141.
288. Sans-DeSanNicolas, L., Caratú, G., Vidal-Cortés, O., Sanchez-Redondo, S., Ferrer, B., Mancuso, F., González-Sanchez, E., Pérez-Alea, M., McGrail, K., Hernandez-Losa, J., et al. (2018). Genetic Profiles of Squamous Cell Carcinomas Associated with Recessive Dystrophic Epidermolysis Bullosa Unveil NOTCH and TP53 Mutations and an Increased MYC Expression. Journal of Investigative Dermatology *138*, 1423–1427.
289. Martins, V.L., Vyas, J.J., Chen, M., Purdie, K., Mein, C.A., South, A.P., Storey, A., McGrath, J.A., and O'Toole, E.A. (2009). Increased invasive behavior in cutaneous squamous cell carcinoma with loss of basement-membrane type VII collagen. Journal of Cell Science *122*, 1788–1799.
290. Knaup, J., Gruber, C., Krammer, B., Ziegler, V., Bauer, J., and Verwanger, T. (2011). TGFβ-signaling in Squamous Cell Carcinoma Occurring in Recessive Dystrophic Epidermolysis Bullosa. Analytical Cellular Pathology *34*, 339–353.
291. van der Kooi-Pol, M.M., de Vogel, C.P., Westerhout-Pluister, G.N., Veenstra-Kyuchukova, Y.K., Duipmans, J.C., Glasner, C., Buist, G., Elsinga, G.S., Westra, H., Bonarius, H.P.J., et al. (2013). High Anti-Staphylococcal Antibody Titers in Patients with Epidermolysis Bullosa Relate to Long-Term Colonization with Alternating Types of Staphylococcus aureus. Journal of Investigative Dermatology *133*, 847–850.
292. Dayal, J.H.S., Mason, S.M., Salas-Alanis, J.C., McGrath, J.A., Taylor, R.G., Mellerio, J.E., Blyth, K., South, A.P., and Inman, G.J. (2021). Heterogeneous addiction to transforming

growth factor-beta signalling in recessive dystrophic epidermolysis bullosa-associated cutaneous squamous cell carcinoma*. Br J Dermatol *184*, 697–708.

293. Annicchiarico, G., Morgese, M.G., Esposito, S., Lopalco, G., Lattarulo, M., Tampoia, M., Bonamonte, D., Brunetti, L., Vitale, A., Lapadula, G., et al. (2015). Proinflammatory Cytokines and Antiskin Autoantibodies in Patients with Inherited Epidermolysis Bullosa. Medicine *94*, e1528.
294. Hoste, E., Arwert, E.N., Lal, R., South, A.P., Salas-Alanis, J.C., Murrell, D.F., Donati, G., and Watt, F.M. (2015). Innate sensing of microbial products promotes wound-induced skin cancer. Nat Commun *6*, 5932.
295. Liao, Y., Ivanova, L., Zhu, H., Plumer, T., Hamby, C., Mehta, B., Gevertz, A., Christiano, A.M., McGrath, J.A., and Cairo, M.S. (2018). Cord Blood-Derived Stem Cells Suppress Fibrosis and May Prevent Malignant Progression in Recessive Dystrophic Epidermolysis Bullosa: Effects of Cord Blood Stem Cells in RDEB. Stem Cells *36*, 1839–1850.
296. Condorelli, A.G., Dellambra, E., Logli, E., Zambruno, G., and Castiglia, D. (2019b). Epidermolysis Bullosa-Associated Squamous Cell Carcinoma: From Pathogenesis to Therapeutic Perspectives. IJMS *20*, 5707.
297. Filoni, A., Cicco, G., Lospalluti, L., Maglietta, A., Foti, C., Annichiarico, G., Resta, L., and Bonamonte, D. (2020). Morphological and morphometric analysis of cutaneous squamous cell carcinoma in patients with recessive dystrophic epidermolysis bullosa: a retrospective study. J Eur Acad Dermatol Venereol *34*, 1707–1714.
298. Phillips, T., Huitema, L., Cepeda, R., Cobos, D. de los, Perez, R.I.M., Garza, M.S., Ringpfeil, F., Dasgeb, B., Uitto, J., Salas-Alanis, J.C., et al. (2020). Aberrant recruitment of leukocytes defines poor wound healing in patients with recessive dystrophic epidermolysis bullosa. Journal of Dermatological Science *100*, 209–216.
299. Beilin, A.K., Evtushenko, N.A., Lukyanov, D.K., Murashkin, N.N., Ambarchian, E.T., Pushkov, A.A., Savostyanov, K.V., Fisenko, A.P., Rogovaya, O.S., Vasiliev, A.V., et al. (2021). Signatures of Dermal Fibroblasts from RDEB Pediatric Patients. IJMS *22*, 1792.
300. Lincoln, V., Chao, L., Woodley, D.T., Murrell, D., Kim, M., O'Toole, E.A., Ly, A., Cogan, J., Mosallaei, D., Wysong, A., et al. (2021). Over-expression of stromal periostin correlates with poor prognosis of cutaneous squamous cell carcinomas. Exp Dermatol *30*, 698–704.
301. Sheipouri, D., Grant, R., Bustamante, S., Lovejoy, D., Guillemin, G.J., and Braidy, N. (2015). Characterization of the Kynurenine Pathway in Skin-Derived Fibroblasts and Keratinocytes: Characterization Of The Kynurenine Pathway. J. Cell. Biochem. *116*, 903–922.
302. Roberti, A., Fernández, A.F., and Fraga, M.F. (2021). Nicotinamide N-methyltransferase: At the crossroads between cellular metabolism and epigenetic regulation. Molecular Metabolism *45*, 101165.
303. Novak Kujundžić, R., Prpić, M., Đaković, N., Dabelić, N., Tomljanović, M., Mojzeš, A., Fröbe, A., and Trošelj, K.G. (2021). Nicotinamide N-Methyltransferase in Acquisition of Stem Cell Properties and Therapy Resistance in Cancer. IJMS *22*, 5681.
304. Yang, W., Wu, Y., Wang, C., Liu, Z., Xu, M., and Zheng, X. (2017). FSTL1 contributes to tumor progression via attenuating apoptosis in a AKT/GSK-3β – dependent manner in hepatocellular carcinoma. Cancer Biomarkers *20*, 75–85.
305. Cheng, S., Huang, Y., Lou, C., He, Y., Zhang, Y., and Zhang, Q. (2019). FSTL1 enhances chemoresistance and maintains stemness in breast cancer cells via integrin β3/Wnt signaling under miR-137 regulation. Cancer Biology & Therapy *20*, 328–337.
306. Jin, T., Zhang, Y., and Zhang, T. (2020). MiR-524-5p Suppresses Migration, Invasion, and EMT Progression in Breast Cancer Cells Through Targeting FSTL1. Cancer Biotherapy and Radiopharmaceuticals *35*, 789–801.

307. Li, L., Huang, S., Yao, Y., Chen, J., Li, J., Xiang, X., Deng, J., and Xiong, J. (2020b). Follistatin-like 1 (FSTL1) is a prognostic biomarker and correlated with immune cell infiltration in gastric cancer. World J Surg Onc *18*, 1–15.
308. Zhang, G., Jin, C., Zhu, Y., Fu, F., Wang, G., and Li, S. (2020). Sulforaphene inhibits the progression of osteosarcoma via regulating FSTL1/NF-κB pathway. Life Sciences *263*, 118485.
309. Lu, T.-P., Tsai, M.-H., Hsiao, C.K., Lai, L.-C., and Chuang, E.Y. (2012). Expression and functions of semaphorins in cancer. Translational Cancer Research *1*.
310. Lu, T.-P., Tsai, M.-H., Lee, J.-M., Hsu, C.-P., Chen, P.-C., Lin, C.-W., Shih, J.-Y., Yang, P.-C., Hsiao, C.K., Lai, L.-C., et al. (2010). Identification of a Novel Biomarker, SEMA5A, for Non–Small Cell Lung Carcinoma in Nonsmoking Women. Cancer Epidemiol Biomarkers Prev *19*, 2590–2597.
311. Sadanandam, A., Varney, M.L., Singh, S., Ashour, A.E., Moniaux, N., Deb, S., Lele, S.M., Batra, S.K., and Singh, R.K. (2010). High gene expression of semaphorin 5A in pancreatic cancer is associated with tumor growth, invasion and metastasis. International Journal of Cancer *127*, 1373–1383.
312. Sadanandam, A., Sidhu, S.S., Wullschleger, S., Singh, S., Varney, M.L., Yang, C.-S., Ashour, A.E., Batra, S.K., and Singh, R.K. (2012). Secreted semaphorin 5A suppressed pancreatic tumour burden but increased metastasis and endothelial cell proliferation. Br J Cancer *107*, 501–507.
313. Saxena, S., Purohit, A., Varney, M.L., Hayashi, Y., and Singh, R.K. (2018). Semaphorin-5A maintains epithelial phenotype of malignant pancreatic cancer cells. BMC Cancer *18*, 1–15.
314. Chen, W., Ding, R., Tang, J., Li, H., Chen, C., Zhang, Y., Zhang, Q., and Zhu, X. (2020). Knocking Out SST Gene of BGC823 Gastric Cancer Cell by CRISPR/Cas9 Enhances Migration, Invasion and Expression of SEMA5A and KLF2. CMAR *12*, 1313–1321.
315. Dziobek, K., Marcin, O., Beniamin, O.G., Nikola, Z., Przemysław, K., Piotr, J., Kamil, K., Robert, K., and Dariusz, B. (2019). Assessment of the Usefulness of the SEMA5A Concentration Profile Changes as a Molecular Marker in Endometrial Cancer. Current Pharmaceutical Biotechnology *21*, 45–51.
316. Kowalski, J., Samojedny, A., Paul, M., Pietsz, G., and Wilczok, T. (2005). Effect of apigenin, kaempferol and resveratrol on the expression of interleukin-1beta and tumor necrosis factor-alpha genes in J774.2 macrophages. Pharmacol Rep *57*, 390–394.
317. Cortes, J.R., Perez-G, M., Rivas, M.D., and Zamorano, J. (2007). Kaempferol Inhibits IL-4-Induced STAT6 Activation by Specifically Targeting JAK3. J Immunol *179*, 3881–3887.
318. Lee, S., Kim, Y.-J., Kwon, S., Lee, Y., Choi, S.Y., Park, J., and Kwon, H.-J. (2009). Inhibitory effects of flavonoids on TNF-alpha-induced IL-8 gene expression in HEK 293 cells. BMB Rep *42*, 265–270.
319. Perera, L.M.B., Sekiguchi, A., Uchiyama, A., Uehara, A., Fujiwara, C., Yamazaki, S., Yokoyama, Y., Ogino, S., Torii, R., Hosoi, M., et al. (2019). The Regulation of Skin Fibrosis in Systemic Sclerosis by Extracellular ATP via P2Y2 Purinergic Receptor. Journal of Investigative Dermatology *139*, 890–899.
320. Lee, H., and Jeong, G. (2021). Therapeutic effect of kaempferol on atopic dermatitis by attenuation of T cell activity via interaction with multidrug resistance-associated protein 1. Br J Pharmacol *178*, 1772–1788.
321. Kon, A., Takeda, H., Ito, N., Hanada, K., and Takagaki, K. (2005). Tissue-specific downregulation of type VII collagen gene (COL7A1) transcription in cultured epidermal keratinocytes by ultraviolet A radiation (UVA) and UVA-inducible cytokines, with special reference to cutaneous photoaging. Journal of Dermatological Science Supplement *1*, S29–S35.
322. Takeda, H., Kon, A., Ito, N., Sawamura, D., Takagaki, K., Hashimoto, I., and Hanada, K. (2005). Keratinocyte-specific modulation of type VII collagen gene expression by pro-

inflammatory cytokines (tumor necrosis factor-alpha and interleukin-1beta). Exp Dermatol *14*, 289–294.

323. Verrecchia, F., Pessah, M., Atfi, A., and Mauviel, A. (2000). Tumor Necrosis Factor-α Inhibits Transforming Growth Factor-β /Smad Signaling in Human Dermal Fibroblasts via AP-1 Activation. Journal of Biological Chemistry *275*, 30226–30231.
324. Verrecchia, F., Tacheau, C., Schorpp-Kistner, M., Angel, P., and Mauviel, A. (2001a). Induction of the AP-1 members c-Jun and JunB by TGF-beta/Smad suppresses early Smad-driven gene activation. Oncogene *20*, 2205–2211.
325. Verrecchia, F., Vindevoghel, L., Lechleider, R.J., Uitto, J., Roberts, A.B., and Mauviel, A. (2001b). Smad3/AP-1 interactions control transcriptional responses to TGF-beta in a promoter-specific manner. Oncogene *20*, 3332–3340.
326. Naso, M., Uitto, J., and Klement, J.F. (2003). Transcriptional Control of the Mouse Col7a1 Gene in Keratinocytes: Basal and Transforming Growth Factor-β Regulated Expression. Journal of Investigative Dermatology *121*, 1469–1478.
327. Wei, T., Xiong, F., Wang, S., Wang, K., Zhang, Y., and Zhang, Q. (2014). Flavonoid ingredients of Ginkgo biloba leaf extract regulate lipid metabolism through Sp1-mediated carnitine palmitoyltranferase 1A up-regulation. Journal of Biomedical Science *21*, 87.
328. Ochiai, A., Miyata, S., Iwase, M., Shimizu, M., Inoue, J., and Sato, R. (2016). Kaempferol stimulates gene expression of low-density lipoprotein receptor through activation of Sp1 in cultured hepatocytes. Sci Rep *6*, 24940.
329. Zhou, B., Jiang, Z., Li, X., and Zhang, X. (2018). Kaempferol's Protective Effect on Ethanol-Induced Mouse Primary Hepatocytes Injury Involved in the Synchronous Inhibition of SP1, Hsp70 and CYP2E1. Am J Chin Med *46*, 1093–1110.
330. Chapman, C.M., Sun, X., Roschewski, M., Aue, G., Farooqui, M., Stennett, L., Gibellini, F., Arthur, D., Pérez-Galán, P., and Wiestner, A. (2012). ON 01910.Na Is Selectively Cytotoxic for Chronic Lymphocytic Leukemia Cells through a Dual Mechanism of Action Involving PI3K/AKT Inhibition and Induction of Oxidative Stress. Clin Cancer Res *18*, 1979–1991.
331. Prasad, A., Khudaynazar, N., Tantravahi, R.V., Gillum, A.M., and Hoffman, B.S. (2016). ON 01910.Na (rigosertib) inhibits PI3K/Akt pathway and activates oxidative stress signals in head and neck cancer cell lines. Oncotarget *7*, 79388–79400.
332. Athuluri-Divakar, S.K., Vasquez-Del Carpio, R., Dutta, K., Baker, S.J., Cosenza, S.C., Basu, I., Gupta, Y.K., Reddy, M.V.R., Ueno, L., Hart, J.R., et al. (2016). A Small Molecule RAS-Mimetic Disrupts RAS Association with Effector Proteins to Block Signaling. Cell *165*, 643–655.
333. Jost, M., Chen, Y., Gilbert, L.A., Horlbeck, M.A., Krenning, L., Menchon, G., Rai, A., Cho, M.Y., Stern, J.J., Prota, A.E., et al. (2017). Combined CRISPRi/a-Based Chemical Genetic Screens Reveal that Rigosertib Is a Microtubule-Destabilizing Agent. Mol Cell *68*, 210-223.e6.
334. Kang, G.-Y., Lee, E.-R., Kim, J.-H., Jung, J.W., Lim, J., Kim, S.K., Cho, S.-G., and Kim, K.P. (2009). Downregulation of PLK-1 expression in kaempferol-induced apoptosis of MCF-7 cells. Eur J Pharmacol *611*, 17–21.
335. Kim, J.H., Kim, Y.S., Choi, J.-G., Li, W., Lee, E.J., Park, J.-W., Song, J., and Chung, H.-S. (2020). Kaempferol and Its Glycoside, Kaempferol 7-O-rhamnoside, Inhibit PD-1/PD-L1 Interaction In Vitro. IJMS *21*, 3239.